MICROINDENTATION CREEP OF CALCIUM-SILICATE-HYDRATE AND SECONDARY HYDRATED CEMENT SYSTEMS

By
Dan-Tam Nguyen

A thesis submitted under the supervision of
Dr. James J. Beaudoin

In partial fulfillment of the requirements for the degree of
Masters of Applied Sciences in Civil Engineering

uOttawa

Department of Civil Engineering
University of Ottawa
Ottawa, Canada
K1N 6N5

August 2014

To my beloved parents

ABSTRACT

The nanostructure, physical properties and mechanical performance of C-S-H, 1.4 nm tobermorite, jennite, and ettringite were studied. C-S-H of variable stoichiometries was examined as a model system in comparison with that produced in the hydration of Portland cement. The current Master's thesis is comprised of four research papers designed to improve the current understanding of the nanostructure and engineering properties of C-S-H systems and modified C-S-H systems. Many of the controversial issues in cement science were identified and were addressed in a comprehensive research study, which examined the key features of the C-S-H systems at the nano-structure level. In Chapter 4, each paper presented new evidence for a number of mechanical aspects of C-S-H materials. Numerous advanced analytical tools were used in order to verify the observations made in each section. The major achievements of the current work are mentioned briefly as follows:

1. It was determined that microindentation is a useful method for determining the creep behavior of C-S-H of various stoichiometries, 1.4 tobermorite, jennite, and ettringite.
2. Microindentation parameters i.e. creep modulus, indentation modulus and indentation hardness are porosity dependent.
3. Microindentation creep measurements on C-S-H (C/S = 0.80 and 1.20) demonstrated that creep modulus, indentation modulus, and indentation hardness are all dependent on mass-loss from the 11%RH condition.
4. Evidence was presented that the nanostructural role of interlayer water in C-S-H has a significant influence on the creep process.

I would like to express my deepest gratitude to my thesis supervisor, Dr. James J. Beaudoin (Researcher Emeritus at NRC and Adjunct Professor at the University of Ottawa), for his guidance, patience, and mentorship he has provided to me throughout my undergraduate and graduate studies. Dr. Beaudoin's intellectual heft is matched only by his genuinely good nature and his ceaseless desire for research, and I am sincerely fortunate to have had the opportunity to work with him.

I would also like to thank Dr. Laila Raki (concrete materials and structural technologies' group leader at NRC) for giving me the opportunity to work with such a great team at M-20. I am highly thankful to Dr. Rouhollah Alizadeh, Messrs. Gordon Chan, Jim Margeson, and Pouya Pourbeik, and Ms. Rahil Khoshnazar for their training on different experimental equipment over the years and assistance in the laboratory; I have been so fortunate to work with such a great team of researchers. Thank you also to Drs. Mamadou Fall and Pouria Ghods for their recommendations and feedback on the current work.

The experimental work of this thesis was conducted at the National Research Council of Canada. I would also like to acknowledge the financial support provided by NSERC and the University of Ottawa through research grants and assistantships.

CONTENT

Paper 3: Microindentation creep, elasticity, and hardness of C-S-H: the structural role of water

Paper 4: Creep of calcium-silicate-hydrates: a particle sliding mechanism

Abbreviations

DMA	Dynamic Mechanical Analysis
GU	General Use
IRC	Institute for Research in Construction
NRC	National Research Council of Canada
SEM	Scanning Electron Microscope
TGA	Thermogravimetric Analysis
XRD	X-Ray Diffraction

Cement Chemistry Notation

A	Al_2O_3
C	CaO
C/S	CaO to SiO_2 molar ratio
C_3A	Tricalcium aluminate
C_3S	Tricalcium silicate
C-S-H	Calcium Silicate Hydrate
F	Fe_2O_3
H	H_2O
S	SiO_2
w/c	Water to cement (or cementitious materials) mass ratio
β-C_2S	Beta dicalcium silica

1

Introduction and Objectives

1.1 Introduction

The binder phase of concrete is comprised of hydrated Portland cement. This phase is porous and its physical and chemical characteristics contribute significantly to its engineering performance. This has led to intensive research effort on the microstructure of cement paste over the last half century. Concrete is the most widely used man-made material in construction. The universal appeal of concrete is due mostly to three factors: concrete's ease of implementation (by mixing aggregate, Portland cement, and water together), its relative low cost of production, and the ability to cast concrete in different forms. Further, research issues in concrete technology pertaining to durability have not been fully resolved. Understanding concrete fundamentals at a microscopic level and the physico-chemical processes associated with the hydration reactions should contribute to a better understanding of the durability issues. The ability to control and modify the properties of the calcium-silicate-hydrate may lead potentially to a reduction in cost of production of concrete as well as repair and maintenance of infrastructure. Moreover, improved concrete technologies concerning durability can directly aid in reducing the production of greenhouse gases, due to the energy intensive production of cement [1].

The advantage of conducting and advancing research in the field of concrete technology permits engineers to design complex structures such as those for blast loads [2]. Concrete durability has remained a major challenge for materials scientists and engineers. The sustainability of concrete buildings and infrastructure has been costly due to the exposure of concrete to aggressive ions. Mehta reported in 1998

that an estimated $50 billion was required for infrastructure repair on bridges alone in the United States [3].

The physical and chemical properties of hydrated cement paste have been studied extensively since 1887 by Le Chatelier and further examined by cement scientists and researchers [4]. Despite ongoing research for over a 120 years, some major unresolved issues include the state of water in the hydration products, the role of water in creep and shrinkage of cement paste, and the mechanisms of sulfate attack and alkali silica reaction. Calcium-Silicate-Hydrate (C-S-H), which is the principal product of the Portland cement hydration process, is a primary contributor to important properties of hardened cement paste e.g. strength and shrinkage. The nanostructure of C-S-H is still not fully understood and debate concerning the arguments, theories, and evidence for some of the observed characteristics exists. The ability to design sustainable concrete structures is greatly dependent on the knowledge of material science and of its application at the nanoscopic-level [5].

The modification of conventional systems and the development of new materials with enhanced properties relies on an understanding the nature of the hydration products at the nanoscopic-scale. In the last decade, application of nanotechnology in materials engineering has grown significantly [6]. Many of the controversial topics in the cement sciences relate to mechanisms that are operative at the nanoscopic-level. The resolution of these will necessarily involve further research of the nanostructure and microstructure of cement paste. This research will involve both innovative experimental work, often coupled with computer simulations e.g. dynamic molecular modeling. The main body of this thesis will be presented in paper-format. The papers will be linked where appropriate with suitable passages.

1.2 Objectives

The current work was designed to contribute to the fundamental knowledge on the nature and engineering behaviour of C-S-H, secondary cement hydrates e.g. gypsum and layered silicate minerals of relevance to cement science. Based on the literature review presented in Chapter 2, specific issues in cement science were identified, and considered for further investigation. The recurring debated topic was found to be primarily concerned with the nanostructure of the C-S-H. The major controversies regarding C-S-H characteristics, specifically the C-S-H present in hydrated Portland cement, concern the role of water on its physical and mechanical properties as well as its layered nature. Some authors consider the C-S-H in hydrated Portland cement to be colloidal in nature and model it as a granular material [7, 8, 9].

The discussion within the research community is mainly due to the fact that the C-S-H generated from the hydration of Portland cement is a nearly amorphous material, containing impurities and exhibiting a wide range of stoichiometries. However, synthetically prepared C-S-H systems, which include C-S-H (I), 1.4 n.m. tobermorite, and jennite, have been suggested as models for the nanostructure of the C-S-H in hardened cement paste [10]. The research reported in this thesis uses the results obtained from several novel experimental methods in order to explain some of the new aspects of the nature of synthetic C-S-H in relation to the C-S-H produced in the hydrated Portland cement. The main objective of this thesis is to improve the understanding of the nanostructural features of the C-S-H as they relate to mechanical performance. As a by-product of this, possible methods of controlling and improving the performance of C-S-H-based materials are considered.

A brief statement of the specific objectives of Chapters 2 to 4 are summarized as follows:

Chapter 2. To identify and discuss the current scientific issues related to the nanostructure and engineering properties of C-S-H materials and their significance relative to the performance of hydrated cement.

Chapter 3. To describe the experimental methods used to study the issues identified in Chapter 2.

Chapter 4. To present the findings comprising four papers authored by the candidate (2 published, 2 submitted for publication). The research was designed to study the relation between the chemistry, stoichiometry, and microindentation creep of the C-S-H phase, and understand the structural role of adsorbed and interlayer water on mechanical performance. Each paper will be preceded with a brief comment on the relevance of the work and its specific objectives.

1.3 Overview

The main body of the thesis is comprised of three chapters, 2 to 4. Chapter 4 contains four research papers. Each paper is formatted according to the layout of a traditional journal paper and is divided into relevant sections such as abstract, introduction, experimental methods, results, discussion, conclusions, and references. Chapter 4 represents the results of investigations designed to study the engineering performance of C-S-H and relevant cement minerals. The studies include investigations of the structural role of water and involve the incremental removal of water from the 11% relative humidity (RH) condition. Theoretically at this condition, there is a monolayer of water present on the surface of the solid as well as the interlayer water. The physical and mechanical properties of phase pure C-S-H materials having

moisture contents below 11% RH were studied in conjunction with those of the C-S-H in hydrated Portland cement subjected to the same relative humidity conditioning. C-S-H specimens with a CaO/SiO_2 ratio (C/S ratio) of 0.8 and 1.2 were examined and compared to hydrated Portland cement with a water-to-cement ratio (w/c) of 0.427. The porosity values of the C-S-H and paste samples were similar. Chapters 2 and 3 offer pertinent information regarding the current research at hand, in order to gain a comprehensive understanding of the current work. An overview of the contents of the chapters 2 to 4 is provided as follows:

Chapter 2. The scope of the literature review, due to the multidisciplinary nature of the current work, is broad and entails aspects of chemistry, physics, and civil engineering. C-S-H, the main hydration product of Portland cement, has been the topic of significant research over the last 120 years. A summary of the relevant findings by other researchers and highlights of the areas which are still not fully understood are presented in the second chapter; these were instrumental in forming the research plan and conducting the research reported in the research papers presented in Chapter 4.

Chapter 3. The experimental methods and techniques are introduced and described in the third chapter. A brief description of the principal concepts for each technique is given in each paper presented in Chapter 4. The major details of the experimental set-up for each method utilized are presented in this chapter. The basic principles behind relevant techniques are described in the current work. The material preparation and the research methods are also explained. Chapter 3 also contains a description of the helium inflow technique. Helium is a non-adsorbing gas that can penetrate the interlayer spaces of C-S-H. The helium inflow technique can track volumetric changes due to the removal of

interlayer water. It is used to further study the properties of C-S-H. C/S ratios of 0.8 and 1.2 are selected as representative stoichiometries for the investigations in these studies. The results are compared to those of the C-S-H in hydrated cement paste. Details are provided in the relevant papers in Chapter 4. It is concluded from the comparison that the nearly amorphous C-S-H in hydrated cement paste acts like a layered material.

Chapter 4. The link between the chemistry and the engineering properties of C-S-H has not been fully established. An attempt to contribute to this goal is contained in the four papers presented in this chapter. Results of experiments on microindentation testing of compacted phase pure C-S-H of variable C/S ratios are studied in this chapter. Studies include investigations of the secondary minerals e.g. ettringite and gypsum. In addition, 1.4 n.m. tobermorite and jennite, which are the primary minerals in composition-based models for C-S-H in hydrated Portland cement, are studied [10]. The behaviour of the modulus of elasticity and creep upon the removal of adsorbed and interlayer water is observed. The C-S-H in hydrated cement paste exhibits a similar response which can be explained by a layered model for the C-S-H in cement paste with an assignment of a structural role to the interlayer water.

1.4 References

1. Mehta, P.K., "Reducing the environmental impact of concrete," *Concrete International*, 61-66, October 2011.
2. Ramachandran, V.S., Concrete Admixtures Handbook: Properties, Science, and Technology, William Andrew Inc., pp. 1153, 1995.

3. Mehta, P.K., “Greening of the concrete industry for sustainable development,” *Concrete International*, 23-28, July 2002.

4. Le Chatelier, H., Experimental Researches on the Constitution of Hydraulic Mortars, translated by J.L. Mack, McGraw, pp. 132, 1905.

5. Ciach, T.D., Gillot, J.E., Swenson, E.G., Sereda, P.J., “Microstructures of calcium silicate hydrates,” *Cement and Concrete Research*, 1, 13-25, 1971.

6. Beaudoin, J.J., “Why engineers need materials science,” *Concrete International*, 21(8), 86-89, 1999.

7. Powers, T.C., “Structures and physical properties of hardened Portland cement paste,” *Journal of the American Ceramic Society*, 41(1), 1-6, 1958.

8. Jennings, H.M., “A model for the microstructure of calcium silicate hydrate in cement paste,” *Cement and Concrete Research*, 30, 101-116, 2000.

9. Jennings, H.M., “Refinements to colloid model of C-S-H in cement: CM-II,” *Cement and Concrete Research*, 38, 275-289, 2008.

10. Taylor, H.F.W., “Proposed structure for calcium silicate hydrate gel,” *Journal of the American Ceramic Society*, 69(6), 464-467, 1986.

2

Calcium Silicate Hydrate – A Literature Review

The literature pertaining to the field of C-S-H investigations is very extensive owing to the important role of the hydrated silicate phase, which governs many of the chemical and mechanical properties of cement-based materials. This chapter provides a critical review and attempts to summarize studies relevant to achieving the main objectives of the current work. An in-depth literature review and/or commentary will also introduce each paper in Chapter 4, where appropriate.

2.1 C-S-H Formation

Portland cement is composed predominantly of four components: C_3S and β-C_2S, which are silicate phases, and C_3A and C_4AF, which are aluminate phases. As denoted in the glossary, cement chemistry has a specific mineralogical notation. C, S, A, F, and H refers to the oxides CaO, SiO_2, Al_2O, Fe_2O_3, and H_2O, respectively. The combination of the calcium silicates in Portland cement and water causes a chemical reaction, which results in the formation of two compounds: crystalline calcium hydroxide and a nearly amorphous calcium-silicate-hydrate, or C-S-H [1]. The hyphens denote variable stoichiometries.

The hydration of C_3S and β-C_2S can be approximated by the following reactions [2], respectively:

$$2(3CaO.SiO_2) + 6H_2O \rightarrow 3CaO.2SiO_2.3H_2O + 3Ca(OH)_2 \quad (1)$$

$$2(2CaO.SiO_2) + 4H_2O \rightarrow 3CaO.2SiO_2.3H_2O + Ca(OH)_2 \quad (2)$$

The chemical formulae for the C-S-H defined in these equations are approximate, as the CaO/SiO_2 ratio of the C-S-H varies within the same cement paste. Furthermore, the molar proportion of H_2O is not easily determined since there is a lack of a complete definition for the state of water in C-S-H. C-S-H constitutes up to about 60% of the hydration products in hardened cement paste and is chiefly responsible for some of its principal properties such as strength, shrinkage, and for its durability. A significant amount of the hydration products are formed within the first few days after mixing for a typical water/cement ratio of 0.3-0.6. The precipitation rate of the C-S-H on the surface of the anhydrous calcium silicates decreases as the rate of the reactions involved in the hydration process decrease. Several theories exist regarding mechanisms associated with the reaction kinetics [3]. Recent theories include processes of nucleation and growth of C-S-H in anhydrous calcium silicate surfaces [4, 5]. One argues that the process is controlled by

the diffusion of ions through the C-S-H barrier layer [2]. The occurrence of C-S-H phases with variable stoichiometry and physical properties is due to the change in the chemistry of aqueous solution and the available reaction volume as the hydration proceeds. Some of the difficulty in understanding the physical and chemical characterizations of C-S-H includes the variable crystalline nature of C-S-H in cement binders and the incorporation of other elements such as aluminium into its structure. These have been a major source of discussion due to ambiguity of the nature of C-S-H and have contributed to the discrepancies in the previously reported research results.

2.2 Characteristics of C-S-H

The physico-mechanical and physico-chemical properties of C-S-H systems are dependent on many factors including methods of preparation, stoichiometry and test conditions and procedures. The scope of the literature in this field is broad. The following section presents a brief overview of some of the research work relevant to the current project.

2.2.1 C/S Ratio

The molar ratio of CaO to SiO_2 in the structure of C-S-H, which is referred to as the C/S ratio, is an important stoichiometric parameter. By determining the amount of calcium hydroxide and unreacted materials, through analytical methods such as thermo-gravimetric analysis or quantitative X-ray diffraction, the C/S ratio of the C-S-H produced in the hydration of calcium silicates can be calculated [3]. The C/S ratio of C-S-H in hydrated cement paste ranges between 0.7 and 2.0, with an average value of 1.75 for that in normally hydrated Portland cement [6].

2.2.2 States of Water

A minimum amount of water is required for completion of the hydration reaction of Portland cement. This limit is considered to be reached at w/c=0.38-0.40 [6]. This is also a minimum requirement for acceptable workability of concrete. The use of excess water cause high porosity in the cement paste microstructure. Moist conditions are however needed after the setting of cement paste for the hydration process and the hardening of hydrated cement paste to proceed satisfactorily. This is also important for controlling volume stability issues like shrinkage. The transportation of aggressive chemicals into concrete and the ease of ionic movement are due mainly to the presence of water within the pore structure and the characteristics of the pore structure itself. Controversy surrounds the role of water in hydrated cement paste, which remains very complex. Many of the important properties of cement paste are microstructure related. The state of water (adsorbed, interlayer, or bulk) influences these properties. Shrinkage and strength are two important properties that are dependent on pore structure, porosity, and the equilibrium state of water in the material [7].

Two distinct traits exist in classifying the state of water in cement paste. The first is determined by the location of the water within the structure. The second depends on the nature of its bonding with and within the solid structure, which is a function of the energy needed for the water removal [8]. Much research has been conducted in an attempt to classify the different states of water in cement paste and in the C-S-H systems. A clear distinction between the various forms of water has not been made [9].

It is generally argued that several forms of water exist within the microstructure of cement paste; these include: water vapour in the pores, capillary water, surface adsorbed water, and interlayer water [10]. There is still considerable debate surrounding the interlayer water state associated with the structure of

C-S-H [11-13]. Different research methods have been employed to distinguish the various states of water in C-S-H systems; these are further discussed in Section 2.3. Many techniques developed have been used to determine the role of water within the C-S-H structure; these include dynamic mechanical analysis (DMA), nuclear magnetic resonance spectroscopy (NMR), and within the present work, microindentation.

2.2.3 Silicate Polymerization

C-S-H is comprised of stacking Ca-O layers supported by defect silicate chains. Calcium ions and water molecules are found between these layers. The silicate tetrahedra, which are bounded by Ca-O layers on both sides, can be found primarily in the form of dimers, pentamers, or a chain of dreierketten. Polymerization of silicate chains is denoted by the mean length of these chains and can be determined from the spectroscopic data obtained from a ^{29}Si MAS NMR experiment. The mean length of a chain represents the number of silicate tetrahedra in a chain and is calculated from the Q^2/Q^1 integral intensity ratio:

$$Mean\ Chain\ Length = 2\left(1 + \frac{Q^2}{Q^1}\right) \qquad (3)$$

Furthermore, the polymerization of C-S-H is dependent on the C/S ratio. It is shown that as the C/S ratio of synthetic C-S-H decreases from about 1.44 to 0.92, the chain length increases from 2.6 to 9.2 [14]. Moreover, polymerization of silicates is characterized by the curing conditions, including temperature and humidity. C-S-H found in moist cured cement paste are mostly composed of dimers, while cement paste cured at low relative humidity conditions (below 10% RH) have a larger degree of polymerization [15]. The degree of hydration affects the mean silicate chain length as well as the volume fraction of the C-S-H produced [16].

2.3 Models

There are two types of C-S-H models: models associated with its structure and those pertaining to the composition of C-S-H. The development of the model based on the C-S-H nano-structure was conceived earlier and is based on the surface area and adsorption-desorption data [11]. Models based on the composition of C-S-H were developed afterwards and advanced through the improvement and invention of new experimental methods. The following section discusses the features of the most important models.

2.3.1 Structure-Based Models

In the 1940's, Powers and Brownyard developed the first model of hardened Portland cement paste, which is known as the P-B model [17]. The purpose of their experiments was to understand the role of water within the structure of the cement paste; their tests were based on measurements of the mass change with varying temperature and humidity conditions. Their theory stipulates that water is found in two forms within the structure of cement paste: evaporable and non-evaporable. The evaporable form of water is the water that is lost under D-drying conditions over the vapour pressure of dry ice at -79°C. The evaporable water was referred to as "gel water" with reference to the four monolayers of water on the surface of the gel and also capillary water. Non-evaporable water represents the remaining water that can be removed by heating up to 1000°C. The P-B model was widely accepted within the community of cement scientists. Controversy arose when Feldman and Sereda presented their model, known as the F-S model in 1968 [18, 19]. The F-S model was based on interpretation of the results of porosity and surface area measurements using nitrogen gas, water isotherms for mass, length change, and modulus of elasticity change at varying humidities. Their experimental work led to a new model for C-S-H, known as the layered model. This approach explained the role of water more thoroughly and assigned a significant

percentage of the water to the interlayer region. Further work by Feldman was conducted using helium diffusion into the C-S-H structure at various humidity conditions. This provided further evidence for the layered nature of the C-S-H [20].

Much of the debate in the cement research community evolves from these two initial models. Brunauer, a critic of the F-S model, suggested that the surface area and porosity of D-dried pastes determined by water vapour adsorption and the application of the BET theory was correct. He also argued that the porosity is only partly measured using nitrogen gas. However, Feldman and Sereda expressed concerns with the nature of the solid particle bonding, the mechanism of water penetration between particles, and the incapability of the P-B model to explain the hysteresis effects in mass-change and length change isotherms [18]. Change with respect to mechanical properties versus relative humidity could not be explained using the P-B model [19, 23]. Daimon et al. further modified the F-S model by using nitrogen and water vapour adsorption isotherms [24]. They called the interlayer space of the structure of C-S-H the inter-crystallite pore space; they also referred to space trapped between the stack of layers as intra-crystallite pore space.

Further development of the C-S-H structural models is still ongoing; Jennings and colleagues have conducted extensive research on C-S-H gel properties based on porosity measurements, density, and mass-change isotherms. The main feature of their model is that C-S-H is composed of globules that have an approximate diameter of 5nm. This model does not seem plausible because it does not comply with the AFM imaging results which measure the C-S-H particle to be 5x20x60 nm^3 in size [25]. The globule model does not explain the fiber-like growth mechanism of C-S-H as proven by X-ray imaging studies [26].

Jennings et al. also proposed that the chemical formula of C-S-H is $(CaO)_{17}(SiO_2)(H_2O)_{18}$ and that its density is 2.604 g/cm^3. They obtained these results using small-angle neutron and X-ray scattering data, assuming that the water in the C-S-H was fully exchanged with heavy water after 24 hours of immersion. However, when comparing Jennings' previous work to his CM-II model [17, 26], the main features are noticeably different; the latter work is similar to the F-S model despite some subtle differences remaining with the respect to the role of water in C-S-H. Jennings' model does not specify if the interlayer water is a singular layer or is composed of several molecular layers of water. They postulate that nanoscale spaces exist in the interlayer area, which is questionable based on helium inflow interpretations [13]. It is suggested that the space in the interlayer region and the small gel pores that form in the globules of C-S-H are similar in nature. Daimon et al. and Feldman and Sereda suggested the existence of small gel pores as well in their models.

2.3.2 Composition-Based Models

Many researchers have attempted to determine the molecular structure of C-S-H; they examined the silicate anions, their arrangement, and other molecular bonds in the C-S-H structure by using diffraction, microscopic, and spectroscopic methods and were not concerned with mechanical properties. The improvements in these experimental methods have helped reveal greater details of the microstructure of C-S-H.

The first dreirerkette-based model of C-S-H was proposed by Bernal et al. [27]. Using crystallographic investigation, it was suggested that the C_3S hydration product is comparable to C-S-H formed in dilute suspension, which is the layered fibrous structure associated with 1.1 nm tobermorite. Taylor and Howison [28] suggested that the accepted C/S ratio of about 0.8 for tobermorite can be increased by

omitting the bridging tetrahedra, which is one of the main features in many other tobermorite-based models for C-S-H [14, 29]. The composition is explained by the C-S-H layers separated by an interlayer region, where H_2O, Ca^{2+}, and OH^- can be found. Other studies have linked the structure of C-S-H to jennite [30, 31]. The main difference between jennite and tobermorite is that in jennite, half of the oxygen atoms from the central Ca-O section of the C-S-H layer are shared with OH^-, and in tobermorite, all the oxygen atoms are shared with the infinite parallel rows of silicate chains.

Taylor suggested that C-S-H in cement paste is a disordered layer structure and is a combination of structures based on both 1.4 nm tobermorite and jennite [32]. Theoretically, this explained the high C/S ratio of C-S-H in cement paste as dimeric 1.4 nm tobermorite (T) and jennite (J) type structures could have a C/S ratio of about 1.25 and 2.25 respectively at early ages. Furthermore, the water to calcium ratio of the C-S-H at 11% RH lies between that of the suggested T-J structure.

Cong and Kirkpatrick further examined the nanostructural aspects of C-S-H [33, 34] by preparing C-S-H in various phases by hydrating β-C_2S and reacting silica fume and calcium oxide in an aqueous solution. Their ^{29}Si and ^{17}O MAS NMR spectroscopy studies were conducted on C-S-H systems with C/S ratios of 0.6 to 1.54. This confirmed the presence of Ca-OH and Si-OH bonds in the C-S-H, the abundance of which depends on the C/S ratio. They proposed a 1.4 nm defect tobermorite structure for C-S-H, where there are missing bridging tetrahedral and short chains that may tilt, rotate, or be displaced along the b-axis. This causes a disordered structure and is responsible for the diverse C-S-H stoichiometries.

2.4 References

1. Taylor, H.F.W., Cement Chemistry, Thomas Telford, 2nd Edition, pp. 459, 1997.
2. Lea, F.M., The Chemistry of Cement and Concrete, Arnold Publishers Ltd. 3rd Edition, pp. 727, 1970.
3. Ramachandran, V.S., "Differential thermal method of estimating calcium hydroxide in calcium silicate and cement pastes," *Cement and Concrete Research*, 9(6) 677-684, 1979.
4. Bullard, J., Jennings, H., Livingston, R.A., Nonat, A., Sherer, G.W., Schwitzer, J.S., Sriverner, K., Thomas, J.J., "Mechanics of Cement Hydration," *Cement and Concrete Research*, 41 1208-1228, 2011.
5. Thomas, J., Biernacki, J.J., Bulllard, J.W., Bishnoi, S., Dolado, J.S., Sherer, G.W., Luttge, A., "Modeling and simulation of cement hydration kinetics and microstructure development," *Cement and Concrete Research*, 41 1257-1278, 2011.
6. Richardson, I.G., "The nature of C-S-H in hardened cements," *Cement and Concrete Research*, 29, 1131-1147, 1999.
7. Wittmann, F.H., "Interaction of hardened cement paste and water," *J. Am. Ceram. Soc.*, 70(5), 323-328, 1987.
8. Mehta, P.K., Monteiro, P.J.M., Concrete: Microstructure, Properties, and Materials, 3rd Edition, McGraw-Hill, 2006.
9. Feldman, R.F., Ramachandran, V.S., "Differentiation of interlayer and adsorbed water in hydrated Portland cement by thermal analysis," *Cement and Concrete Research*, 16, 607-620, 1971.
10. Pellenq, R.J.-M., Lequeux, N., Van Damme, H., "Engineering the bonding scheme in C-S-H: the iono-covalent framework," *Cement and Concrete Research*, 38, 159-174, 2008.
11. Ramachandran, V.S., Feldman, R.F., Beaudoin, J.J., Concrete Science, Heyden, 1981.

12. Jennings, H.M., “Refinements to colloid model of C-S-H in cement: CM-II,” *Cement and Concrete Research*, 38, 275-289, 2008.

13. Beaudoin, J.J., Alizadeh, R., “Discussion of the paper ‘Refinements to colloid model of C-S-H in cement: CM-II,’ by Jenning, H.M.,” *Cement and Concrete Research*, 38(7), 1026-1027, 2008.

14. Chen, J.J., Thomas, J.J., Taylor, H.F.W., Jennings, H.M., “Solubility and structure of calcium silicate hydrate,” *Cement and Concrete Research*, 34(9), 1499-1599, 2004.

15. Macphee, D.E., Lachowski, E.E., Glasser, F.P., “Polymerization effects in C-S-H: implications for Portland cement hydration,” *Advances in Cement Research*, 1(13), 131-137, 1998.

16. Richardson, I.G., Groves, G.W., “Models for the composition and structure of calcium silicate hydrate (C-S-H) gel in hardened tricalcium silicate pastes,” *Cement Concrete Research*, 22, 1001-1010, 1992.

17. Beaudoin, J.J., “On the Validity of Colloidal Models for Hydrated Cement Paste.” Cement Lab. Web. 30 Apr. 2013.

18. Feldman, R.F., Sereda, P.J., “A model for hydrated Portland cement paste as deduced from sorption-length change and mechanical properties,” *Matériaux et Constructions*, 1(6), 509-520, 1968.

19. Feldman, R.F., Sereda, P.J., “A new model for hydrated Portland cement and its practical implications,” *Engineering Journal*, 53(8-9), 53-59, 1970.17.

20. Feldman, R.F., “Density and porosity studies of hydrated Portland cement,” *Cement Technology*, 3(1), 5-14, 1972.

21. Brunauer, S., Emmit, P.H., Teller, E., “Adsorption of gases in multimolecular layers,” *J. Am. Chem. Soc.*, 60, 309-319, 1938.

22. Brunauer, S., Odler, I., Yudenfreund, M., “The new model of hardened Portland cement,” *Highway Research Record*, 328, 89-101, 1970.

23. Feldman, R.F., “Assessment of experimental evidence for models of hydrated Portland cement,” *Highway Research Record*, 370, 8-24, 1972.

24. Daimon, M., Abo-El-Enein, S.A., Rosara, G., Goto, S., Kondo, R., “Pore structure of calcium silicate hydrate in hydrated tricalcium silicate,” *J. Am. Ceram. Soc*., 60(3-4), 110-114, 1977.

25. Tennis, P.D., Jennings, H.M., “A model for two types of C-S-H in the microstructure of Portland cement pastes,” *Cement and Concrete Research*, 30(6), 855-863, 2000.

26. Gartner, E., Kurtis, K.E., Monteiro, P.J.M., “Proposed mechanism of C-S-H growth tested by soft X-ray microscopy,” *Cement and Concrete Research*, 30(5), 817-822, 2000.

27. Gernal, J.D., Jeffery, J.W., Taylor, H.F.W., “Crystallographic research on the hydration of Portland cement. A first report on investigations in progress,” *Mag. Concre. Res*., 4(11), 49-54, 1952.

28. Taylor, H.F.W., Howison, J.W., “Relationships between calcium silicates and clay minerals,” *Clay Miner. Bull.*, 3(16), 98-111, 1956.

29. Cong, X., Kirkpatrick, R.J., “^{29}Si MAS NMR study of the structure of calcium silicate hydrate,” *Adv. Cem.Based Mater.*, 3, 144-156, 1996.

30. Carpenter, A.B., Chalmers, R.A., Gard, J.A., Speakman, K., Taylor, H.F.W., “Jennite, a new mineral,” *American Mineralogist*, 3, 160-170, 1966.

31. Gard, J.A., Taylor, H.F.W., Cliff, G., Lorimer, G.W., “A re-examination of jennite,” *American Mineralogist*, 62, 365-368, 1977.

32. Taylor, H.F.W., “Proposed structure for calcium silicate hydrate gel,” *J. Am. Ceram. Soc.*, 69(6), 464-467, 1986.

33. Cong, X., Kirkpatrick, R.J., “^{29}Si MAS NMR study of the structure of calcium silicate hydrate,” *Adv. Cem. Based Mat.*, 3, 144-156, 1996.

34. Cong, X., Kirkpatrick, R.J., “^{29}Si and ^{17}O NMR investigations of the structures of some crystalline calcium silicate hydrates,” *Adv. Cem. Based Mat.*, 3, 133-143, 1996.

3

Experimental Methods

In this chapter, the test methods used to characterize the structure of C-S-H and determine the microindentation parameters and other indices of engineering behaviour are described. The details of C-S-H synthesis, humidity conditioning, drying methods, and the powder compaction technique are described.

3.1 Experimental Tools

3.1.1 Helium Inflow

The flow of helium gas into the structure of Portland cement paste at various increments of moisture loss from the 11% RH condition, has been used to study the volumetric stability of the system. Feldman and colleagues have been using helium gas as a nanostructural probe to evaluate Portland cement and C_3S pastes' structural response to loss of moisture since the early 70's [1-6]. The volume of the nanospaces vacated by water can be measured using helium inflow measurements. The volume of the solid phase of the sample is changed by removing water incrementally from the hydrate structure and its effect can be systematically and quantitatively estimated. The results from the helium inflow measurements for Portland cement paste systems correspond with the behaviour of a layered material despite its X-ray amorphous character [7].

The technique for helium inflow measurements has been described in previous papers [1, 2]. The procedure, which is based on gas laws, entails using a helium pycnometer and assumes that helium is an ideal gas. It is normally used for measurements of solid volumes. This measurement is instantaneous. Inert helium gas fills the small pores of a material, which allows for the true calculations of a solid volume. The density and porosity can then be calculated from the known mass and the apparent volume.

A secondary phenomena occurs if the sample remains exposed to helium gas over an extended period. Following the initial solid volume measurement, the helium gas, which is maintained at a constant pressure of 2 atm, begins to diffuse into the very small regions of the sample that are not accessible to the helium at first. The inflow can be examined and the results obtained for the adjusted volume (that takes into account interlayer space) can be plotted mass-loss. The material's nanostructure and its

equilibrium state with regards to water vapour play a vital role in the inflow of helium and its characteristics. The time-dependent flow is interpreted as entering the interlayer regions of the structures. Pores are instantly filled and therefore, are not involved in the inflow measurement. Helium pycnometry has proven to be a technique that is capable of revealing nanostructural characteristics which are not measureable using other tools [8].

Helium gas was used as a nano-structural probe in this study to investigate the structural changes in C-S-H (I) (C/S = 0.8 and 1.2) due to the removal of interlayer water. Changes to the 002 basal spacing were correlated with helium inflow characteristics. New evidence supporting the “layered” nature of C-S-H in hydrated cement paste was presented. Furthermore, the viability of considering C-S-H (I) as a physical model for the C-S-H in hydrated Portland cement was discussed.

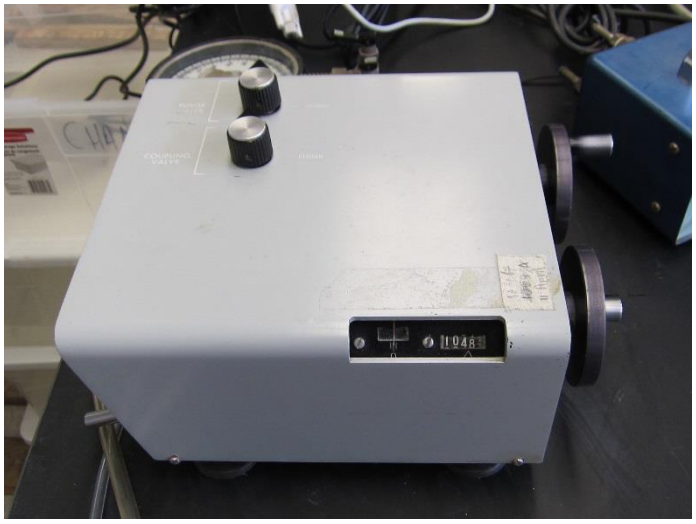

Figure 3.1: Helium pycnometer apparatus

3.1.2 Microindentation

All the microindentation tests were performed using a CSM Instruments Instrumented Indentation Tester. The apparatus is housed in an environmental chamber. The initial set of tests was conducted at 11% RH on specimens equilibrated at 11% RH. Subsequent tests were conducted at varying moisture contents after a step-wise removal of water in increments of 1% up to a total of 8%. These tests outlined in papers 3 and 4 of Chapter 4 are particularly useful in analyzing the structural role of water in C-S-H. Microindentation tests were conducted using a Berkovich indenter. The CSM microindentation instrument has a load range of 0.03-30 N with a resolution of 0.3 mN. The rate of loading in the current experiments was 2000 mN/min. The specimens were tested at porosity values of about 43%. There were approximately 25 indents on each sample at each moisture content for a total of approximately 225 indents for each material system. The composition of the solid phase (with the exception of the moisture content) for each C-S-H system remains constant. Pure materials do not require as many indents as composite materials as phase separation procedures such as the use of deconvolution methods are not necessary.

The indentation depth was recorded as a function of time at the maximum load of 1000 mN for a 600 s dwell period. The logarithmic creep was determined through curve fitting of the indentation-depth versus time curves during the 600s dwell time by the following equation:

$$\Delta h(t) = x_1 ln(x_2 t + 1) + x_3 t + x_4 \qquad (1)$$

The creep modulus, C, is then calculated from: $C = P_{max}/(2a_U x_1)$ where $a_U = [A_c/\pi]^{1/2}$. A_c is the projected area of contact between the indenter probe and the indenter surface. It is determined using the Oliver

and Pharr method as a function of the maximum indentation depth [9]. The indentation modulus (M) and indentation hardness (H) were obtained from the software that uses the Oliver and Pharr method. $M = \pi^{1/2}S/[2(A_c)^{1/2}]$ where $S = dP/dh\ |_{h = hmax}$ is the initial slope of the unloading branch of the P-h curve. P is the maximum indentation load. Indentation hardness $H = P/A_c$. The stiffness, S, is determined as illustrated in Figure 3.1.

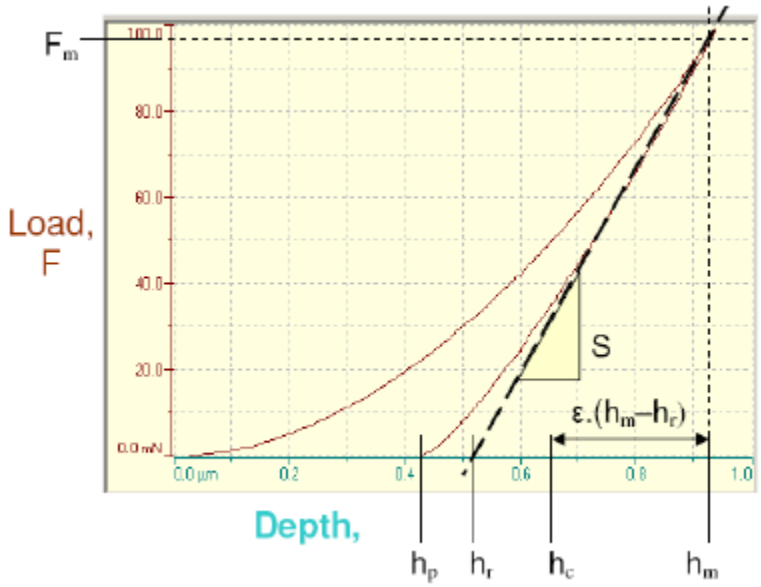

Figure 3.2: Determination of the stiffness [10]

The following schematic outlines the calculations:

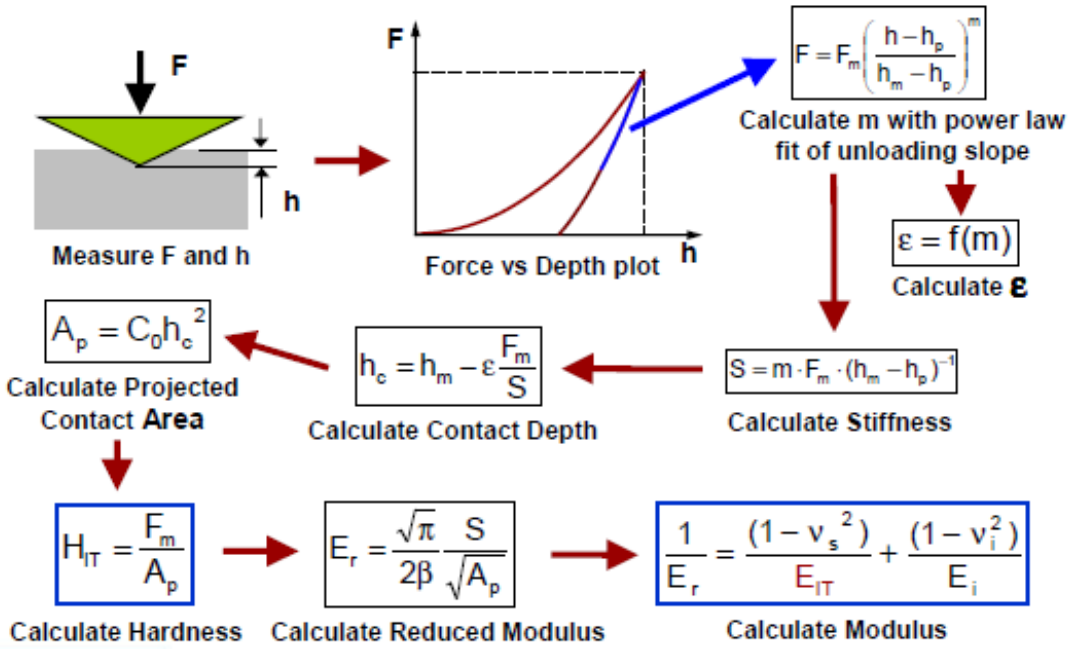

Figure 3.3: Schematic of modulus of elasticity calculation [10]

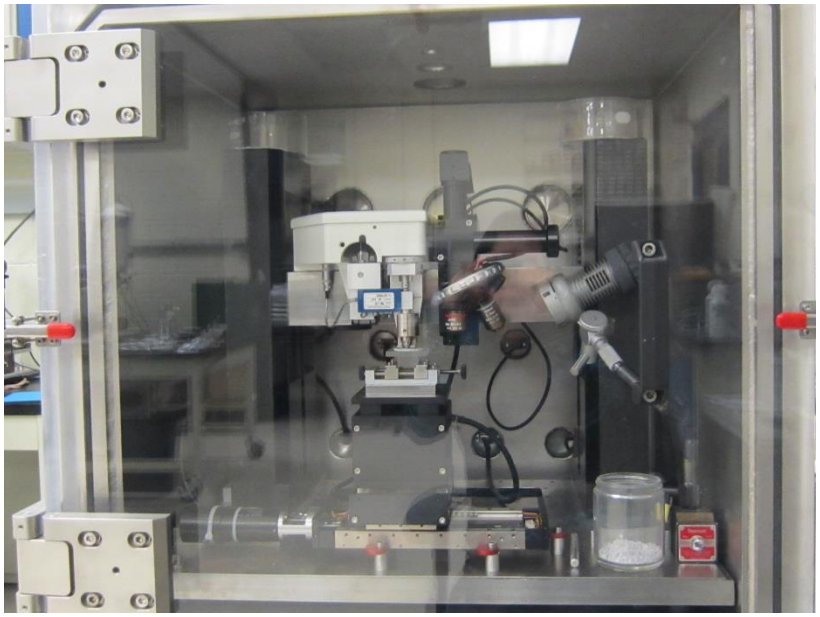

Figure 3.4: Microindentation apparatus

3.2 Materials

The following section describes the C-S-H preparation method, its humidity conditioning, drying, and compaction. The C-S-H, 1.4 nm tobermorite, jennite, and ettringite were prepared synthetically. The latter three compounds were prepared for companion studies. Other materials were obtained from commercial sources.

3.2.1 Synthesis of C-S-H, 1.4 nm Tobermorite, and Jennite

C-S-H: The synthesis of C-S-H samples was achieved by mixing stoichiometric amounts of CaO and SiO_2 in distilled and de-aired water at room temperature. CaO was obtained by calcining reagent grade $CaCO_3$ (Sigma-Aldrich) at 900°C in a muffle furnace for 24 hours. Freshly obtained CaO through this method is more reactive than the reagent-grade pure CaO. Amorphous SiO_2 (Cab-O-Sil, Grade M-5, Cabot corporation) was used. C-S-H preparation with a C/S ratio of 0.8 and 1.2 were produced. In each preparation, a water to solid mass ratio of about 10 was used. The amount of materials for each C/S ratio is given in Table 3.1.

Table 3.1: The Mass of Materials Used to Prepare C-S-H at Various C/S Ratios

C/S Ratio	CaO, g	SiO_2, g	H_2O, g
0.8	25.90	34.68	700
1.2	31.95	28.53	700

The CaO and SiO_2 were dry-mixed and shaken in N_2 purged high-density polyurethane bottles. The water was then added to the mixture and the bottle was additionally shaken. A significant amount of heat would generally be produced due to the hydration reaction of CaO. Extra care was taken in handling the bottle

in order to properly finish the shaking step. After the initial shaking, the plastic bottles were placed on rotating racks at the speed of 16 rpm. In order to complete the crystallization and ordering of C-S-H layers and achieve a well-aged material, the hydration process lasted 6 months.

After 6 months, the samples were filtered in order to remove excess water. The paste-like material (surface-wet) was then dried under vacuum for 3-4 days. During the drying step, extra care was taken to avoid or minimize exposure of the material to the atmosphere. This was due to CO_2 in the air which could cause undesirable carbonation of the materials. After drying, the C-S-H powders were stored in N_2 purged glass vials until further use.

In order to compare the behaviour of C-S-H with that of cement paste, Portland cement paste (made with type GU cement, w/c = 0.4) was also prepared. The Portland cement paste sample was cut into thin circular slices of approximately 1 mm in thickness for helium flow measurements.

The C-S-H preparations and cement paste slices were conditioned for three weeks in a vacuum desiccator over the vapour pressure of a saturated lithium chloride solution. The lithium chloride solution provides a relative humidity of about 11% at room temperature, which is a desirable base for studying the stoichiometry of C-S-H [11]. Theoretically, there is a monolayer of adsorbed water on the surface of particles at this specific humidity in addition to the interlayer water. This state was used as the starting condition for all the experiments in the present research.

1.4 nm tobermorite: The reactants (CaO and SiO_2) were prepared in a similar manner to those for C-S-H. The C/S ratio was 0.9. The reactants were placed in a high density polyethylene bottle mixed in excess

deionized water (water/solids=11) and maintained at 80°C using a heating wrap. The mixture was continuously agitated with a magnetic stirrer for a period of 4 months.

Jennite: The reactants (CaO and SiO_2) were prepared as described above. The C/S ratio was 1.4. The reactants were placed in a high density polyethylene bottle mixed in excess deionized water (water/solids = 11) and maintained at 80°C using a heating wrap. The mixture was continuously agitated with a magnetic stirrer for a period of 4 months.

Figure 3.5: Vacuum-sealed desiccator conditioning samples at 11% RH.

3.2.2 Characterization of Materials

C-S-H: Characterization of all the C-S-H materials by X-ray diffraction (XRD) and thermal methods gave results directly comparable to C-S-H (I) as reported by Taylor [12]. The C-S-H samples have a definite X-ray pattern with three main peaks at about 1.250, 0.304, and 0.280 nm as reported in the literature [12].

The location of the low angle d_{002} XRD peak that occurs between 5° and 10°, 2θ (commonly referred to as 002 basal spacing) depends on the C/S ratio of the C-S-H. The reflection can be used to calculate the mean distance between the layers of C-S-H based on Bragg's law.

The thermogravimetric curves of C-S-H (mass-loss and heat flow versus temperature) are qualitatively and quantitatively similar to those reported for the C-S-H gel [12]. A relatively low mass-loss was observed in the region of 400-600°C for the C-S-H (I) used in this study, which suggests that the residual amount of $Ca(OH)_2$ is small or negligible. The mass-loss from room temperature to about 110°C is usually considered to be due to the evaporable water. Loss of constitutional water likely contributes to the additional gradual mass-loss at higher temperatures.

C-S-H that is formed in the hydration of Portland cement or calcium silicate phases, has a generally spongy and amorphous texture as shown in Figure 3.6. However, the synthetic C-S-H is well-ordered and depicts flaky and foil-like crystals. It can be inferred from the SEM images that as the C/S ratio decreases, the C-S-H flakes become smaller but more connected to each other forming a continuous network.

1.4 nm Tobermorite and Jennite: Characterization of 1.4 nm tobermorite and jennite by X-ray diffraction give spectra comparable to those produced by Yu and Kirkpatrick [18]. TGA curves were also similar.

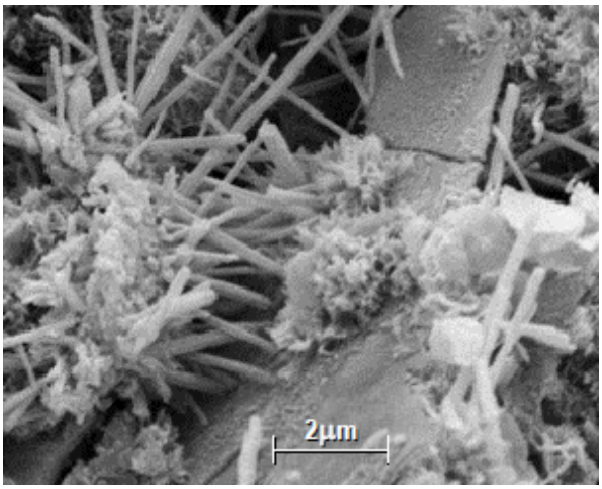

Figure 3.6: SEM Image of Portland cement hydration products
(Courtesy of Mr. Jim Margeson, NRC)

3.2.3 Compaction of Powders

Compacted powders of C-S-H, 1.4 nm tobermorite, jennite, and secondary hydrated phases were prepared in these studies. A rigid body of the material was required for the helium inflow investigation and microindentation creep experiments. In Portland cement hydration studies, the cement paste hardens and can be cut into various shapes depending on the type of test. However, it is necessary to prepare solid samples by compressing the fine powder of materials such as a synthetic C-S-H in order to determine the mechanical properties [13, 14]. Furthermore, handling the compacted specimens for mass-change measurements is simplified. Moreover, the limitations inherent in the use of natural rigid porous materials is avoided. Control and the extension of the range of porosity is also possible.

It has been demonstrated that the compacted samples of hydrated Portland cement powders display similar properties to hardened Portland cement paste [15]. Essentially, the bonds between the particles in a compacted sample mimic those that form during the setting and hardening. The bridging of the

surface of particles together primarily involves the formation of van der Waals's attractions. Solid-state reactions can be postulated.

This technique entails the compaction of powders through pressure compaction in steel moulds, consisting of a cylinder and two closely-fitted pistons. The steel mould and prepared samples are shown in Figures 3.7 and 3.8.

Figure 3.7: Steel mould used for pressure compaction

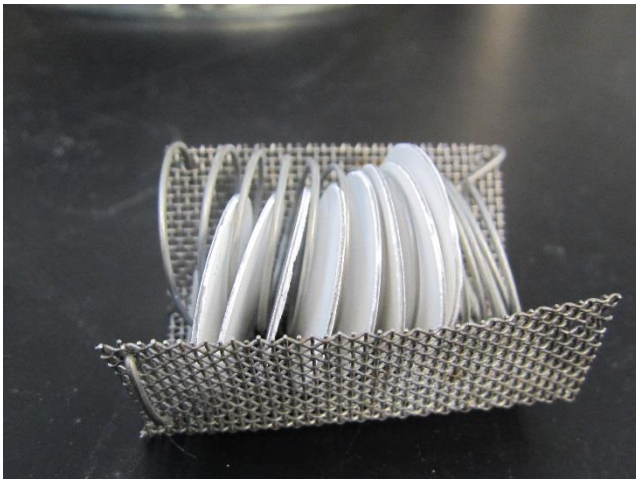

Figure 3.8: Compacted samples

The mould is first mounted vertically with the bottom piston. The powder is then placed in the cylinder. The surface of the powder is leveled by pushing the bottom piston up so the powder is somewhat flush with the mould; using a spatula, the powder was swept across the top of the mould to ensure the powder was evenly distributed within the mould. The bottom piston was carefully brought down and the top piston is then placed in the cylinder. The assembly is mounted in a compression machine. The pressure is gradually increased to the specified value where it is maintained for about 30 seconds before releasing. The compacted sample is removed by pressing out the pistons.

The compacted sample may crack due to the relaxation if the density of the powder is not uniform in the sample. This can occur if the pressure exceeds a limiting value (depending on the nature of the powder) or if the powder is too wet. The experimental plan required the powders to be conditioned at 11% RH, where the desired state has a monolayer of water on the surface of the solid particles; this humidity level is favourable for making compacted powder samples. Further, the C-S-H and other silicates used for this study was in the form of a very fine powder that could pass through a 150 μm sieve (mesh No. 100).

Test samples having various porosity values were compressed into circular discs for this study. It is critical to control the porosity of the compacted samples in order to compare the experimental results between the materials at different stoichiometries [16, 17].

3.2.4 Removal of Water from C-S-H

The experimental plan, as previously mentioned, was to measure the changes in various properties of C-S-H on drying the 11% RH conditioned specimens. This was a key component of the work presented in paper 3 and 4, Chapter 4. Water removal from the specimens was attained by the application of a

combination of vacuum and heat. A glass cell wrapped with a heating mantel was used, which was also connected to a vacuum hose. The initial drying increments for the 11% RH conditioned samples were obtained at room temperature using only vacuum. The temperature was gradually increased using the voltage adjustment (with a VARIAC W5MT3) on the heating mantel for higher mass-loss levels in the samples. The temperature inside the cell under vacuum had been previously calibrated for the voltage.

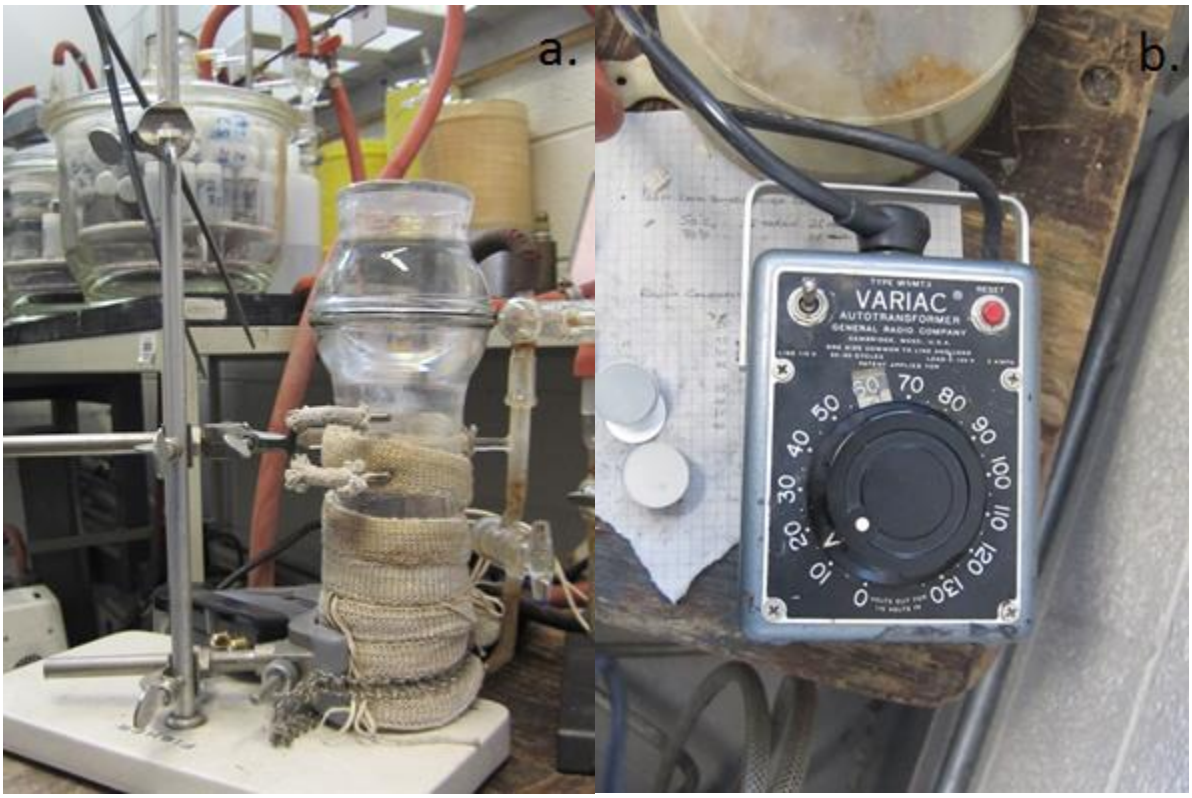

Figure 3.9: a. Vacuum-sealed heating cell used for experimentation, b. VARIAC W5MT3 used to adjust voltage on the heating mantel.

The drying temperatures generally never exceeded 50°C for most of the mass-loss range and 108°C (along with a 24h vacuum) for mass loss of about 8%, in order to minimize the alteration of the C-S-H structure. Considering the ample amount of time spent on the removal of water at each increment, these drying steps can be considered to be at semi-equilibrium states. Extra care was taken to increase the temperature gradually so that the moisture gradients did not cause any cracking to the samples. A special

steel mesh cage and forceps were designed to place and remove the specimens in the drying-cell with additional care. All the powder samples were handled in small glass vials and the compacted and sliced samples were placed on a special steel net rack.

Conventional drying procedures of hydrated Portland cement cannot completely preserve the microstructure [1]. The method used in this study has the advantage, that the C-S-H microstructure is formed at 11% RH, which is a low humidity, through the compaction of the powder. There was no drying of the porous body required to obtain the 11% RH state. The saturated sample, as was the case for the hydrated paste, has to be dried to 11% RH. The cement paste drying may alter the C-S-H microstructure and possibly cause the formation of micro-cracks.

3.3 References

1. Feldman, R.F., "The flow of helium into the interlayer spaces of hydrated Portland cement pastes," *Cem. Concr. Res.*, 1(3), 285-300, 1971.
2. Feldman, R.F., "Helium flow and density measurements of the hydrated tricalcium silicate water systems," *Cement and Concrete Research*, 2(1), 123-136, 1972.
3. Feldman, R.F., "Helium flow characteristics of rewetted specimens of dried hydrated Portland cement paste," *Cement and Concrete Research*, 3, 7777-791, 1973.
4. Feldman, R.F., "Application of the helium inflow technique for measuring surface area and hydraulic radius of hydrated Portland cement," *Cement and Concrete Research*, 10, 657-664, 1980.

5. Feldman, R.F., Ramachandran, V.S., “Microstructure of calcium hydroxide depleted Portland cement paste, I: density and helium flow measurements,” *Cement and Concrete Research*, 12, 179-189, 1982.

6. Feldman, R.F., Beaudoin, J.J., “Effect of applied stress on the helium inflow characteristics of hydrated Portland cement,” *Cement and Concrete Research*, 13, 470-476, 1983.

7. Alizadeh, R., Beaudoin, J.J., Raki, L., “C-S-H (I): A nanostructural model for the removal of water from hydrated cement paste,” *J. Am. Ceram. Soc.*, 90(2), 670-672, 2007.

8. Beaudoin, J.J., Alizadeh, R., “Detection of nanostructural anomalies in hydrated cement systems,” *Journal of Cement and Concrete Composites*, 29(2), 63-69, 2007.

9. Oliver, W.C., Pharr, G.M., “An improved technique for determining hardness and elastic modulus using load and displacement sensing indentation experiments. *J. Mater Res.*, 7, 1564-1583, 1992.

10. Conté, N., “CSM Instruments,” *Instrumented Indentation Testing Course*, 25-40, 2008.

11. Feldman, R.F., Ramachandran, V.S., “A study of the state of water and stoichiometry of bottle-hydrated Ca_3SiO_5,” *Cement and Concrete Research*, 4(2), 155-166, 1974.

12. Taylor, H.F.W., Cement Chemistry, Thomas Telford, 2nd Edition, pp. 459, 1997.

13. Taylor, H.F.W., “Proposed structure for calcium silicate hydrate gel,” *Journal of the American Ceramic Society*, 69(6), 464-467, 1986.

14. Beaudoin, J. J., “Comparison of mechanical properties of compact calcium hydroxide and Portland cement paste systems,” *Cement and Concrete Research*, 13, 319-324, 1983.

15. Sereda, P.J., Feldman, R.F., Swenson, E.G., “Effect of sorbed water on some mechanical properties of hydrated Portland cement paste and compacts,” *Highway Research Board spec. Report 90*, 58-73, 1966.

16. Feldman, R.F., Beaudoin, J.J., “Microstructure and strength of hydrated cement,” *Cement and Concrete Research*, 6(3), 389-400, 1976.

17. Beaudoin, J.J., “Effect of humidity and porosity on fracture of hardened Portland cement,” *Cement and Concrete Research*, 12(6), 705.716, 1982.

18. Yu, P., Kirkpatrick, R.-J., “Thermal dehydration of tobermorite and jennite,” *Concrete Science and Engineering*, 1, 185-191, 1999.

4

Microindentation Studies of Calcium-Silicate-Hydrate and Secondary Hydrated Phases

Four papers addressing creep, elasticity, hardness, and the structural role of water in the behaviour of calcium-silicate-hydrate

This chapter is comprised of four research papers. The titles of these papers are as follows:

Paper 1: Microindentation creep of monophasic calcium-silicate-hydrates (Cement and Concrete Composites, April 2014, Volume 48, pp 118-126)

Paper 2: Microindentation creep of secondary hydrated cement phases and C-S-H (Materials and Structures, September 2013, Volume 46, Issue 9, pp 1519-1525)

Paper 3: Microindentation creep, elasticity, and hardness of C-S-H: the structural role of water (Submitted for publication)

Paper 4: Creep of calcium-silicate-hydrates: a particle sliding mechanism (Submitted for publication)

4.1 Introduction

The mechanical properties of compacted samples of synthetic C-S-H, cement paste, 1.4 nm tobermorite, and jennite as well as those of secondary hydrated cement phases were determined at variable stoichiometries. The results of these investigations are reported and discussed in papers 1 and 2. In addition, the creep modulus, indentation modulus, and indentation hardness of the C-S-H systems were monitored at various increments of mass-loss from 11%RH following the removal of the adsorbed and interlayer water and discussed in terms of the state of water present in the microstructure of C-S-H. These results are discussed in papers 3 and 4. Results were compared to that for the hydrated Portland cement. It was demonstrated that C-S-H in the hydration products of Portland cement displays an analogous mechanical behaviour to that of synthetic C-S-H. The response of these systems to the removal of water was explained by a layered model for the C-S-H. A model was proposed to describe the changes occurring at various stages of the mechanical performance of C-S-H. It is noted that the microindentation results reported in papers 3 and 4 show similar trends to data obtained from dynamic mechanical analysis measurements i.e. curves of storage modulus and indentation modulus versus mass-loss as well as curves of creep modulus versus mass-loss and tan δ (internal friction) versus mass loss have similar characteristics. This was particularly useful in characterizing the model and providing evidence for a particle-sliding creep mechanism.

4.2 Paper 1: Microindentation Creep of Monophasic Calcium-Silicate Hydrates

This first paper utilized microindentation methods to determine creep behaviour of monophasic calcium-silicate-hydrates. The research in this paper also supported the view that compacted powders are useful models for studying the indentation creep of calcium silicates and minimizing surface roughness effects. Furthermore, it was found that creep of pure C-S-H phases is greater than the creep of hydrated cement paste or hydrated C_3S due to the restraining effect of calcium hydroxide and clinker phase in the paste and that the creep of 1.4 nm tobermorite and jennite is generally less than that of synthetic C-S-H and greater than that of hydrated cement paste or hydrated C_3S. The C/S ratio of the C-S-H preparations studied appeared to influence the three microindentation parameters (indentation modulus, hardness, and creep modulus). The porosity dependence of creep modulus and the general equivalence of density values determined by helium pycnometry and by calculations employing unit cell dimensions are discussed in terms of postulates for the existence of two types of C-S-H. The compatibility of the creep modulus data for 1.4nm tobermorite and jennite with models of C-S-H present in cement paste is also described.

Microindentation Creep of Monophasic Calcium-Silicate-Hydrates

(*Cement and Concrete Composites*, 48, 118-126, 2014)

D.-T. Nguyen[a], R. Alizadeh[b], J. J. Beaudoin[c], P. Pourbeik[a] and L. Raki[c]

[a] Department of Civil Engineering, University of Ottawa, Ottawa, ON, Canada
[b] Giatec Scientific Inc., Ottawa, ON, Canada
[c] National Research Council Canada, Construction Portfolio, Ottawa, ON, Canada

Abstract

Microindentation creep results for monophasic synthetic C-S-H (C/S = 0.6 – 1.5), 1.4nm tobermorite, jennite and calcium hydroxide at 11% RH are reported. Creep results for well hydrated cement paste and C_3S 'composite' systems are also described. The significance of the co-linear behavior of creep modulus functions of indentation modulus and indentation hardness for C-S-H obtained by microindentation and nanoindentation methods is discussed. The porosity dependence of creep modulus and the general equivalence of density values determined by helium pycnometry and by calculations employing unit cell dimensions (obtained using x-ray crystallography techniques) are also discussed in terms of postulates for the existence of two types of C-S-H. Comment on the compatibility of the creep modulus data for 1.4nm tobermorite and jennite with models of C-S-H present in cement paste is provided.

Keywords: Microindentation, Creep, C-S-H

1. Introduction

There has been a plethora of publications over several decades dealing with the creep behavior of cement-based materials [1]. These have included numerous contributions on creep mechanisms. Indentation techniques for measuring creep of cement systems have been introduced recently [2]. They have the advantage of significantly reducing the time scale for observing creep phenomena. Recent studies utilizing nanoindentation techniques conclude that creep is likely due to the rearrangement of nanoscale particles associated with theories of granular physics [3, 4]. Creep is then said to originate from a rearrangement of nanoscale C-S-H particles around limited packing densities of 3 compositionally similar but structurally distinct C-S-H phases: low density (LD), high density (HD) and ultra-high density (UHD). The separation of these phases is based on deconvolution methods applied to indentation modulus and indentation hardness frequency distributions obtained from nanoindentation tests performed on hydrated cement paste. It was stated that creep properties of C-S-H have never been measured directly [2]. Further the role of interlayer water in the creep process was not delineated. Stress relaxation measurements of C-S-H having varied C/S ratios were subsequently reported by the current authors [5]. It was observed that removal of water from interlayer spaces modified the viscoelastic behavior of C-S-H. A sliding mechanism involving the translation of C-S-H layers themselves taking into account the interaction of silica tetrahedral and cations in the interlayer region at various moisture contents was proposed. This mechanism is in contradistinction to that proposed by Vandamme and Ulm [2].

A study was designed to determine the indentation creep behavior of pure C-S-H phases prepared from compacted specimens including synthetic C-S-H, 1.4 nm tobermorite and jennite. Microindentation techniques were used as these systems are monophasic and interference from other phases is avoided. Issues with the relative size of homogenous domains and the interaction volume beneath the indenter

that may arise in an indentation experiment, as well as surface roughness influences, are avoided. Creep measurements on calcium hydroxide, hydrated C_3S and hydrated Portland cement were also included in the study. Hydrated C_3S and hydrated Portland cement paste are, of course, multicomponent systems containing phases other than hydrated silicates. The creep measurements for these materials represent 'composite' behavior and are included for comparison purposes. Attempts at separation of frequency distributions of microindentation parameters, in this context, would of course be meaningless.

The microindentation creep, indentation modulus and indentation hardness results are reported. Insights on the mechanism of creep in cement-based materials are provided. The merits of interpreting creep as a nanogranular-centered phenomenon and the existence of two types of C-S-H based on nanoindentation measurements are debated.

2. Experimental

2.1 Materials

Six cementing systems were prepared including four monophasic materials: synthetic calcium-silicate-hydrate (C-S-H with C/S = 0.6, 0.8, 1.0, 1.2 and 1.5); 1.4 nm tobermorite; jennite; hydrated Portland cement paste (water/cement ratio = 0.40); hydrated C_3S (water/solid ratio = 0.40); reagent grade calcium hydroxide (obtained from Anachemia).

C-S-H: synthetic C-S-H was produced from the pozzolanic reaction between CaO and amorphous silica in excess water (water/solids = 11). Calcium oxide was obtained by calcining reagent grade calcium carbonate at 900°C. Reactive silica (CAB-O-SIL, grade M-5 from Cabot Corporation, USA) was heated at 110°C to remove any surface adsorbed water. Distilled water was de-aired and used for the reactions. All

materials were kept sealed in N_2 purged bottles until they were used. Variation in C/S ratio was achieved by adjusting the stoichiometric amounts of the reactants. The reaction period was 6 months. The material was then filtered and dried under vacuum for 4 days at room temperature. The dried C-S-H was stored in N_2 purged glass vials before the experiments. Characterization of these materials by X-ray diffraction (XRD) and thermal methods gave results directly comparable to C-S-H (I) as reported by Taylor [6].

1.4 nm tobermorite: the reactants (CaO and SiO_2) were prepared as described above. The C/S ratio was 0.9. The reactants were placed in a high density polyethylene bottle mixed in excess deionized water (water/solids = 11) and maintained at 80 °C using a heating wrap. The mixture was continuously agitated with a magnetic stirrer for a period of 4 months. The material was then filtered and dried under vacuum for 4 days at room temperature. The XRD spectrum and TGA curve were similar to those obtained by Yu and Kirkpatrick [7].

Jennite: the reactants (CaO and SiO_2) were prepared as described above. The C/S ratio was 1.4. The reactants were placed in a high density polyethylene bottle mixed in excess deionized water (water/solids = 11) and maintained at 80 °C using a heating wrap. The mixture was continuously agitated with a magnetic stirrer for a period of 4 months. The material was then filtered and dried under vacuum for 4 days at room temperature. The XRD pattern was similar to that obtained by Yu and Kirkpatrick [7], Gard and Taylor [8] and Hara and Inoue [9]. The TGA curve matched that published by Yu and Kirkpatrick [7].

Portland cement paste: The Portland cement paste (made with Type I Portland cement) was prepared using a water/cement ratio of 0.40. Rectangular prisms (250 x 100 x 12 mm) were cast. The samples were vibrated and stored in a moist curing room for 24 h. They were then demoulded and curing was continued for 3 years in a saturated lime solution. Thin slices (1 x 12 x 60 mm) were cut from the paste prism using

an Isomet diamond saw. Selected slices were also ground into a fine powder and passed through sieve No. 100 (nominal opening size of 0.149 mm) for fabrication into compacted specimens.

Hydrated C_3S paste: Tricalcium silicate paste was prepared using a water/solid ratio of 0.40. Specimens with circular cross-section (25 mm in diameter) were cast in glass cylinders. The specimens were demoulded after 24h and sheathed in a rubber membrane containing a few drops of lime saturated water. They were then stored in stoppered glass tubes for 32 years. The use of 32 year old samples assures that the degree of hydration approaches 100%. Slices 1 mm thick were then cut and ground into a fine powder for fabrication into compacted specimens.

2.2 Humidity Conditioning and Environmental Control

Specimens for all six systems were conditioned for several weeks at 11% RH in vacuum desiccators containing saturated lithium chloride solution. The powders were conditioned at 11% RH before compaction and for one week days after compaction. Theoretically there is a monolayer of water on the surfaces of the particles in addition to interlayer water at this humidity. The choice of 11% RH is a particularly significant datum point in the study of porous calcium silicate hydrate systems as the influence of capillary water on mechanical performance can be negated. The effects of 'structural' water can be isolated and controlled by incremental removal of interlayer water from this moisture condition if required. Mechanical properties e.g. modulus of elasticity and hardness are humidity dependent [10]. Modulus of elasticity on first drying is at a maximum value as opposed to hardness which reaches a minimum value at this humidity [11]. The associated mechanisms are discussed in a detailed description of the Feldman-Sereda microstructural model for cement paste.

Precautions were taken to minimize any contamination of the samples due to carbonation. Desiccators were purged with nitrogen gas (in a glove box) prior to conditioning of the samples. The microindentation tester was located within an environmental chamber kept at 11% RH. In general, carbonation is minimized at low humidities. The chamber also contained CO_2 absorbers. Transfer of samples prior to indentation testing took place from the desiccators placed in the chamber. Finally, the samples were periodically checked for any carbonation after testing using TGA methods. Generally, TGA methods indicated that the precautions were satisfactory with little or no carbonation detected.

2.3 Preparation of Compacted Specimens

Solid circular disc samples for all the powdered materials (from the six cementing systems) were prepared by pressure compaction in steel moulds with a cross-section of 25 mm. The thickness of most of the disc samples was nominally 1 mm. Numerous studies on the use and validity of compacts as models for hydrated cement systems have been published [10, 12-15]. It has been shown that compacted specimens of powdered hydrated Portland cement have similar mechanical property-porosity relationships to that of the original hardened paste of the same material [10]. The porosity of compacted samples was determined using helium pycnometry or in the case of the phase pure minerals by calculation using published density values. The calculation is made knowing the apparent volume and the solid volume of the sample. Porosity is varied by controlling the compaction pressure.

2.4 Microindentation measurements

All the microindentation tests were performed using a CSM Instruments Instrumented Indentation Tester. The apparatus is housed in an environmental chamber. All tests were conducted at 11% RH on specimens

equilibrated at 11% RH. Tests were conducted using a Berkovich indenter. The CSM microindentation instrument has a load range of 0.03-30 N with a resolution of 0.3 mN. The rate of loading in the current experiments was 2000 mN/min. The specimens were tested over a wide range of porosity values varying from about 10% to as high as 60%. There were approximately 25 indents on each sample at each porosity level for a total of approximately 125 indents for each material system. The composition of the solid phase for monophasic systems remains constant. Pure materials do not require as many indents as composite materials as phase separation procedures such as the use of deconvolution are not necessary.

The surfaces of C-S-H and cement paste samples were examined by optical microscopy. The indents were obtained at loads of 1 N and 5 N. The 5 N load was chosen to demonstrate that even at a load 5 times higher than what was used in the test program cracking was not an issue. There were no visible cracks (magnification 100x) on the surface of the specimen away from the indentation or at the corners of the indentation as demonstrated in Figure 1. The material shown is a compact of C-S-H (C/S = 1.5) prepared at a porosity of 28%. In addition, the depth of distortion and fracture of the crystals under the apex of an indentation is roughly equivalent to the length of the diagonal of the indentation as previously reported by Sereda in an SEM observation for compacted gypsum samples [16]. Atkins et al. demonstrated for non-porous materials that the depth of the deformed zone is approximately a hemisphere and practically unaffected by the detailed shape of the indentation itself [17]. Applying this conclusion to porous systems the depth to which the microstructure is disturbed at the apex of the indentation should be the radius of the hemisphere of the deformed zone.

The indentation depth was recorded as a function of time at the maximum load of 1000 mN for a 600 s dwell period. The logarithmic creep was determined through curve fitting of the indentation-depth versus time curves during the 600 s dwell time by the following equation:

$$\Delta h(t) = x_1 ln(x_2 t + 1) + x_3 + x_4 \qquad (1)$$

The average penetration depth (h_m) for P_m = 1N is dependent on the C-S-H preparation and porosity level. In general h_m is approximately 10,000 nm or 10 µm. The disturbed volume size is estimated to be approximately 2.09 x 10^3 µm^3 assuming the deformed zone is hemispherical.

The tip calibration involves calculation of the contact area A_c utilizing a polynomial expressed as a function of penetration depth (h). The first term of the polynomial is $A_c = 23.96h^2$. Calibrations are typically conducted with a fused quartz reference sample with known indentation characteristics. Calculations of contact area versus depth of penetration using only the first term of the polynomial (Berkovich indenter) indicate that deviations from the reference are negligible especially if the depth of penetration is greater than 200 nm. Therefore, no further corrections to the calculations were made in this paper.

A logarithmic function as proposed by Vandamme [18] was used to fit the overall creep data obtained from the nanoindentation tests. Vandamme established that the overall error was less than 1%. A similar finding was obtained for all the curves obtained in this study with the overall error being much less than 1%. Two examples are cited: they are typical curves for C-S-H with C/S ratios = 0.80 and 1.20. The logarithmic expressions for the time dependent deformations (Δh(t)) as determined using the CSM Instruments regression analysis software are: Δh(t)= 223.99 ln (0.563t + 1) + 0.951t – 10.471 for C/S = 0.80 and Δh(t) = 150.13 ln (0.956t + 1) – 0.003t -8.419 for C/S = 1.20. The standard error for the x_1 and x_2

parameters in the dominant first term are 0.466 and 0.001 (C/S = 0.80) and 0.420 and 0.027 (C/S = 1.20). The maximum load applied was 1004.52 mN and 1006.66 mN respectively. The goodness of fit is excellent and justifies the use of the creep modulus based on a logarithmic assumption of the experimental creep curve.

The creep modulus, C, is then calculated from: $C = P_{max}/(2a_U x_1)$ where $a_U = [A_c/\pi]^{1/2}$. A_c is the projected area of contact between the indenter probe and the indenter surface. It is determined using the Oliver and Pharr method as a function of the maximum indentation depth [19]. The indentation modulus (M) and indentation hardness (H) were obtained from the software that uses the Oliver and Pharr method. $M = \pi^{1/2}S/ [2\beta(A_c)^{1/2}]$ where $S = dP/dh \mid_{h = hmax}$ is the initial slope of the unloading branch of the P-h curve. P is the maximum indentation load. Indentation hardness, $H = P/A_c$.

The creep modulus parameter was conceived by Vandamme [18]. He argued that the creep behavior reaches no asymptote over time and identified the two functions that capture this behavior: a power function where the modulus is proportional to t^{α} and a logarithmic function where the modulus is proportional to $\ln(t/\tau)$. The power function generally overestimates the creep deformation at large times. The logarithmic function is less accurate at early ages but more precise with respect to the long term creep behavior of concrete. The specimens in this study are essentially fully hydrated cements or phase pure silicates. As such they are more representative of microstructures for mature cement-based materials. Application of the logarithmic function in this case seems appropriate. Vandamme concluded that the observed logarithmic dependence of the time-dependent behavior and the Creep Modulus versus Hardness scaling could be explained by a rearrangement of the C-S-H particles. He further argued that creep may be due to a sliding of the C-S-H particles with respect to each other leading to a rearrangement of collections of C-S-H particles. A sliding mechanism of C-S-H layers has been previously proposed by

Feldman [20] and Alizadeh [5]. The primary difference is that the latter authors include the effects of interlayer water ingress or egress on creep i.e. interlayer water is considered part of the solid C-S-H. The presence of structural water should have a major effect on the translation of the silicate sheets during the creep process as its removal affects the intrinsic properties of the solid itself.

A concern with the definition of creep modulus may be its lack of normalization and the effect of high indentation modulus values on its absolute value. The majority of the materials investigated are calcium-silicate-hydrate phases and should not have a pronounced negative effect on the use of the creep modulus parameter for comparative purposes.

The calculation of a_u was made using a value for the contact area, A_c, obtained using the first term of the polynomial expressing A_c as a function of penetration depth. As indicated the divergence of A_c from a reference sample (as indicated earlier) is considered negligible especially at values of h > 200 nm.

3. Results and Discussion

3.1 Microindentation of calcium-silicate-hydrates

Microindentation measurements and analysis are reported here for several monophasic calcium silicate hydrates including: synthetic C-S-H (C/S = 0.6 to 1.5); 1.4nm tobermorite and jennite. In addition, results for pure calcium hydroxide, cement paste hydrated for 3 years and C_3S hydrated for 32 years were obtained. Microindentation is appropriate for monophasic materials as frequency distribution plots of indentation modulus and indentation hardness are not bimodal and the measurements of these properties represent those of the single phase. Measurements for the hydrated C_3S and Portland cement paste represent average 'composite' values of all the hydrated phases present in these systems. No

deconvolution of frequency plots for the hydrated pastes was attempted as clearly the property values for any individual phase would reflect those of neighboring phases.

Numerous nanoindentation experiments have been conducted on cement pastes and deconvolution techniques have been used to determine the mechanical characteristics of individual phases [3, 4]. These methods have been central to arguments postulating the presence of two types of C-S-H. There is some debate as to the validity of utilizing these techniques and the conclusions that have been drawn from their application. This will be discussed in the ensuing sections of this paper.

Plots of creep modulus versus indentation modulus and indentation hardness for calcium hydroxide, cement paste, hydrated C_3S and C-S-H (C/S = 0.6, 0.8 1.0, 1.2 and 1.5) are presented in Figures 2 and 3 respectively. The plots include published data for C-S-H obtained by nanoindentation techniques involving the use of deconvolution methods [4]. Discussion of the significance of this data will be given later. The data to construct each curve was obtained on compacted specimens described earlier. Compacts for each material were prepared at several different porosities by varying the compaction pressure. The number of microindents is therefore relatively large i.e. up to 125 for each curve considering that the C-S-H materials are monophasic. The required number of indents for nanoindentation measurements in cement paste systems would be much greater, assuming of course that there are no issues regarding the validity of applying deconvolution techniques to frequency diagrams.

It is argued that for pure monophasic materials such as synthetic C-S-H, tobermorite and jennite a bimodal or multimodal frequency distribution of the indentation parameters would not be expected particularly if the peaks are descriptors of the presence of separate phases. It is emphasized that this is not the case for hydrated silicates such as hydrated C_3S and hydrated Portland cement. These silicate systems also contain

substantial amounts of crystalline calcium hydroxide and in the case of the Portland cement system smaller amounts of secondary sulfoaluminate phases. The frequency distributions for these systems would be expected to be multimodal. The microindentation data for these systems provides a 'composite' response as indicated earlier and one cannot differentiate the contribution of separate phases from the results. The intent however is to compare the 'composite' properties of these systems to those of the pure phases. It is noteworthy that the nanoindentation results for C-S-H obtained by Vandamme and Ulm [2] obtained using deconvolution procedures and plotted as creep modulus versus indentation hardness in Figure 3 are coincident with the results directly obtained from microindentation measurements on pure C-S-H in this study.

It is noted that the indentation modulus data for calcium hydroxide reported in the paper ranges from about 10 to 25 GPa. The porosity of the compacted samples ranges from about 10 to 25%. Values of close to 40 GPa reported in the literature were obtained by Beaudoin extrapolating the modulus versus porosity curves to 0 % porosity [21]. Wittman obtained slightly lower values using similar methods [22]. Monteiro and Chang obtained values of 39.7 to 44.9GPa using Brillouin spectra [23]. It is important to emphasize that the literature values represent the modulus of non-porous calcium hydroxide.

The following observations were made in this study. Creep modulus curves are generally linear. Creep modulus as a function of indentation modulus or hardness modulus over the entire range of the argument is ranked in the following order: calcium hydroxide > cement paste > hydrated C_3S > C-S-H. Creep is therefore in the inverse order. It is well known that creep of cement systems is dependent on porosity. Generally creep increases as porosity increases and strength and stiffness decreases. C-S-H is the principle binding phase in cement-based materials. Stiff inclusions such as calcium hydroxide restrain deformation and hence reduce creep. The modulus of elasticity values have been reported to be similar to those of

cement paste for equivalent porosity values [10]. Calcium hydroxide is a layered mineral with some cleavage along the interlayer plane (0001) possible. Nevertheless it creeps less than the other systems studied. Synthetic C-S-H is a layered material. The stress relaxation phenomena associated with C-S-H has been shown to be dependent on humidity and the removal of interlayer water from the 11% RH condition [5]. It was argued that the removal of this interlayer water is itself associated with the translation of the silicate sheets of the C-S-H nanostructure when the latter is subjected to sustained stress. This is contrary to the postulates advanced by Vandamme and Ulm based on interpretation of nanoindentation creep data [2]. These workers ascribe the origin of creep to translation of nanogranular particulates.

The nanoindentation creep data for C-S-H (in cement paste) obtained by Vandamme and Ulm [2] are approximately co-linear with the microindentation data obtained in this study (Figures 2 and 3). Their data lies in a lower porosity region at higher values of indentation modulus and indentation hardness. Porosity appears to be the only distinguishing feature between the microhardness and nanohardness data. This is porosity that in both sets of data is accessible to helium differing only in size distribution. Higher compaction pressures would likely extend the microhardness data into the nanohardness data region. The advantage working with compacts of monophasic materials is that the porosity effect can be clearly established. The possibility that there is a distinction between low density (LD) C-S-H and high density (HD) C-S-H or that two types of C-S-H exist may be artificial.

The pore structures of C-S-H, tobermorite and jennite samples were characterized using nitrogen adsorption methods. The pore size distributions indicated that about 97% of the pore space contained pores with diameters less than 0.10 μm. The pore size distributions for all the C-S-H samples had a sharp peak of medium intensity at 20×10^{-4} μm and a large broad peak between 30×10^{-4} μm and 400×10^{-4} μm. The distribution for tobermorite had a large sharp peak at about 20×10^{-4} μm and a large broad peak

between 25 x 10^{-4} μm and 200 x 10^{-4} μm. The jennite distribution was similar except the second peak was very small. The pore size distribution for cement paste exhibited primarily a large sharp peak at 20 x 10^{-4} μm. The estimated volume size of the disturbed zone beneath the microindenter was 2.09 x 10^{3} μm^3.

The effect of porosity on micro and nanoindentation measurements is not surprising as the porosity dependence curves for creep modulus, indentation modulus and indentation hardness are similar for all the systems studied. The plots in Figure 4(a), (b), (c) respectively illustrate the dependence of indentation modulus, indentation hardness and creep modulus, on porosity for C-S-H, cement paste and hydrated C_3S. The creep modulus data for cement paste and hydrated C_3S appear to be along the upper bound of the data sets. It is apparent that in general low values of C/S ratio correspond to low values of the indentation parameters. This appears to be in contradiction to previously reported results obtained using DMA methods [24].

A possible argument for this discrepancy is as follows. The microindentation test is actually not 'non-destructive' on a micro-scale considering the microstructural disturbance of the area under the indenter. It has been reported previously [16] that the mechanisms responsible for the humidity dependence of elastic stiffening and microhardness of hydrated cement are different. That being the case the stress field below the indenter may influence the failure mechanism of the particles in the disturbed zone. E is influenced to a greater extent by the structural role of interlayer water. In a 'destructive' test the stiffness may be influenced by both the structural role of interlayer water and the fracture of Si-O bonds. The population of Si-O bonds is greater in the C-S-H with a higher degree of polymerization i.e. low C/S ratio. Perhaps this is the reason low C/S ratio systems are weaker in a microindentation test. It could also explain why creep modulus is lower (i.e. higher creep) when C/S ratio is lower! In other words the results may be test method dependent and reflect the extent to which a test is truly non-destructive.

Models for the nanostructure of C-S-H in hydrated cement paste where the structural units consist of 1.4 nm tobermorite and jennite-like elements have recently been advanced [25]. It is instructive to examine the creep modulus functions for these pure phases (Figures 5, 6). The creep modulus versus indentation modulus curves for 1.4 nm tobermorite and jennite are similar with the curve for jennite being slightly higher. Both curves lie between the curves for hydrated C_3S and synthetic C-S-H (C/S = 1.2). Differences between the creep modulus curves for 1.4 nm tobermorite and jennite are more pronounced when plotted against indentation hardness. The jennite curve is actually closer to the hydrated cement paste curve and the curve for 1.4 nm tobermorite lies between the curves for hydrated C_3S and synthetic C-S-H. The proximity of the curves for 1.4 nm tobermorite and jennite to those of hydrated cement paste and synthetic C-S-H provide support that structural models for cement paste based on these hydrated silicates have credence.

The creep modulus data for all the C-S-H preparations (C/S = 0.6, 0.8, 1.0, 1.2 and 1.5) is plotted in Figures 6 and 7. The creep modulus versus indentation modulus and indentation hardness data for all C/S ratios except C/S = 0.6 are closely nested on a single curve. The data for C-S-H with C/S ratio = 0.6 lies above the other data. The difference is greater for the indentation modulus curve. The lower creep for this C/S ratio preparation may be due to the greater degree of polymerization with a fewer number of surface defects.

3.2 Significance of porosity and density determinations

It is instructive to examine the implications of porosity and density determinations not only on creep indentation measurements but on the broader question of the existence of two types of C-S-H postulated from nanoindentation experiments on cement paste [26]. Porosity calculations for bottle hydrated cement and d-dried hydrated cement paste using three different fluids-helium, methanol and saturated

lime solution are useful for this purpose [27]. Helium-based density values for the bottle-hydrated cement conditioned to 11% RH were determined using the instantaneous solid volume or this value corrected for: the monolayer volume; the space detected by the time-dependent flow of helium or the presence of interlayer water in the space detected by helium flow assigning a density of 1.25 g/cm^3 to the interlayer water. Density values ranged from 2.30 to 2.37 g/cm^3 with the highest value obtained by taking into account the helium flow. Methanol-based density values taking into account similar corrections ranged from 2.25 to 2.32 g/cm^3. Corresponding values for density determinations using lime-saturated water were slightly higher and ranged from 2.35 to 2.39 g/cm^3. Density values determined in the 'D-dry' state utilizing helium, methanol and lime-saturated water were 2.28, 2.28, and 2.61 g/cm^3 respectively. It is important to comment that the value of 2.61 g/cm^3 represents the density of the silicate sheets in the C-S-H structure as the calculation considers the space occupied by the 'interlayer' water as pore space. This invalidates the use of water as a displacement fluid for both porosity and density determinations when the hydrated cement specimens are in the dry state. This is due to the fact that interlayer water is considered part of the solid structure and as such contributes to the solid volume in a density calculation.

Density values of D-dried cement paste using helium as a displacement fluid range from 2.19 g/cm^3 for w/c = 0.40 to 2.30 g/cm^3 for w/c = 0.30. Use of methanol gives a value of 2.27 g/cm^3. Water gives higher density values of 2.64 to 2.66 g/cm^3. Density values of 2.60 g/cm^3 were reported for C-S-H by Allen and co-workers using small angle neutron scattering (SANS) techniques [28]. A density value of 2.56 g/cm^3 obtained by Pellenq et al. [29] obtained using atomistic modeling methods has been cited as validation of the estimates provided by SANS experiments. It appears however that the density value obtained by modeling was in error. The cell parameter 'a' should be half of that cited. Corrections to the cell descriptors including the number of resident water molecules results in an estimated density value of 2.33 g/cm^3 [30]. It would appear then that atomistic modeling would in fact validate density values obtained

by pycnometric methods and not the SANS value. Clearly these values represent the density of the individual silicate sheets themselves. Published values for the density of pure C-S-H phases based on crystallographic determinations for C-S-H (I), 1.4 nm tobermorite and jennite are 2.25-2.35, 2.23 to 2.28 and 2.33 g/cm^3 respectively [6]. These values are very similar to those measured experimentally for hydrated cement conditioned to 11% RH using helium, methanol and water as displacement fluids and density values determined on D-dried cement using helium and methanol as displacement fluids. It is further suggested that any porosity not detected by helium and methanol would be at a minimum as the close correspondence of the density values determined by pycnometric methods and those determined by crystallographic determinations is noteworthy.

3.3 C-S-H: a nanogranular material?

The engineering behavior of C-S-H has been described by Jennings and co-workers as nanogranular in nature [31]. It is apparent that the significance of the packing factors (that are central to arguments for nanogranular behavior) as calculated by Jennings and co-workers needs to be reinterpreted as 'interlayer' water comprises a significant portion of the so-called 'porosity' inherent in the concept. It is difficult to visualize 'structural' water as part of a model for C-S-H described in terms of compaction factors.

The packing density was determined from the following equations described in reference [23].

$\eta_{sat} = 1- (\rho_{sat}-\rho_{dry)/} \rho_w$ (1)

where: ρ_{sat} and ρ_{dry} are in this case the wet and dry C-S-H density values.

$\eta_{dry} = \rho_{dry}/\rho_s$ (2)

where: ρ_w and ρ_s are the mass density of the saturating fluid phase (water) and the particle

$\eta = ½ (\eta_{sat} + \eta_{dry})$ (3)

Substitition shows that $\eta_{sat} = 1 – [(M_s + M_w)/V- M_s/V)] =1 – M_w/V = 1 –$ porosity (as determined by water). V = volume of solid + volume of voids (or water); V_s = volume of solid; M_s = mass of solid; M_w = mass of water

$\eta = V_s/V = 1 –$ porosity (4)

It is clear that these authors have used the equivalent of water porosity to calculate the packing factor. This kind of calculation assumes that interlayer water is equivalent to pore water which is erroneous. Porosity and density measurement are discussed further in the note that follows.

The numerical values of the limit packing densities (random packing (64%) and ordered face-centred cubic or close packed (74%)) corresponding to the so-called LD and HD C-S-H are a cornerstone of the arguments for the validity of colloidal models for the nanostructure of hydrated cement and the 'nanogranular' behavior of the hydrated cement solids [32]. They are also central to arguments interpreting nanoindentation data (i.e. frequency distributions of indentation modulus and hardness) as supporting the existence of two types of C-S-H [33]. Packing factor estimates based on solid densities determined using water as a displacement fluid are misleading as solid volumes cannot be correctly determined in this manner. These results using arguments based on packing factor determined in this manner are at best fortuitous.

It is relevant to examine porosity values for a cement paste (w/c = 0.40) hydrated for 3 years. Feldman obtained a porosity value of 37.8% using water as a displacement fluid [27]. This is comparable to the value of 36% calculated by Jennings for what he terms as LD-C-S-H [33]. It is readily apparent that there is

very little if any capillary pore space at this w/c ratio. It is also clear that Jennings calculations are based on water residing in all the 'pores' of the LD-C-S-H. These of course would include the 'interlayer' spaces making it difficult to provide a valid assessment of the true density of the C-S-H. Direct determination of porosity at higher w/c values gives of course higher values as the amount of 'capillary' pore space increases.

3.4 Two types of C-S-H?

Plots of creep modulus versus indentation modulus and indentation hardness including our results (microindentation of monophasic C-S-H compacts) and those of Vandamme and Ulm (nanoindentation) [2] can be considered to be co-linear. The data points attributed to this work were obtained by varying the porosity of the system by compacting the C-S-H powders. Lower porosities could be obtained at very high compaction pressures with data points extending into the region of the Vandamme and Ulm results. This suggests that the latter are not necessarily representative of two types of C-S-H. The conformance of the directly determined density values (using pycnometric methods) of C-S-H with those calculated from crystallographic data suggests that fundamentally the C-S-H if present in more than one form in cement paste (i.e. variable C/S ratio) is compositionally similar as density variation is small. Cement paste with w/c << 0.40 likely does contain small gel pores due to the imperfect consolidation of layers. Regions of variable pore size distribution in low w/c pastes may exist due to space constraints for the deposition of hydration products. A greater concentration of clinker grains (potential sites for inner product formation) also exists. Product formation in these two scenarios could account for two types of C-S-H. These phases, however, would be distinguished only by porosity differences. However, these would not necessarily produce a bimodal distribution (of nanoindentation parameters) reflective of the contribution of two types of C-S-H.

It has been reported that during the hydration of C_3S generally two distinct calcium silicate hydrate gels are formed [34, 35]. These are referred to as 'inner' and 'outer' product C-S-H. Inner product C-S-H forms within the boundary of the original particles and outer product forms within originally water-filled space. TEM microanalysis conducted by Richardson and Groves [36] indicates that inner and outer product C-S-H differs in morphology but not substantially in Ca/Si ratio [36]. This was confirmed by Taylor and Newbury in their X-ray area scans of a 23 year old paste (w/c = 0.45) [37]. The 'denser' inner product may have lower levels of porosity. Nevertheless, this porosity is readily detectable by helium pycnometry. The compositional similarity and density of the 'inner' product C-S-H (either measured or calculated i.e. crystallographic is similar to the value for 'outer' product C-S-H as indicated in this work. Other than the morphology distinction it is essentially the same C-S-H. From a nanoindentation perspective differences in the indentation parameters arising from two different types of C-S-H would be detected only if a distinct and significant zone of influence under the indenter could be distinguished; this has yet to be proven. It would appear unlikely that two types of 'uniformly-dispersed' C-S-H exist. Further in a mature paste the bulk of the hydrates represent the 'outer' product. It is clear from this study that the dependence of the indentation parameters on porosity covers a wide range of porosity representing a *continuum of pore sizes* and does not necessarily infer the existence of two types of C-S-H with specific compaction factors.

It is emphasized that the microindentation data for cement paste or hydrated C_3S cannot be used to distinguish the presence of LD C-S-H or HD C-S-H due to the large size of the volume indented. Rather the data represent a 'composite' effect that includes the influence of secondary phases e.g. calcium hydroxide, sulfoalumunates and residual clinker grains. This issue is not a factor for the monophasic C-S-H materials and related minerals. It is felt that it is meaningful to compare the composite behavior of hydrated cement (real systems) with that of pure C-S-H phases. It is noted from the discussion above and the likely presence of C-S-H/CH nanocomposite systems (i.e. intimate mixtures of nano-sized C-S-H and

nano-sized CH) in cement paste that results obtained from nanoindentation tests may possibly be challenged and at the very least may require further validation.

3.5 Commentary on the significance of nanoindentation measurements

The work of Trtik et al. and Lura et al. is especially relevant for the interpretation of nanoindentation experiments on cement paste as it relates to the postulation of two types of C-S-H [38, 39]. They question the notion that multi-peak signatures in statistical nanoindentation experiments can be explained only by the presence of two distinct C-S-H phases. Their results indicate that the homogenous C-S-H regions in cement paste are too small to cause independent and separated peaks in the elastic modulus plots. They argue that spurious peaks in the frequency plots can be produced by the presence of other phases including unhydrated cement and calcium hydroxide. This view has been challenged by Ulm et al. [40]. They cite energy dispersive spectroscopy studies [41] of paste regions having a similar size to the interaction volume beneath a nanoindenter. They state that hydration phases in cement pastes constitute compositionally homogenous regions larger than a few microns. It is noted, however, that the main conclusion of reference [41] is that the nanoindentation response is almost always a 'composite' response of C-S-H and CH in apparent contradiction to the arguments advanced in reference [40]. Ulm et al. also cite a range of Si/Ca ratios, $0.4 < Si/Ca < 0.8$ as representing the composition variation of 'pure' C-S-H in 'real' cement pastes. A difficulty with their analysis as it relates to the nanoindentation measurements is the low water/cement ratio of the samples i.e. 0.30. These pastes contain a very high concentration of clinker phases. Chen et al. even by eliminating zones with residual clinker in low water/cement ratio paste observed a composite response of C-S-H and CH [41]. The regions represented can therefore not be considered as homogenous regions of C-S-H. The size of 'real' homogenous regions would therefore be uncertain at least on the basis of their analysis. Further statements (based on the information presented

in reference [29]) that the molecular properties of C-S-H in cement paste are well known are inconsistent with established observations of the nanostructure of C-S-H (in cement paste) that relate to the amount of monomer and the absence of both Ca-OH bonds and a basal-spacing [30]. Richardson has emphasized the importance and utility of proper crystal-chemical and geometrical reasoning in structural studies [42]. He notes that in the Pellenq model a large proportion of the Ca-O distances are either shorter than the minimum calculated from known structures of calcium-silicate-hydrates or longer than the maximum distance and that more than half of the Ca atoms are coordinated to fewer than six O atoms. Six and sevenfold are the natural coordination states for these phases.

The Swiss workers draw attention to the controversy re. the existence of two nanogranular C-S-H phases in cement paste and argue that the nanogranular position is in conflict with the results produced by low-dose cryo-transmission electron microscopy and limited dose electron diffraction which concludes that the C-S-H shows a sheet-like structure [43]. They also point out that surface roughness estimates for cement paste specimens based on Focused Ion Beam (FIB)-nanotomography (on the scale relevant to nanoindentation) in which 3D images are obtained using a marching object sampled over a large number of positions cannot be lower than several hundred nanometers casting doubts on the validity of test results with the maximum indentation depths of the same order of magnitude. They demonstrated using virtual micromechanical experiments that depending on the respective sizes of the homogenous domains and the interaction volume peaks may appear in the elastic modulus histogram that do not correspond to the stiffness of any of the phases present in the microstructure. Their composite modeling “appears to substantiate the assumption that random peaks in the elastic modulus frequency plots may be generated by the distribution of the phases rather than indicating the presence of a phase with a specific elastic modulus within the region of the peak”. They propose that the HD peak could be a spurious peak due to the presence of other phases, namely unhydrated cement, CH and other crystalline hydration products

within the influence volumes of the indenter. In addition, they suggest a possible solution for using a statistical grid indentation technique may be the reduction of surface roughness by constructing artificial systems such as special compacts of hydration products. The compact specimens used in the current study had maximum asperity heights of 100 nm as determined using AFM methods. The compacts are also comprised (with the exception of cement paste and hydrated C_3S) of monophasic pure systems. The limitations inherent in the application of nano-indentation methods to cement paste are not a factor in this system when microindentation methods are used. Trtik et al. also draw attention to the requirement that the linear size of homogenous domains of a single phase needs to be larger than about 3 μm given a maximum indentation depth of about 300 nm. Hardly any such regions of C-S-H exist in the microstructure of C-S-H in cement paste.

4. Conclusions

1. Microindentation is a useful method for determining the creep behavior of monophasic calcium-silicate-hydrates.
2. Compacted powders are useful models for studying the indentation creep of calcium silicates and minimizing surface roughness effects.
3. Creep of pure C-S-H phases is greater than the creep of hydrated cement paste or hydrated C_3S due to the restraining effect of calcium hydroxide and clinker phase in the paste.
4. The C/S ratio of the C-S-H preparations studied appeared to influence the three microindentation parameters. In general lower C/S ratio preparations have lower values of creep modulus, indentation modulus and indentation hardness. The preparation with C/S = 0.6 had the lowest creep modulus or highest creep possibly due to the high degree of polymerization and low number of defects.

5. Creep of 1.4nm tobermorite and jennite is generally less than that for synthetic C-S-H and greater than the creep of hydrated cement paste or hydrated C_3S.
6. Nanostructural models of C-S-H comprised of 1.4nm tobermorite and jennite structural units are compatible with the indentation creep observations made in this study.
7. Creep data for C-S-H obtained from micro and nanoindentation measurements is co-linear. The porosity dependence of the creep measurements is similar for both scales.
8. The linear porosity dependence of indentation creep over a wide porosity range and the convergence of pycnometric density determinations with crystallographic determinations supports the view that only one type of C-S-H is present. This is in agreement with the findings of Trtik et al. who have questioned the interpretation of frequency diagrams for indentation modulus and indentation hardness and hence the existence of two types of C-S-H.

5. References

1. A.M. Neville, Creep of concrete: plain, reinforced and prestressed, North Holland Pub. Co., pp. 622, 1970.
2. M. Vandamme and F.-J. Ulm, Nanogranular origin of creep, Proc. Nat. Acad. Sci. (USA), 106 (26), 10552-10557, 2009.
3. G. Constantinedes, F.-J. Ulm and K. Van Vliet, On the use of nanoindentation for cementitious materials, Mater. And Struct., 36, 191-196, 2003.
4. M. Vandamme, F.-J. Ulm and P. Fonollosa, Nanogranular packing of C-S-H at substochiometric conditions, Cem. Concr. Res., 40, 14-26, 2010.
5. R. Alizadeh, J. J. Beaudoin and L. Raki, Viscoelastic nature of calcium silicate hydrate, Cem. Concr. Comp., 32, 369-376, 2010.

6. H.F.W. Taylor, Proposed structure for Calcium Silicate Hydrate Gel, J. Amer. Ceram. Soc. 69, (6), 464-467, 1986.

7. P. Yu and R.J. Kirkpatrick, Thermal dehydration of tobermorite and jennite, Concr. Sci. and Eng., 1, 185-191, 1999.

8. J. A. Gard and H. F.W. Taylor, Calcium silicate hydrate (II) ("C-S-H(II)", Cem. Concr. Res., 6, 667-678, 1976.

9. N. Hara and N. Inoue, Formation of jennite from fumed silica, Cem. Concr. Res., 10, 677-682, 1980.

10. P.J. Sereda, R.F. Feldman and E.G. Swenson, Effect of sorbed water on some mechanical properties of hydrated Portland cement pastes and compacts, Highway Research Board, Special Report 90, 58-73, 1966.

11. R.F. Feldman, Sorption and length change isotherms of methanol and water on hydrated Portland cement, Proc., V Int. Symp. Chem. Cem., Tokyo, Vol. 3, 53-66, 1968.

12. I. Soroka and P.J Sereda, The structure of cement- stone and use of compacts as structural models, Proc. 5th Int. Symp. on the Chem. of Cem., Vol. 3., Tokyo, 67-73,1968.

13. R.F. Feldman, Factors affecting the Young's modulus-porosity relation of hydrated Portland cement compacts, Cem. Concr. Res., 2(4), 375-386, 1972.

14. P.J. Sereda and R. F.Feldman, Compacts of powdered material as porous bodies for use in sorption studies, J. Appl. Chem., 13, 150-158, 1963.

15. J.J. Beaudoin, Comparison of mechanical properties of compacted calcium hydroxide and Portland cement paste systems, Cem. Concr. Res., 13, 319-324, 1983.

16. P.J. Sereda, Significance of microhardness of porous inorganic materials, Cem. Concr. Res., 2, 717-729, 1972.

17. A.G. Atkins, A. Silverio and D. Tabor, Indentation hardness and the creep of solids, J. Inst.Metals, 94, 369-378, 1966.

18. M. Vandamme, The nanogranular origin of concrete creep: A nanoindentation investigation of Microstructure and fundamental properties of calcium-silicate- hydrates, PhD thesis, MIT, pp.366, 2008.

19. W.C. Oliver and G.M. Pharr, An improved technique for determining hardness and elastic modulus using load and displacement sensing indentation experiments, J. Mater. Res.7, 1564-1583, 1992.

20. R.F. Feldman, Mechanism of creep of hydrated Portland cement paste, Cem. Concr. Res., 2(5), 521-540, 1972.

21. J.J. Beaudoin, Comparison of mechanical properties of compacted calcium hydroxide and Portland cement paste systems, Cem. Concr. Res., 13, 319-324, 1983.

22. F.H. Wittmann, Estimation of the modulus of elasticity of calcium hydroxide, Cem. Concr. Res., 16,971-972, 1986.

23. P.J.M. Monteiro and C.T. Chang, The elastic moduli of calcium hydroxide, Cem. Concr. Res., 25(8), 1605-1609, 1995.

24. R. Alizadeh., J.J. Beaudoin and L. Raki, Mechanical properties of calcium-silicate-hydrates, Mat. and Sruct., 44, 13-28, 2011.

25. I. Richardson and G.W. Groves, Models for the composition and structure of calcium silicate hydrate (C-S-H) gel in hardened tricalcium silicate pastes, Cem. Concr. Res., 22, 1001-1010, 1992.

26. H. M. Jennings, A model for the microstructure of calcium silicate hydrate in cement paste, Cem. Concr. Res., 30, 101-116, 2000.

27. R.F. Feldman, Density and porosity studies of hydrated Portland cement, 3(1), 5-14, 1972.

28. A.J. Allen, R.C. Oberthur, D. Pearson, P. Schofield and C.R. Wilding, Development of the fine porosity and gel structure of hydrating cement systems, Philosophical Mag. B, 56 (3), 263-288, 1987.

29. J.-M. Pellenq, A. Kushima, R. Shahsavari, K. J. Van Vliet, M. J. Buehler, S. Vip and F.-J. Ulm, A realistic molecular model of cement hydrates, Proc. Natl. Acad. Sci., USA, 106, 16102-16107, 2009.

30. I. G. Richardson, Problems with a 'realistic' model for the binding phase in concrete, private communication (to J. J. Beaudoin), Nov. 31, 2009.

31. H.M. Jennings, Refinements to colloidal model of C-S-H in cement: CM-II, Cem. Concr. Res. 38, 275-289, 2008.

32. F.-J. Ulm, M. Vandamme, C. Bobko and J.A. Ortega, Statistical indentation for hydrated nanocomposites: Concrete, bone and shale, J. Amer. Ceram. Soc. 90[9], 2677- 2692, 2007.

33. H.M. Jennings, J.J. Thomas, J. S. Gevrenov, G. Constantinides and F.-J. Ulm, A multi-technique investigation of the nanoporosity of cement paste, Cem. Concr. Res., 37, 329-336, 2007.

34. G.W. Groves, P.J. Le Sueur and W. Sinclair, J. Amer. Ceram. Soc., 69, 353, 1986. Transmission electron microscopy and microanalytical studies of ion-beam-thinned Sections of tricalcium silicate paste, J. Amer. Ceram. Soc., 69(4), 353-356, 1986.

35. S. Diamond, Cement paste microstructure- an overview at several levels, Hydraulic cement pastes, Proc. Conf., University of Sheffield, Cement and Concrete Association, 2-30, April, 1976.

36. I.G. Richardson and G.W. Groves, Microstructure and microanalysis of hardened ordinary Portland cement pastes, J. Matls. Sci., 28, 265-277, 1993.

37. H.F.W. Taylor and D.E. Newbury, An electron microprobe study of a mature cement paste, Cem. Concr. Res., 14, 565-573, 1984.

38. P. Trtik, B. Munch and P. Lura, A critical examination of statistical nanoindentation on model materials and hardened cement pastes based on virtual experiments, Cem. Concr. Comp., 31, 705-714, 2009.

39. P. Lura, P. Trtik and B. Munch, Validity of recent approaches for statistical nanoindentation of cement pastes, Cem. Concr. Comp., 33, 457-465, 2011.

40. F.-J. Ulm, M. Vandamme, H.M. Jennings, J. Vanzo, M. Bentivegna, K. J. Krakowiak, G. Constantinides, C.P. Bobko, K.J. Van Vliet, Does microstructure matter for Statistical nanoindentation techniques?, Cem. Cn. Comp., 32, 92-99, 2010.

41. J.J. Chen, L. Sorelli, M. Vandamme, F.-J. Ulm and G. Chanvillard, coupled grid-indentation/SEM-EDX study on low water/cement ratio Portland cement paste: evidence for C-S-H/CH nanocomposites, J. Amer. Ceram. Soc., 93, 1484-1493, 2010.

42. I.G. Richardson, The importance of proper crystal-chemical and geometrical reasoning demonstrated using layered single and double hydroxides, Acta Crystallographica, Sec. B, 69, 150-162, 2013.

43. C. Roβler and J. Stark, Limited-dose electron microscopy reveals the crystallinity of fibrous C-S-H phases, J. Amer. Ceram. Soc., 89(2), 627-632, 2006.

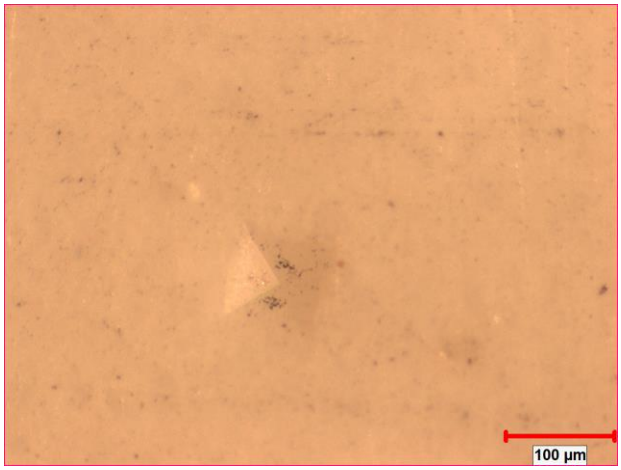

Figure 1: Optical photo of an indent obtained with the Berkovich indenter. C-S-H specimen (C/S =1.5) loaded at 5 N. Magnification 100x.

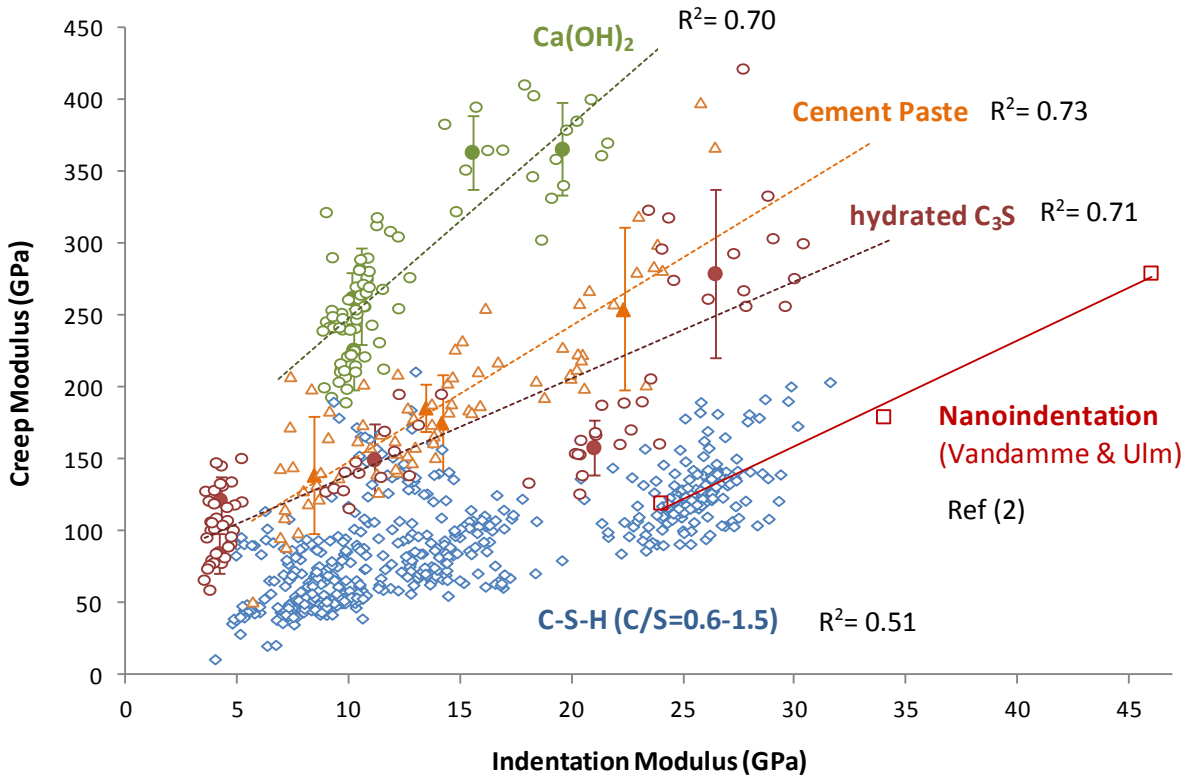

Figure 2: Creep modulus versus indentation modulus: calcium hydroxide; cement paste; hydrated C_3S; C-S-H (C/S = 0.6, 0.8, 1.0, 1.2, and 1.5).The solid markers represent the mean values for a cluster of data points obtained on compacts prepared at a given compaction pressure. The error bars indicate one standard deviation from the mean.

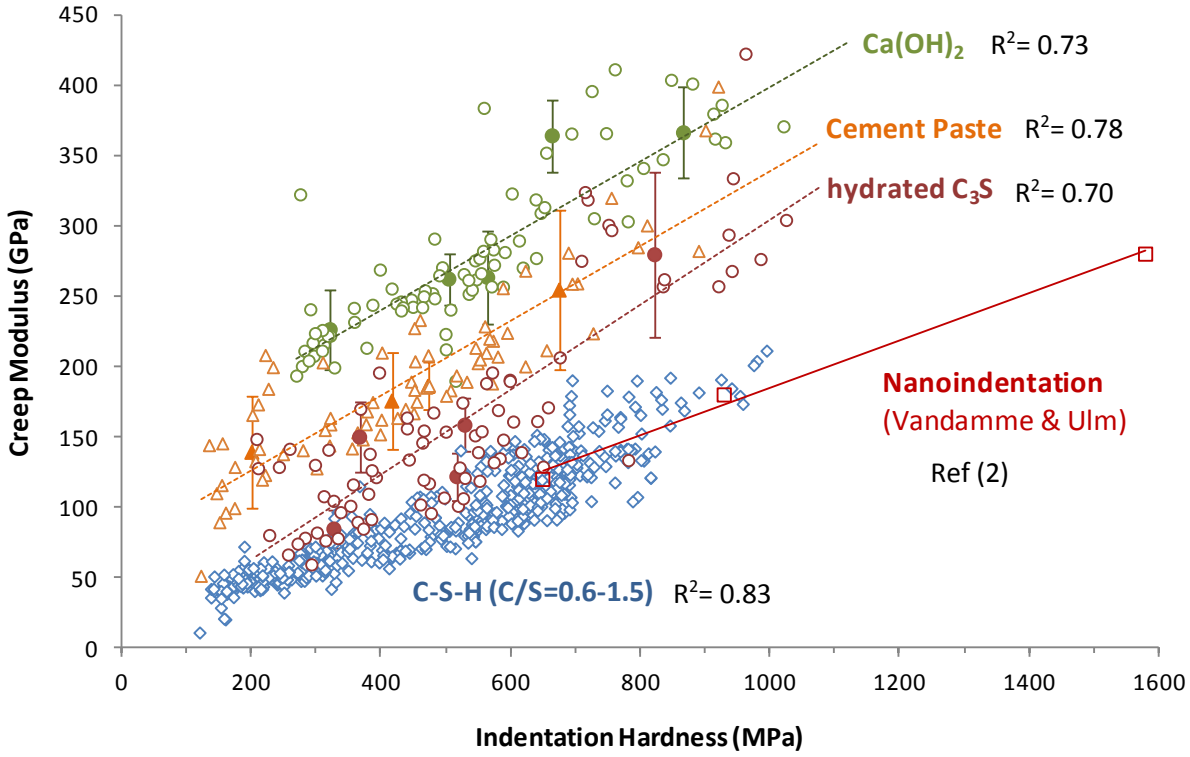

Figure 3: Creep modulus versus indentation hardness: calcium hydroxide; cement paste; hydrated C_3S; C-S-H (C/S = 0.6, 0.8, 1.0, 1.2, and 1.5). The solid markers represent the mean values for a cluster of data points obtained on compacts prepared at a given compaction pressure. The error bars indicate one standard deviation from the mean.

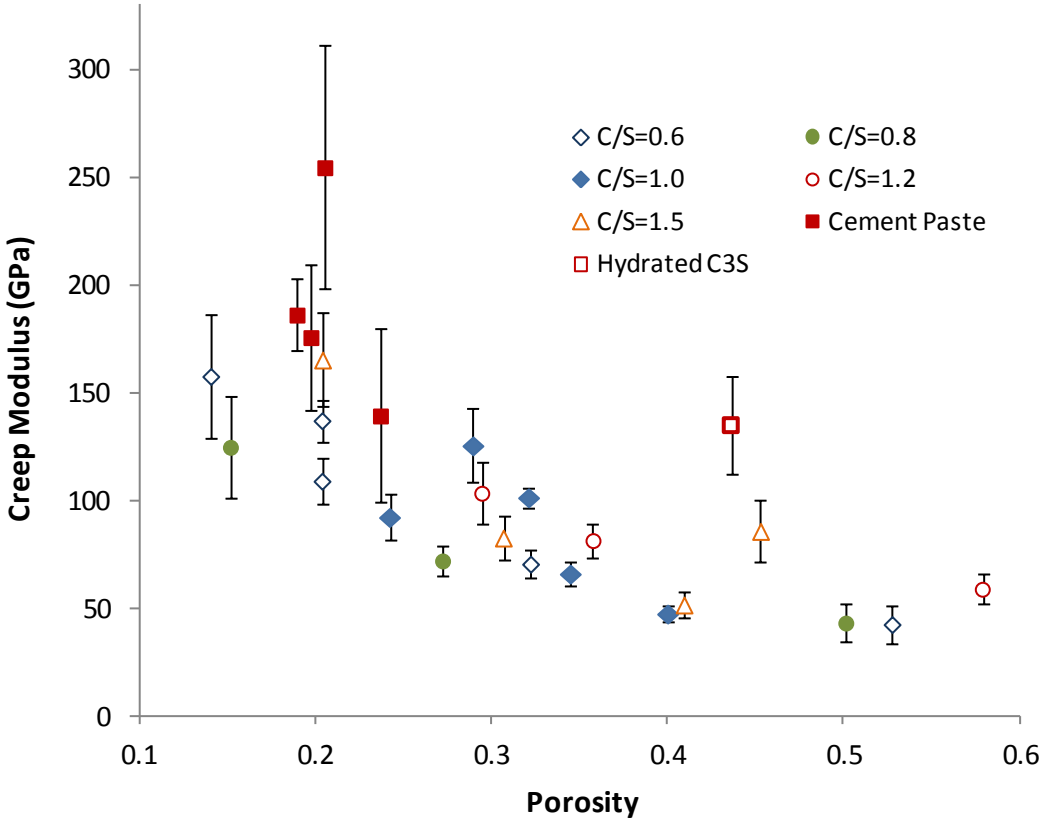

Figure 4.a: Creep modulus versus porosity: C-S-H (C/S = 0.6, 0.8, 1.0, 1.2, and 1.5); cement paste; hydrated C_3S.

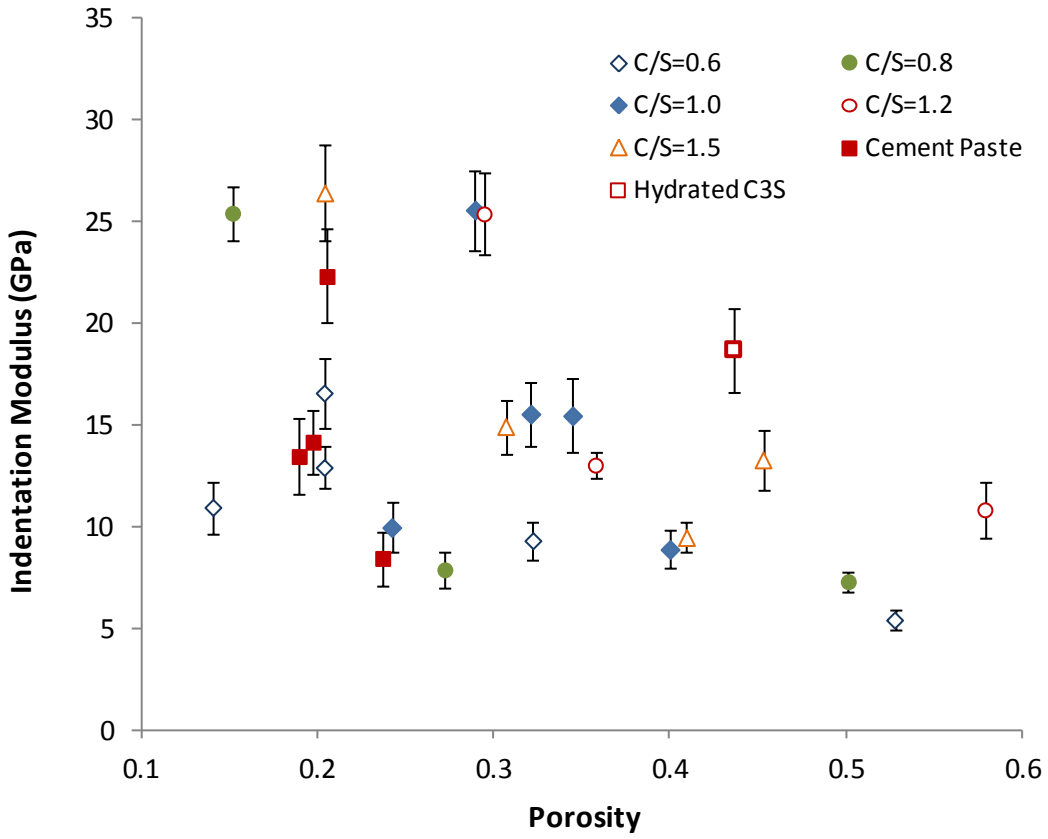

Figure 4.b: Indentation modulus versus porosity: C-S-H (C/S = 0.6, 0.8, 1.0, 1.2, and 1.5); cement paste; hydrated C_3S.

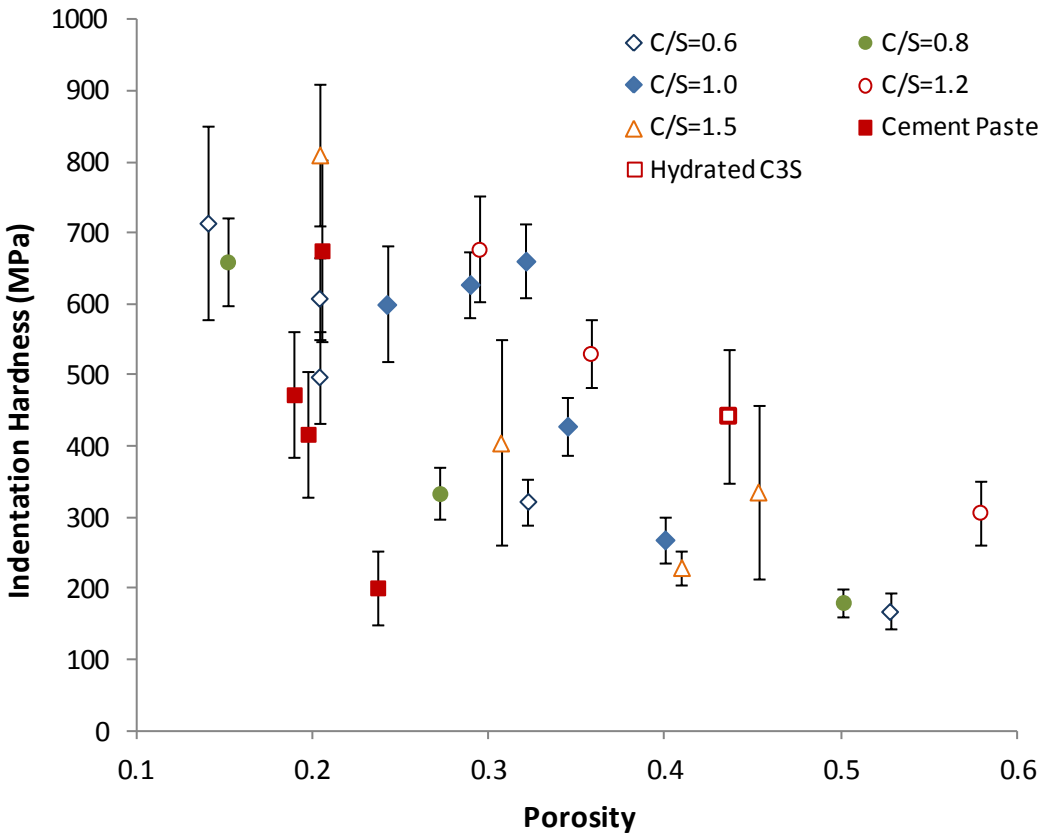

Figure 4.c: Indentation hardness versus porosity: C-S-H (C/S = 0.6, 0.8, 1.0, 1.2, and 1.5); cement paste; hydrated C_3S.

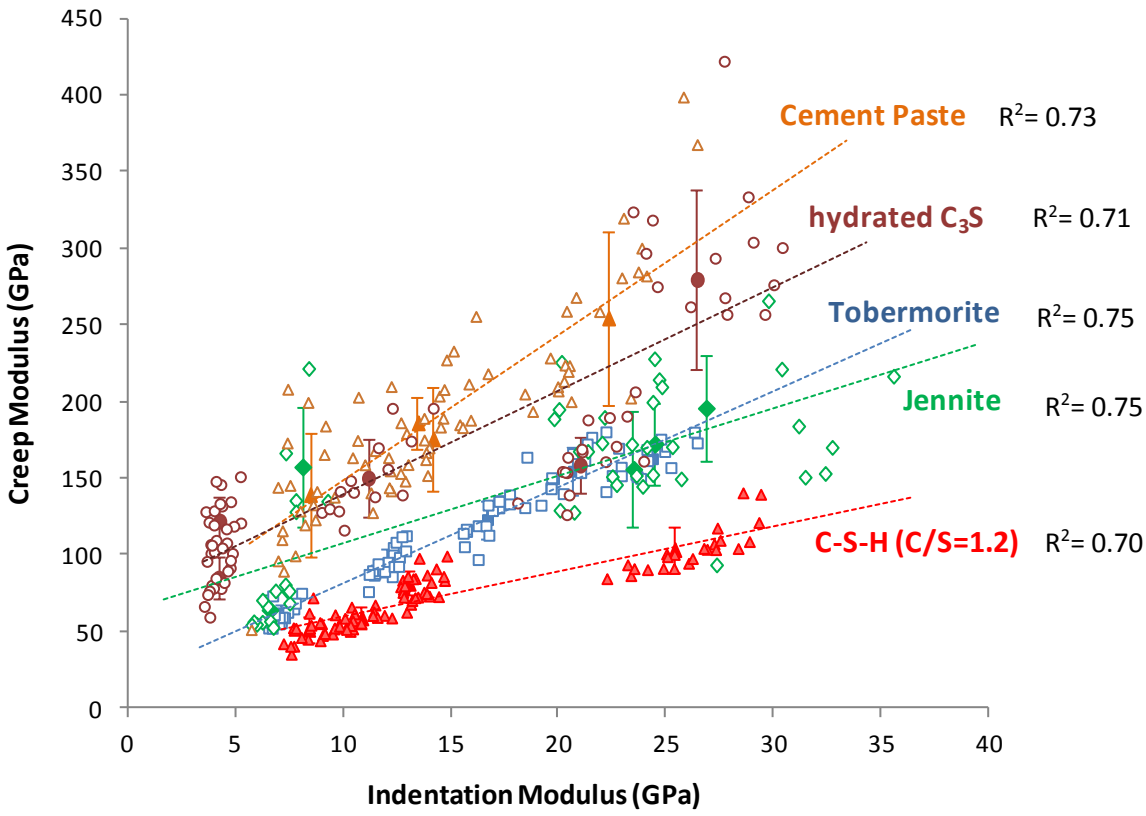

Figure 5: Creep modulus versus indentation modulus: 1.4 nm tobermorite; jennite; cement paste; hydrated C_3S; C-S-H (C/S = 1.2). The solid markers represent the mean values for a cluster of data points obtained on compacts prepared at a given compaction pressure. The error bars indicate one standard deviation from the mean.

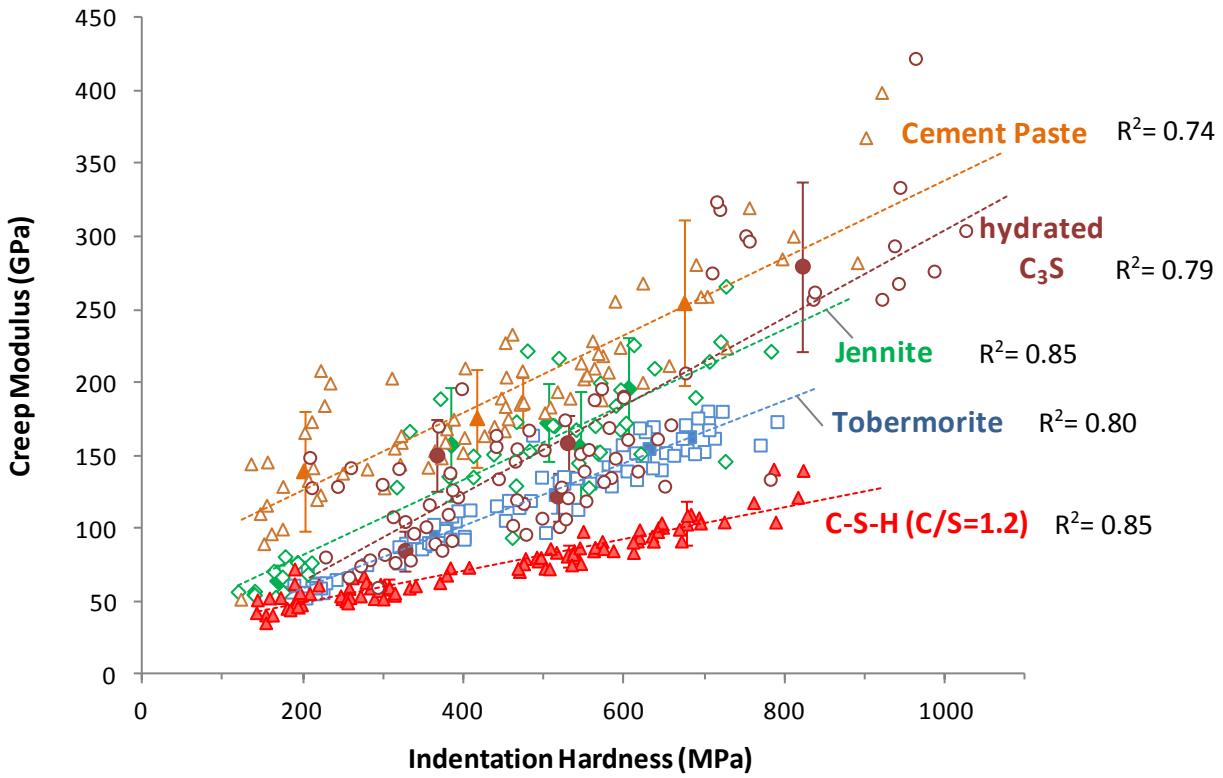

Figure 6. Creep modulus versus indentation hardness: 1.4 nm tobermorite; jennite; cement paste; hydrated C_3S; C-S-H (C/S = 1.2). The solid markers represent the mean values for a cluster of data points obtained on compacts prepared at a given compaction pressure. The error bars indicate one standard deviation from the mean.

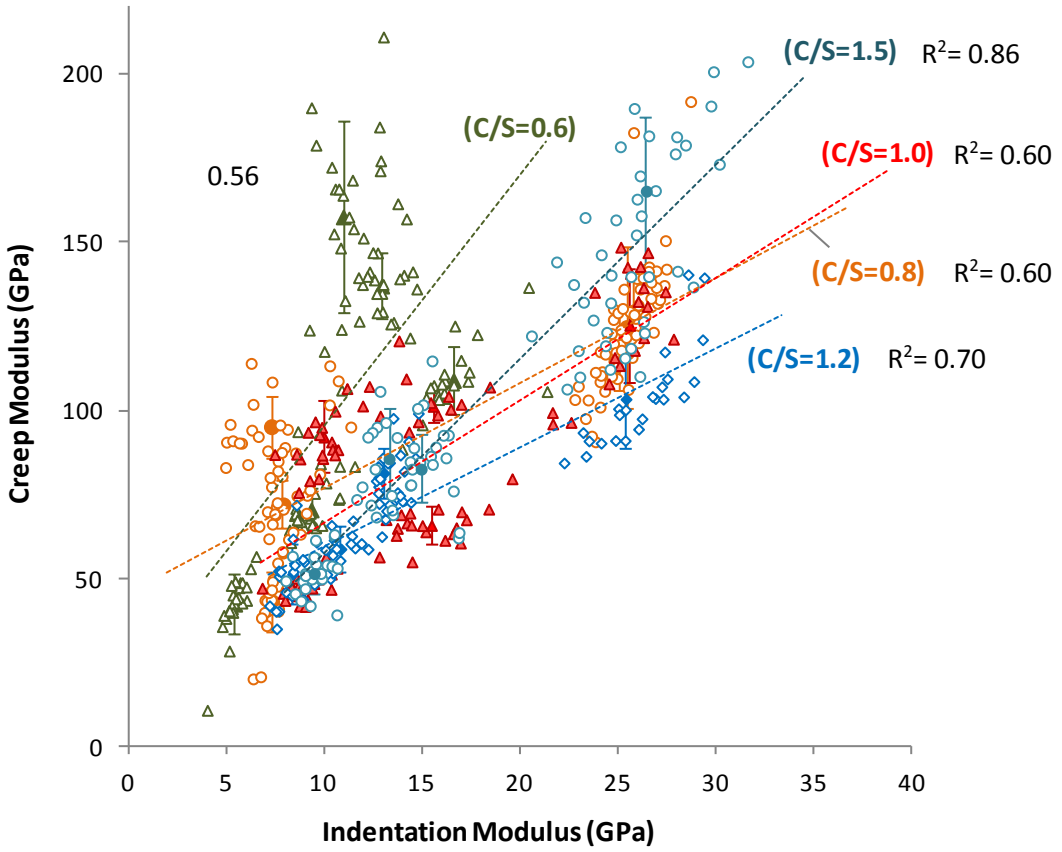

Figure 7: Creep modulus versus indentation modulus: C-S-H preparations (C/S = 0.6; 0.8; 1.0; 1.2; 1.5). The solid markers represent the mean values for a cluster of data points obtained on compacts prepared at a given compaction pressure. The error bars indicate one standard deviation from the mean.

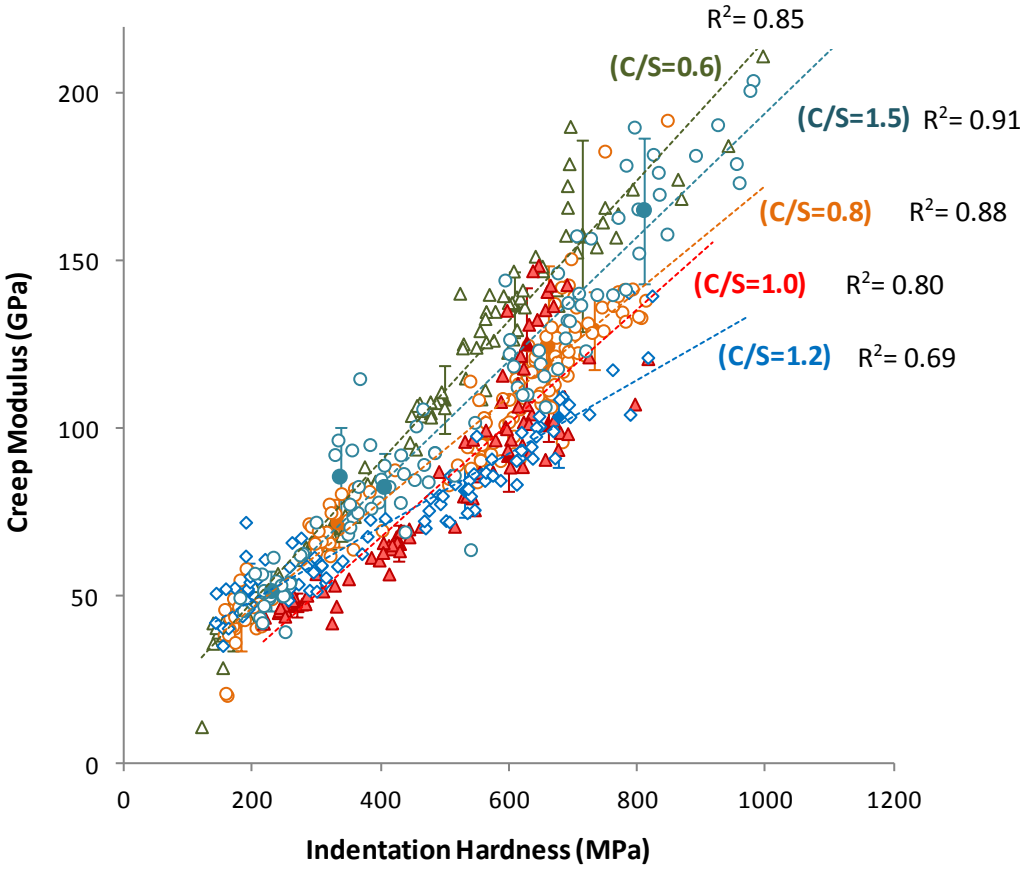

Figure 8: Creep modulus versus hardness modulus: C-S-H preparations (C/S = 0.6; 0.8; 1.0; 1.2; 1.5). The solid markers represent the mean values for a cluster of data points obtained on compacts prepared at a given compaction pressure. The error bars indicate one standard deviation from the mean.

4.3 Paper 2: Microindentation Creep of Secondary Hydrated Cement Phases and C-S-H

The second paper provided evidence for the view that microindentation methods using compacted powder specimens can provide a rapid assessment of the creep behavior of pure 'secondary' hydrated cement phases. Microindentation creep measurements were obtained on compacted specimens of several secondary hydrated cement phases in equilibrium with water vapor at 11% RH. Porosity is an important parameter in determining creep rate as equivalent values of indentation hardness and modulus are obtained at different values of porosity for different hydrated cement phases. The contribution of the secondary phases in hydrated cement-based materials to creep with respect to the more 'active' C-S-H phase is discussed in this paper.

Microindentation Creep of Secondary Hydrated Cement Phases and C-S-H

(*Materials and Structures*, 46(9), 1519-1525, 2013)

Dan-Tam Nguyen[a], R. Alizadeh[b], J. J. Beaudoin[c] and L. Raki[c]

[a] Department of Civil Engineering, University of Ottawa, Ottawa, ON, Canada
[b] Giatec Scientific Inc., Ottawa, ON, Canada
[c] National Research Council Canada, Construction, Ottawa, ON, Canada

Abstract

Microindentation creep measurements were obtained on compacted specimens of several secondary hydrated cement phases in equilibrium with water vapor at 11% RH. Values of creep modulus, indentation modulus and indentation hardness for calcium hydroxide, ettringite, gypsum and calcium carbonate are reported. The porosity dependence of these parameters was established and the significance of porosity on the time-dependent deformation of these materials was discussed. In addition the microindentation creep behavior of pure C-S-H and C_3S paste hydrated 32 years was determined. The discussion focuses on the relative importance of the contribution of the secondary phases in hydrated cement-based materials to creep with respect to the more 'active' C-S-H phase.

Keywords: Microindentation; Creep; Ettringite; Gypsum; Calcium Carbonate; C-S-H

1. Introduction

Creep of cement-based materials has been studied for decades due to its importance in the behavior and design of concrete structures [1]. The origins of creep continue to be the subject of much debate. Creep in papers on the nanogranular nature of cement paste has been attributed to nanoparticle sliding [2]. This view is in conflict with studies on the viscoelastic nature of pure C-S-H [3]. The concept of nanoparticle (or

nanoglobule) sliding is primarily concerned with the point-to-point contact movements between the nanoparticles under load. In the viscoelastic theory, however, a role is considered for the nanostructural changes within the particles such as sliding of the C-S-H layers. It is apparent that water has a nanostructural role in the sliding of individual C-S-H sheets. This is not the case for the nanoparticle sliding model. Creep is explained here in terms of the translation of silicate sheets and the role of interlayer water in the C-S-H nanostructure.

C-S-H is generally considered to be the most active phase contributing to the time-dependent deformation of hydrated cement binders. Published information on the creep of 'secondary' hydrated cement phases eg. calcium hydroxide, ettringite, gypsum, calcium carbonate, is scarce. Calcium hydroxide alone occupies up to 26% by volume of hydrated cement paste. Therefore, it was an objective of this study to establish the relative importance of these 'secondary' phases on the creep of cement binders. In addition creep measurements of the pure C-S-H phase are also scarce [4]. It was a further objective of this work to obtain creep data for pure C-S-H and well-hydrated C_3S paste in order to provide context for the creep results obtained for the 'secondary' hydrated phases.

Creep results for cement paste using nanoindentation techniques have recently been reported [2]. These methods have the advantage of providing time-dependent creep data in a significantly shorter time period than conventional procedures. The contribution of the C-S-H phase to the indentation parameters is obtained by deconvolution of frequency spectra. The deconvolution concept has been challenged but is beyond the scope of this particular paper [5, 6].

The results of a microindentation creep study of the 'secondary' phases in hydrated cement are reported in this study. Microindentation techniques are appropriate as the compounds tested are monophasic and

problems associated with separation of phases in multiphasic systems are avoided. The results for the hydrated C_3S are reported as 'composite' values as no attempt was made to separate the parameters for different phases in this material.

2. Experimental

2.1 Materials

Ettringite: Pure ettringite was synthesized using the sucrose method proposed by Struble 1986 [7]. Two solutions containing the reactants in stoichiometric proportions were mixed. One contained $Al_2(SO_4)_3$ and the other CaO dissolved in a 10% sugar solution. The mixture was rotated for several hours and filtered. The product was characterized by X-ray diffraction.

Gypsum: Reagent grade gypsum supplied by Anachemia was used.

Calcium hydroxide: Reagent grade calcium hydroxide supplied by Anachemia was used.

Calcium carbonate: Reagent grade calcium carbonate supplied by Fisher Scientific was used.

C-S-H: synthetic C-S-H was produced from the pozzolanic reaction between CaO and amorphous silica in excess water. Calcium oxide was obtained by calcining reagent grade calcium carbonate at 900°C. Reactive silica (CAB-O-SIL, grade M-5 from Cabot Corporation, USA) was heated at 110°C to remove any surface adsorbed water. Distilled water was de-aired and used for the reactions. All materials were kept sealed in N_2 purged bottles until they were used. Variation in C/S ratio was achieved by adjusting the stoichiometric amounts of the reactants. Preparations had C/S ratios of 0.6, 0.8, 1.0, 1.2 and 1.5. The reaction period was 6 months. The material was then filtered and dried under vacuum for 4 days at room temperature. The dried C-S-H was stored in nitrogen purged glass vials before the experiments. Characterization of these

materials by X-ray diffraction (XRD) and thermal methods gave results directly comparable to C-S-H (I) as reported by Taylor 1986 [8].

Hydrated C_3S Paste: Tricalcium silicate paste was prepared using a water/solid ratio of 0.40. Specimens with circular cross-section (25mm in diameter) were cast in glass cylinders. The specimens were demolded after 24h and sheathed in a rubber membrane containing a few drops of lime saturated water. They were then stored in stoppered glass tubes for 32 years. Slices 1 mm thick were then cut and ground into a fine powder for fabrication into compacted specimens.

2.2 Humidity Conditioning

Specimens for all systems were conditioned for several days at 11% RH in vacuum desiccators containing saturated lithium chloride solution. The powders were conditioned at 11% RH before compaction and for a few days after compaction. Theoretically, there is a monolayer of water on the surfaces of the particles in addition to interlayer water at this humidity.

2.3 Preparation of Compacted Specimens

Solid circular disc samples for all the powdered materials were prepared by pressure compaction in steel moulds with a cross-section of 25 mm. The thickness of most of the disc samples was nominally 1 mm. Numerous studies on the use and validity of compacts as models for hydrated cement systems have been published [9-12]. It has been shown that compacted specimens of powdered hydrated Portland cement have similar mechanical property-porosity relationships to that of the original hardened paste of the same material [10]. The porosity of compacted samples was determined using helium pycnometry or in the case

of the phase pure minerals by calculation using published density values. The calculation is made knowing the apparent volume and the solid volume of the sample. Porosity is varied by controlling the compaction pressure.

2.4 Microindentation measurements

All the microindentation tests were performed using a CSM Instruments Instrumented Indentation Tester. The apparatus is housed in an environmental chamber. All tests were conducted at 11% RH on specimens equilibrated at 11% RH.Tests were conducted using a Berkovich indenter. The nanoindentor tip is a three-sided pyramid which is geometrically self-similar. It has a flat profile with a total included angle of 142.3 degrees and a half angle of 65.35 degrees measured from the axis to one of the pyramid flats. The Berkovich tip has the same projected area-to-depth ratio as a Vickers indentor. The CSM microindentation instrument has a load range of 0.03-30 N with a resolution of 0.3 mN. The specimens were tested over a wide range of porosity values varying from about 10% to as high as 60%. There were approximately 25 indents on each sample at each porosity level for a total of approximately 125 indents for each material system. The composition of the solid phase for monophasic systems remains constant. Pure materials do not require as many indents as composite materials as phase separation procedures such as the use of deconvolution are not necessary.

The indentation depth (h) was recorded as a function of time at the maximum load of 1000 mN for a 600 s dwell period. The loading rate was 2000mN/min. The logarithmic creep was determined through curve fitting of the indentation-depth versus time curves during the 600s dwell time by the following equation:

$$\Delta h(t) = x_1 ln(x_2 t + 1) + x_3 + x_4 \qquad (1)$$

The creep modulus, C, is then calculated from: $C = P_{max}/(2a_U x_1)$ where $a_U = [A_c/\pi]^{1/2}$. A_c is the projected area of contact between the indenter probe and the indenter surface. It is determined using the Oliver and Pharr method as a function of the maximum indentation depth [13]. The indentation modulus (M) and indentation hardness (H) were obtained from the software that uses the Oliver and Pharr method. $M = \pi^{1/2}S/[2(A_c)^{1/2}]$ where $S = dP/dh|_{h = hmax}$ is the initial slope of the unloading branch of the P-h curve. P is the maximum indentation load. Indentation hardness (H) was estimated from the relation $H = P/A_c$.

3. Results and Discussion

3.1 Mechanical performance of the systems investigated

Numerous publications have documented the mechanical behavior of hydrated Portland cement paste and its role in determining the engineering performance of concrete [14]. This is particularly true for studies of creep behavior which is an important consideration in the design of concrete structures. There is, however, a paucity of data concerning the engineering properties of pure hydrated cement phases. A brief summary of some pertinent properties is germane to this discussion. Typical modulus of elasticity values for gypsum and calcium carbonate [15], calcium hydroxide [16-18], ettringite [19] and C-S-H [20] determined experimentally are 45.7GPa, 79.6 GPa, 35.0-48.0 GPa, 35.0GPa and 34 GPa respectively. These values were determined using a variety of techniques and sample preparation methods. Samples were made utilizing powder compaction methods [9] to form solid bodies or in some cases single crystals were examined using Brillouin spectroscopy [18, 19]. It is apparent that values of the elastic constants are generally similar with the exception of the value for calcium carbonate. Additional information on mechanical strength properties is available for calcium hydroxide [16]. Flexural strength values of calcium hydroxide compacts range from 5.9 to 14.2 MPa over a porosity range of 21.0 to 34.2%. Cement paste values vary from about 3.0 to 10.0 over a similar porosity range. Fracture mechanics parameters for

calcium hydroxide and C-S-H compacts prepared with a wide range of porosity values have also been reported [20]. Calcium hydroxide generally has a lower fracture resistance than C-S-H. The C-S-H with the highest fracture resistance had the highest value of polymer to dimer ratio. This is generally the case for low C/S ratio C-S-H. For example, the magnitude of the storage modulus (E') obtained from Dynamic Mechanical Analysis measurements over a wide range of porosity varies inversely with C/S ratio [20].

The authors were able to identify only one reference to direct measurement of the creep behavior of calcium hydroxide [4]. Direct creep measurements on the other systems studied were not identified. It was observed that calcium hydroxide compacts do creep even at 0% RH and show at the very beginning a trend similar to that observed in cement paste systems. This result is significant as there is a large amount of this phase in cement paste (20-26% by volume) underlying the importance of understanding the role of calcium hydroxide in the creep behavior of cement-based materials. The argument can be extended to the role of the other cement phases on creep of cement-based materials as there contribution at this point is uncertain.

3.2 Microindentation Creep Measurements

Creep modulus versus indentation modulus and indentation hardness data for the cement phases investigated are plotted in Figures 1 and 2 respectively. Curves for hydrated C_3S are also plotted in the figures for comparison. Ettringite and hydrated C_3S creep (inverse of creep modulus) at about the same rate and creep significantly more than gypsum and calcium hydroxide at all values of indentation modulus and indentation hardness. Creep rate of calcium carbonate, although over a more limited range of data, is similar to the creep rate for gypsum. The 'free' water contained by specimens of secondary phases when conditioned at 11% RH is essentially adsorbed water on surfaces. Ettringite also contains about 2 moles

of ‘mobile’ water in the channels of its structure. This water is not removed unless drying takes place below 11% RH [22]. The creep rate of C-S-H is significantly greater than the creep rate of the cement phases as well as the creep rate for hydrated C_3S. The data for the C-S-H plotted in Figures 1 and 2 is for C/S = 1.2 only for purposes of clarity. Data for other C/S ratios are located along the same line.

The interlayer water in C-S-H has a role in the stress dependent translation of the silicate sheets in the nanostructure [3]. Hydrated C_3S contains a significant amount of calcium hydroxide that has a high creep modulus in addition to C-S-H. It would therefore be expected that calcium hydroxide would have a restraining effect on the creep of C-S-H. Calcium hydroxide has a hexagonal unit cell with weak interlayer forces, negligible hydrogen bonding and good cleavage along the (0001) plane [23]. Gypsum is monoclinic with (010) cleavage. It would appear that the influence of cleavage planes that are randomly oriented in the specimen does not enhance the creep rate of calcium hydroxide and gypsum in cement systems as these phases have the lowest creep rate for the systems studied. Further, it is suggested that calcium hydroxide in Portland cement paste and calcium hydroxide in compacts can both be considered to be formed under confined conditions. Modulus of elasticity versus porosity curves for paste and calcium hydroxide compacts are similar [16]. Large platy crystals of calcium hydroxide will form only in large voids in the paste and are not likely to have a significant influence on behavior. The bulk of the calcium hydroxide forms as small crystals and some of it may even be nanocrystalline [24]. The shape of the calcium hydroxide surface has been shown to change when exposed to testing in the AFM [25]. These changes are possibly due to exposure to carbon dioxide and humidity in the air. In the experiments reported in this study the measurements were conducted in an environmental chamber under low humidity conditions. Carbonation was limited. Moreover, there is a very insignificant amount of free lime in the phase pure C-S-H samples. In addition, the microindentation creep tests are not as sensitive as AFM to the slight surface changes. Ettringite is generally in the form of hexagonal, prismatic or acicular crystals

and has a relatively low density of 1.775 g/cm^3. Its creep rate is similar to that for hydrated C_3S and may involve translational strain along channels in the 'c' direction of the unit cell. The 'sensitivity' for displacement in this direction may be the reason that ettringite has a greater creep rate than calcium hydroxide. Calcium carbonate has a relatively high density (2.771 g/cm^3) but does have a (1014) cleavage plane. This may account for the similarity in creep rate to gypsum in the region of the plotted data when it otherwise might be expected to have a higher creep modulus or lower creep rate.

The C-S-H formed as a result of cement hydration is the most significant contributor to overall creep deformation. Nevertheless it is apparent that 'secondary' reaction products in cement systems can contribute in a meaningful manner to the creep behavior of hydrated cement paste.

3.3 Microindentation parameters-porosity dependence

The porosity dependence of the microindentation parameters (creep modulus, indentation hardness and indentation modulus) for the studied systems is illustrated in Figure 3(a), (b) and (c). The creep modulus versus porosity data (Figure 3(a)) for hydrated C_3S and ettringite lie on the upper bound of the data sets indicating that on a porosity basis creep rate would be lower for these materials. One data point (for calcium hydroxide) at about 35% porosity also lies on this bound. The indentation hardness versus porosity data for hydrated C_3S and ettringite (Figure 3(b)) lie on the upper bound of the data sets. Data for calcium hydroxide has lower values over the entire porosity range. The curves in Figure 1 (creep modulus versus indentation modulus) for ettringite and hydrated C_3S are also similar. The relative position of the indentation hardness curves for ettringite and hydrated C_3S are also similar. The creep modulus versus indentation hardness and indentation modulus curves for calcium hydroxide in Figure 1 are positioned above those for ettringite and hydrated C_3S. This corresponds to the observation (in Figure 3(b)

and 3(c)) that the porosity required to achieve the same indentation modulus and indentation hardness is lower for calcium hydroxide. This is also compatible with the view that calcium hydroxide is weaker than ettringite and hydrated C_3S. It is also important for engineering design considerations to be aware of porosity effects on the performance of cement-based materials and their constituent phases.

The relative position of the indentation modulus versus porosity curves (Figure 3(c)) for all the systems studied is similar to that for the data in Figure 3(a) and 3(b). The data for gypsum, calcium carbonate and calcium hydroxide are generally well nested over the entire porosity range. Creep modulus versus porosity data for C-S-H (Figure 3(a)) lies on the lower bound of all the data sets. It is apparent that C-S-H has a lower creep modulus and therefore higher creep rate over the entire porosity range investigated than all the other hydrated cement phases. This parallels the information presented in Figure 1 and further underscores the importance of determining porosity in assessing creep behavior and characterizing cement-based materials.

4. Conclusions

1. Microindentation methods using compacted powder specimens can provide a rapid assessment of the creep behavior of pure 'secondary' hydrated cement phases.
2. Microindentation parameters i.e. creep modulus, indentation modulus and indentation hardness are porosity dependent.
3. Porosity is an important parameter in determining creep rate as equivalent values of indentation hardness and modulus are obtained at different values of porosity for different hydrated cement phases.

4. C-S-H generally has a greater creep rate than that of the other hydrated cement phases over a wide range of porosity.
5. Ettringite, calcium hydroxide and hydrated C_3S have a relatively low creep rate on a porosity basis. Gypsum and calcium carbonate have a relatively high creep rate approaching that of C-S-H.
6. Creep of cement phases depends on many factors including crystal structure, defects, translation of cleavage planes, intrinsic mechanical properties in addition to porosity effects.
7. Consideration should be given to determining the influence of 'secondary' phases in hydrated cement when assessing on creep behavior of cement-based materials.

5. References

1. Neville A.M. (1970) Creep of concrete: plain, reinforced and prestressed, North Holland Pub. Co., Amsterdam, pp 622.
2. Vandamme M., Ulm F.-J. (2009) Nanogranular origin of creep, Proc. Nat. Acad. Sci. (USA), 106 (26):10552-10557
3. Alizadeh R., Beaudoin J.J., Raki L. (2010) Viscoelastic nature of calcium silicate hydrate, Cem. Concr. Comp., 32: 369-376
4. Tamtsia B.T., Beaudoin J.J., Marchand J. (2002) Time-dependent load-induced deformation of Ca(OH)2, Adv. Cem. Res., 14(4): 135-139
5. Trtik P., Munch B., Lura P. (2009) A critical examination of statistical nanoindentation on model materials and hardened cement pastes based on virtual experiments, Cem. Concr. Comp., 31: 705-714

6. Lura P., Trtik P., Munch B. (2011) Validity of recent approaches for statistical nanoindentation of cement pastes, Cem. Concr. Comp., 33: 457-465

7. Struble L.J. (1986) Synthesis and characterization of ettringite and related phases, Proc. 8th Int. Conf. Chem. Cem., Rio de Janeiro, Brazil, Vol.6 :582-588

8. Taylor H.F.W. (1986) Proposed structure for Calcium Silicate Hydrate Gel, J. Amer. Ceram. Soc. 69(6): 464-467

9. Soroka I., Sereda P.J. (1968) The structure of cement- stone and use of compacts as Structural models, Proc. 5th Int. Symp. on the Chem. of Cem., Tokyo, Vol. 3: 67-73

10. Feldman R.F. (1972) Factors affecting the Young's modulus-porosity relation of Portland cement compacts, Cem. Concr. Res., 2: 375-386

11. Sereda P.J., Feldman R.F. (1963) Compacts of powdered material as porous bodies for use in sorption studies, J. Appl. Chem., 13: 150-158

12. Sereda P.J., Feldman R.F., Swenson EG (1966) Effect of sorbed water on some mechanical properties of hydrated Portland cement pastes and compacts, Highway Research Board, Special Report 90: 58-73

13. Oliver W.C., Pharr G.M. (1992) An improved technique for determining hardness and elastic modulus using load and displacement sensing indentation experiments, J. Mater. Res.7: 1564-1583

14. Ramachandran V.S, Feldman R.F., Beaudoin J.J. (1981) Concrete Science, Heyden & Son Ltd., London, pp. 427

15. Haecker C.-H., Garboczi, E.J., Bullard J.W., Bohn R.B., Sun Z., Shah S.P., Voigt T. (2005) Modeling the linear elastic properties of Portland cement paste, Cem. Concr. Res., 35:1948-1960

16. Beaudoin J.J. (1983) Comparison of mechanical properties of compacted calcium hydroxide and Portland cement paste systems, Cem. Concr. Res., 13: 319-324

17. Wittmann F.H. (1986) Estimation of the modulus of elasticity of calcium hydroxide, Cem. Concr. Res., 16: 971-972

18. Speziale S., Jiang F., Mao Z,. Monteiro P.J.M., Wenk H.-R., Duffy T.S., Schilling F.R. (2008) Single-crystal elastic constants of natural ettringite, Cem. Concr. Res., 38: 885-889

19. Speziale S., Reichmann H.J., Schilling F.R., Wenk H.R., Monteiro P.J. (2008) Cem. Concr. Res., 38: 1148-1153

20. Beaudoin J.J., Gu P., Myers R.E. (1998) The fracture of C-S-H and C-S-H/CH mixtures, Cem. Concr. Res., 28(3): 341-347

21. Alizadeh R., Beaudoin J.J., Raki L. (2011) Mechanical properties of calcium silicate hydrates, Mat. and Struct., 44: 13-28

23. Taylor (1997) Cement Chemistry (2nd edition), Thomas Telford Pub., London, pp. 459

22. Skoblinskaya NN, K. G. Krasilnikov (1975), Changes in crystal structure of ettringite on dehydration. 1, Cem. Concr. Res. 5(4): 381-394

24. Chen J., Vandamme M., Ulm F.-J., Chanvillard G. (2010) A coupled nanoindentation/SEM-EDS study on low water/cement ratio portland cement paste: Evidence for C-S-H/$Ca(OH)_2$ nanocomposites, J. Amer. Ceram. Soc., 93: 1484-1493 hydrated Portland cement compacts, Cem. Concr. Res., 2(4): 375-386

25. Peled A., Weiss J. (2011) Hydrated cement paste constituents observed with Atomic Force and Lateral Force Microscopy, Constr. and Bldg Matls, 25, 4299-4302

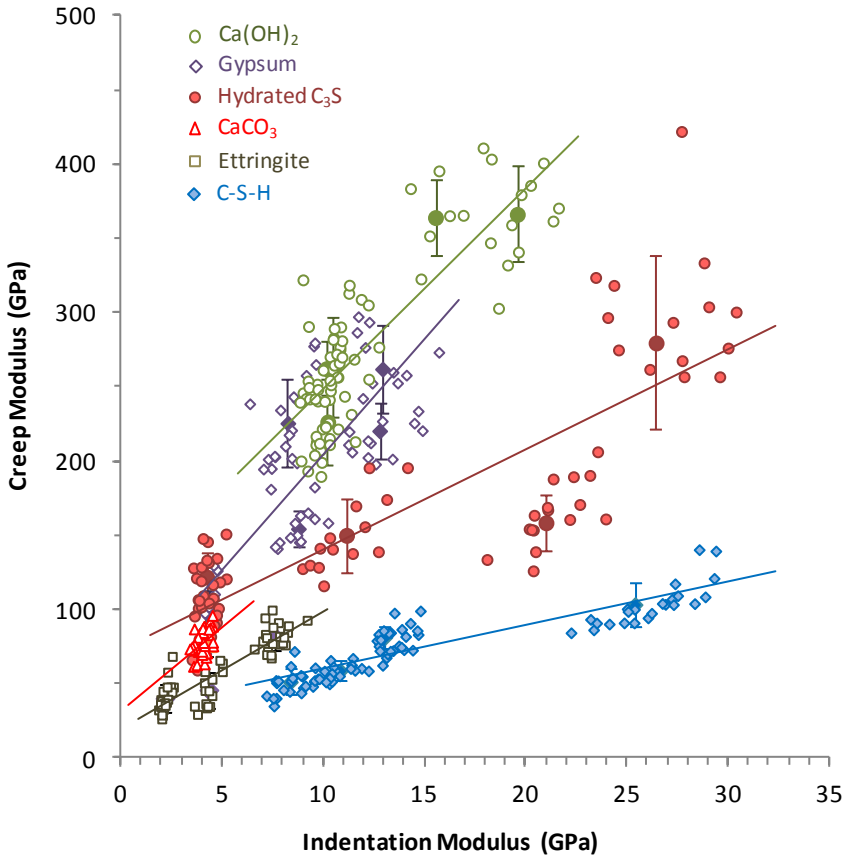

Figure 1: Creep modulus versus indentation modulus for secondary hydrated cement phases, C-S-H and hydrated C_3S. The error bars are indicative of the standard deviation of the results in each data cluster i.e. indentation data for a particular C-S-H sample at a given porosity value. The plot point on the error bar represents the average value of each cluster.

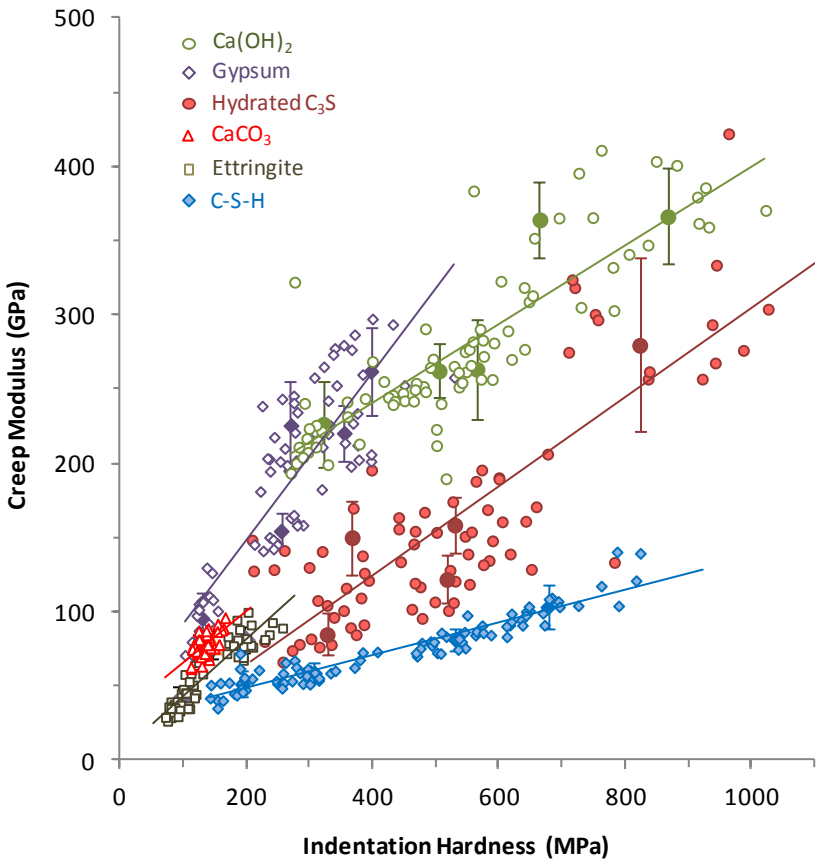

Figure 2: Creep modulus versus indentation hardness for secondary hydrated cement phases, C-S-H and hydrated C_3S. The error bars are indicative of the standard deviation of the results in each data cluster i.e. indentation data for a particular C-S-H sample at a given porosity value. The plot point on the error bar represents the average value of each cluster.

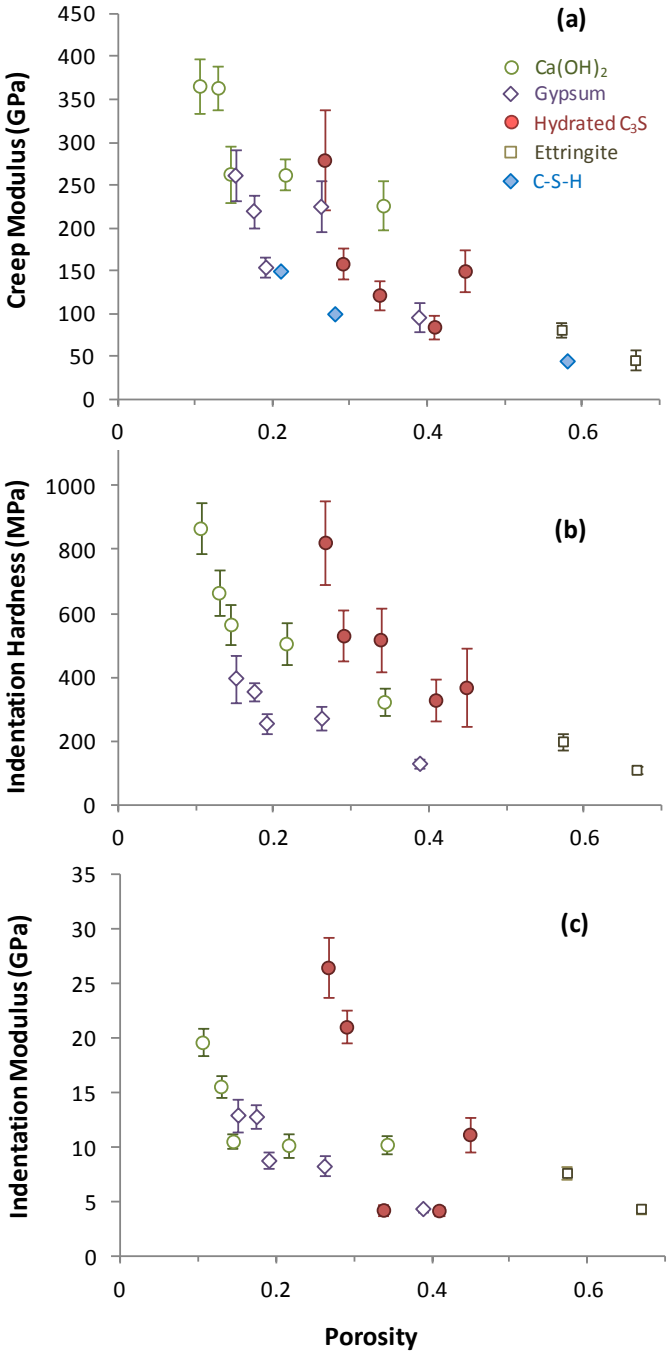

Figure 3: Microindentation parameters versus porosity for secondary hydrated cement phases, C-S-H and hydrated C_3S: (a) creep modulus; (b) indentation hardness; (c) indentation modulus. The error bars are indicative of the standard deviation of the results in each data cluster i.e. indentation data for a particular C-S-H sample at a given porosity value. The plot point on the error bar represents the average value of each cluster.

4.4 Paper 3: Microindentation Creep, Elasticity and Hardness of C-S-H: The Structural Role of Water

The results of microindentation creep, elasticity, and hardness studies conducted on compacted specimens of pure C-S-H are presented in the third paper. It was demonstrated that creep modulus, indentation modulus and indentation hardness are all dependent on mass-loss from 11% RH condition. The research also examined the oscillatory nature of the microindentation parameters as a function of mass-loss, which can be explained in terms of removal of adsorbed and interlayer water, increase in the degree of polymerization, possible cross-linking of the silicate chains and the role of calcium ions in the interlayer region. A possible creep mechanism may involve the relative displacement (‘sliding’) of C-S-H sheets relative to one another. Microindentation was used because it is a method that is rapid and reliable for determining time and moisture dependent mechanical properties of pure C-S-H phases.

Microindentation Creep, Elasticity and Hardness of C-S-H: The Structural Role of Water

(Submitted for publication)

Dan-Tam Nguyen[a], R. Alizadeh[b], J. J. Beaudoin[c] and L. Raki[c]

[a] Department of Civil Engineering, University of Ottawa, Ottawa, ON, Canada
[b] Giatec Scientific Inc., Ottawa, ON, Canada
[c] National Research Council Canada, Construction, Ottawa, ON, Canada

Abstract

Microindentation creep, elasticity and hardness studies were conducted on compacted specimens of pure C-S-H. Indentation parameters were determined at 11% RH and at various stages of dehydration up to a mass-loss of 8%. The oscillating nature of the dependence of these parameters on moisture content was similar to the previously observed dependence of the storage modulus as determined by dynamic mechanical analysis methods. These dependencies were explained in terms of the structural role of water in the nanostructure of the C-S-H. Evidence for a creep mechanism based on the 'sliding' of C-S-H sheets relative to one another is presented.

1. Introduction

The creep of concrete and other cement-based materials has been the subject of intensive investigation for decades [1]. Despite this there remains no unanimity concerning the mechanisms responsible for creep. Models for creep of hydrated cement paste are generally microstructure dependent i.e. the origins of creep are rooted in the stress-dependent translation of fundamental particles. A 'sliding' mechanism associated with the translation of 5 nm 'globules' at points of contact has been advanced by Vandamme and Ulm [2]. No assignment to the role of water has been advanced by these authors. The present authors

also subscribe to the validity of a 'sliding' mechanism. The role of water in the viscoelastic response of layered calcium-silicate-hydrates differentiates their approach from those of the previous authors [3]. Microindentation creep, elasticity and hardness measurements of pure C-S-H phases have been conducted by the present authors [4]. This study extends this work to examine the role of water on the creep behavior of pure C-S-H phases. The testing protocols included microindentation creep, elasticity and hardness measurements of pure compacted C-S-H powders conditioned to 11% RH and measurements obtained after step-wise dehydration to a mass loss of up to 8%. Water held at 11% RH is essentially surface adsorbed and interlayer water. These results clearly demonstrate that the nature of the 'structural' water in the layered silicates is an important factor to consider in any study of creep mechanisms. An assessment of the influence of the removal of structural water on the creep of C-S-H is presented here.

2. Experimental

2.1 Materials

C-S-H: synthetic C-S-H was produced from the pozzolanic reaction between CaO and amorphous silica in excess water (water/solids = 11). Calcium oxide was obtained by calcining reagent grade calcium carbonate at 900°C. Reactive silica (CAB-O-SIL, grade M-5 from Cabot Corporation, USA) was heated at 110°C to remove any surface adsorbed water. Distilled water was de-aired and used for the reactions. All materials were kept sealed in N_2 purged bottles until they were used. Variation in C/S ratio was achieved by adjusting the stoichiometric amounts of the reactants. The C-S-H used in this work had C/S ratios of 0.80 and 1.20. The reaction period was 6 months. The material was then filtered and dried under vacuum for 4 days at room temperature. The dried C-S-H was stored in nitrogen purged glass vials before the

experiments. Characterization of these materials by X-ray diffraction (XRD) and thermal methods gave results directly comparable to C-S-H (I) as reported by Taylor [5].

2.2 Humidity Conditioning

Specimens for the two C-S-H systems were conditioned for several weeks at 11% RH in vacuum desiccators containing saturated lithium chloride solution. The powders were conditioned at 11% RH before compaction and for one week days after compaction. Theoretically there is a monolayer of water on the surfaces of the particles in addition to interlayer water at this humidity.

2.3 Preparation of Compacted Specimens

Solid circular disc samples for all the powdered materials (from the six cementing systems) were prepared by pressure compaction in steel moulds with a cross-section of 25 mm. The thickness of most of the disc samples was nominally 1 mm. Numerous studies on the use and validity of compacts as models for hydrated cement systems have been published [6-10].It has been shown that compacted specimens of powdered hydrated Portland cement have similar mechanical property-porosity relationships to that of the original hardened paste of the same material [10]. The porosity of compacted samples was determined using helium pycnometry and verified by calculation using published density values. The calculation is made knowing the apparent volume and the solid volume of the sample.

2.4 Drying of C-S-H

Drying of the C-S-H (from the 11% RH condition) was carried out in a glass vacuum vessel equipped with a heating wrap. Drying took place either with the application of vacuum alone or a combination of vacuum and heat. The incremental removal of water up to a mass loss of 5% was carried out using vacuum alone. Removal of water at greater mass losses (6 to 8%) involved the application of both vacuum and heat (up to 96°C) for various periods ranging from 1 to 4 days depending on the temperature.

2.5 Microindentation measurements

All the microindentation tests were performed using a CSM Instruments Instrumented Indentation Tester. The apparatus is housed in an environmental chamber. The initial set of tests was conducted at 11% RH on specimens equilibrated at 11% RH. Subsequent tests were conducted at varying moisture contents after step-wise removal of water in increments of 1% up to a total of 8%. Microindentation tests were conducted using a Berkovich indenter. The CSM microindentation instrument has a load range of 0.03-30 N with a resolution of 0.3 mN. The rate of loading in the current experiments was 2000 mN/min. The specimens were tested at porosity values of 43%. There were approximately 25 indents on each sample at each moisture content for a total of approximately 225 indents for each material system. The composition of the solid phase (with the exception of the moisture content) for each C-S-H system remains constant. Pure materials do not require as many indents as composite materials as phase separation procedures such as the use of deconvolution methods are not necessary.

The indentation depth was recorded as a function of time at the maximum load of 1000 mN for a 600 s dwell period. The logarithmic creep was determined through curve fitting of the indentation-depth versus time curves during the 600 s dwell time by the following equation:

$$\Delta h(t) = x_1 ln(x_2 t + 1) + x_3 + x_4 \qquad (1)$$

The creep modulus, C, is then calculated from: $C = P_{max}/(2a_U x_1)$ where $a_U = [A_c/\pi]^{1/2}$. A_c is the projected area of contact between the indenter probe and the indenter surface. It is determined using the Oliver and Pharr method as a function of the maximum indentation depth [11]. The indentation modulus (M) and indentation hardness (H) were obtained from the software that uses the Oliver and Pharr method. $M = \pi^{1/2}S/[2(A_c)^{1/2}]$ where $S = dP/dh|_{h = hmax}$ is the initial slope of the unloading branch of the P-h curve. P is the maximum indentation load. Indentation hardness $H = P/A_c$.

3. Results and Discussion

3.1 Removal of Interlayer Water from C-S-H-DMA Experiments

It has been demonstrated that the presence of interlayer water in the C-S-H nanostructure has a significant effect on volume stability and engineering performance [3, 12]. It is therefore relevant to provide brief comment on this work as it is germane to the subject of this paper i.e. microindentation creep.

Previous studies of the mechanical properties of calcium silicate hydrates using dynamic mechanical analysis (DMA) techniques have indicated that the removal of adsorbed and interlayer water molecules is critical to the structural integrity of the C-S-H framework [12]. The oscillatory nature of the storage

modulus (E') versus mass loss curves (for C-S-H preparations with C/S ratios = 0.8-1.5) starting from the 11% RH condition was explained in terms of the stiffening effects of interlayer water and chemical/compositional changes due to dehydration including an increase in the degree of polymerization, possible cross-linking of the silicate chains and the role of calcium ions in the interlayer region. The possibility of strong 'surface-cation-surface' ionic-covalent interactions between the C-S-H sheet and the interlayer exists [13]. It may be a factor influencing the viscoelastic response of C-S-H to sustained load. Stress relaxation experiments performed on compacted C-S-H specimens conditioned at 11% RH and dried to various moisture levels clearly demonstrate the 'structural' role of interlayer water on time-dependent deformations of C-S-H [3]. Viscoelasticity of C-S-H is modified by the change in moisture content associated with the interlayer water. Variations in stress relaxation with the removal of interlayer water are likely to be due to cross-linking of silicate tetrahedral and the interaction of calcium ions with the silicate chains. These effects are analogous to those influencing the storage modulus (E') response to removal of interlayer water from 11% RH.

3.1 Removal of Interlayer Water from C-S-H-Microindentation Experiments

The microindentation parameters, creep modulus, indentation modulus and indentation hardness were determined from microindentation measurements on compacted C-S-H samples prepared at C/S ratios of 0.80 and 1.2. A series of experiments were conducted at various moisture contents starting from the 11% RH condition followed by the incremental removal of water up to a mass loss of about 8%. Creep modulus versus indentation modulus data for C/S = 0.80 are presented in Figure 1. The data falls into two 'mass loss' regions. A linear curve with a shallow slope is obtained for mass losses between 0 and 5%. A second curve with a much steeper slope is obtained for mass losses between 6 to 8%. It is evident from the curves

that moisture content has an effect on both indentation modulus and creep modulus. This is made clearer in a plot of indentation modulus versus mass-loss for C-S-H (C/S = 0.80) in Figure 2.

Figure 2 also contains a storage modulus (E') versus mass loss curve derived from the authors' previous work using DMA methods [12]. The similarities in the character of the two curves are striking. There are three similar and distinct mass loss regions for each curve (mass loss up to 7%). A steep reduction in both stiffness and indentation modulus observed in the first region (up to about 2% mass loss) is attributed to the loss of adsorbed water and some interlayer water. An increase in both E' and indentation modulus occurs as the mass loss increases from about 2% to 4-5%. These increases are attributed to the increase in degree of polymerization, effects associated with the cross-linking of the silicate chains and ionic-covalent interactions involving calcium ions as described in the previous section. Further mass loss results in a decrease in modulus for both curves (up to 7 and 8% mass loss for the indentation modulus and storage modulus respectively). This is likely the result of the removal of the final quantities of interlayer water which provide structural stability to the layered nanostructure. The structural collapse at this C/S ratio is gradual as evidenced by the linear and continual decrease in basal-spacing as water is removed. There is an increase in indentation modulus at 8% mass loss which may be a result of additional cross-linking in these particular samples. The significance of the similarity between the indentation modulus data (obtained using microindentation methods) and the storage modulus data (obtained from dynamic mechanical analysis, DMA) on the removal of water from C-S-H is that the two measurement techniques are very different and provide independent corroboration of the structural role of water in C-S-H.

A plot of indentation modulus versus mass-loss for the C-S-H (C /S = 1.20) is provided in Figure 3. The general shape of the curve is similar to that for the C/S = 0.80 material. There is an initial decrease in the modulus (8.0 to 4.5 GPa) up to a mass-loss of 1% followed by a continuous increase to a maximum of

about 14.5 GPa at 6% mass-loss. This is followed by a rapid decrease in modulus to about 3.1 GPa at 7% mass-loss. The arguments associated with the three regions of mass-loss are similar to those for the C/S = 0.80 material presented above. Figure 3 also contains a plot of storage modulus (E') determined from DMA measurements versus mass-loss. The plot has quantitatively similar characteristics to those of the indentation modulus plot in the mass-loss range of 2 to 8%. The reference values (at 11% RH) and values of the indentation modulus at 1% mass-loss are significantly lower than the storage modulus values. The interlayer positions of both C-S-H systems are approximately filled with water at 11% RH. The C/S ratio = 1.20 material also has a lower degree of polymerization and contains a greater number of defects i.e. missing 'bridging' silica tetrahedra. The microindentation test is 'destructive' in the stress zone beneath the indenter. The DMA test is 'non-destructive'. This coupled with the larger number of defects at this C/S ratio may account for the initially lower values of indentation modulus compared to those obtained by DMA methods. The 002 X-ray basal-spacing versus mass-loss is also plotted in Figure 3. There is a pronounced decrease in the basal-spacing beginning at 2% mass-loss and continuing to about 7% mass-loss. The closer proximity of the silicate sheets and the attendant interactions between them (described previously) may account for the quantitative similarity of the modulus values in this mass-loss region.

Creep modulus versus mass-loss data for both C-S-H systems are presented in Figure 4. The oscillatory nature of the curve mimics that of the indentation modulus curve but the changes are much lower in magnitude for the latter. The curve for C/S = 0.80 is described first. There is a relatively small decrease in creep modulus at 1% mass loss followed by an increase to a maximum of 106 GPa at 5% mass loss. This is followed by a decrease to about 78 GPa at 6% mass loss and a large increase to about 180 GPa as the mass loss is increased to 8% GPa. The nanostructure-based factors that influence creep and the concomitant role of water are therefore likely to be similar to those factors that influence the dependence of indentation modulus on moisture content. The large increase in creep modulus as mass loss increases

from 6 to 8% is likely due to increased cross-linking and ionic-covalent interactions between the silicate sheets. The curve for C/S = 1.2 has some similarities and differences from the curve for C/S = 0.80. The initial creep modulus value at the reference condition (11% RH) is higher for the C/S = 0.80 material. This means that the creep rate is lower in this system that contains fewer defects. Drying, however, affects the magnitude of the creep modulus of the two C-S-H systems in an opposite manner. The creep modulus for both C-S-H systems increases up to 5% mass-loss with the modulus for the C-S-H (C/S = 1.20) increasing at a much faster rate. The respective modulus values for C/S = 1.20 and 0.80 are 160 and 110 GPa at 5% mass-loss. This implies that after drying from the 1% mass-loss level the magnitude of creep is significantly greater for the C/S = 0.80 system. The creep modulus of the C/S = 1.20 system reaches a maximum of 225 GPa at a mass-loss of 6% followed by a rapid decrease to 80 GPa at 7% mass-loss. The modulus for the C/S = 0.80 system decreases to 80 GPa at 6% mass-loss followed by a rapid increase to 185 GPa at 8% mass-loss. Drying appears to affect the general character of the creep modulus versus mass-loss curves in a similar manner as it does the indentation modulus mass-loss curves. Differences due to C/S ratio are however more pronounced for the creep modulus data. The structural collapse that occurs on drying would appear to bring the C-S-H sheets (C/S = 1.20) much closer together resulting in increased modulus or much less creep at mass-losses up to 6%. Decreases in modulus at higher mass-loss values may be a result of the removal of compositional water. This may be delayed to higher mass-loss values at C/S = 0.80 due to the removal process involving a larger amount of interlayer water as the silicate chain length is longer.

The effect of drying from the 11% RH condition on the indentation hardness of both C-S-H systems is illustrated in Figure 5. There are similarities in the general character of the hardness versus mass-loss curve (C/S = 0.80) with that of the indentation modulus versus mass-loss curve (Figure 2).There is a decrease in hardness (640 to 380 MPa) as mass-loss increases to 2%. This is followed by an increase to a

maximum (560 MPa) at about 4% mass-loss and a subsequent decrease to 330 MPa at 6% mass-loss. Further mass-loss to 8% results in a significant increase in hardness to 680 MPa. The mechanisms involved in the cyclic dependence of hardness on mass-loss are similar to those described for the indentation modulus and storage modulus data presented in Figure 2 and described previously. The reference hardness value (at 11%RH) for the C/S = 0.80 system (640 MPa) was greater than that for the C/S = 1.20 system (480 MPa). The difference is in accordance with the indentation modulus values and is attributed to the shorter silicate chains and larger number of missing 'bridging' silica tetrahedra (structural defects) in the C/S = 1.20 system. The hardness values increase to a maximum (710 MPa) at about 6% mass-loss and generally exceed those of the C/S = 0.80 system. The structural collapse that occurs on drying would appear to bring the C-S-H sheets (C/S = 1.20) much closer together with an attendant strengthening effect. Decreases in hardness at higher mass-loss values (similar to indentation modulus values) may be a result of the removal of compositional water. This may also be delayed to higher mass-loss values at C/S = 0.80 due to the removal process involving a larger amount of interlayer water as the silicate chain length is longer.

It is apparent that the removal of surface adsorbed and interlayer water from C-S-H is an integral part of the creep process. The structural nature of this water influences the relative stability of the C-S-H sheets and their abilty to deform and translate under a sustained load. The microindentation data support the view that a possible creep mechanism may involve the 'sliding' of C-S-H sheets relative to each other.

4. Conclusions

1. Microindentation creep measurements on C-S-H (C/S = 0.80 and 1.20) demonstrate that creep modulus, indentation modulus and indentation hardness are all dependent on mass-loss from the 11% RH condition.
2. The oscillatory nature of the indentation modulus versus mass-loss curve (C/S = 0.80) mimics both qualitatively and quantitatively the storage modulus (E') versus mass-loss curve obtained independently using dynamic mechanical analysis methods. This is also the case for the C/S = 1.20 system except at low values of mass-loss. The character of these curves was also mimicked by the indentation hardness and creep modulus versus mass-loss curves.
3. Differences in the magnitude of the microindentation parameters at mass-losses greater than 2% for the two C-S-H systems studied as a result of drying may be due to the structural collapse that occurs on drying that would appear to bring the C-S-H sheets (C/S = 1.20) much closer together possibly with an attendant strengthening effect.
4. The oscillatory nature of the microindentation parameters as a function of mass-loss can be explained in terms of removal of adsorbed and interlayer water, increase in the degree of polymerization, possible cross-linking of the silicate chains and the role of calcium ions in the interlayer region.
5. A possible creep mechanism may involve the relative displacement ('sliding') of C-S-H sheets relative to one another.
6. Microindentation methods are rapid and reliable procedures for determining time and moisture dependent mechanical properties of pure C-S-H phases.

5. References

1. A.M. Neville, Creep of concrete: plain, reinforced and prestressed, North Holland Pub. Co., pp. 622, 1970.
2. M. Vandamme and F.-J. Ulm, Nanogranular origin of creep, Proc. Nat. Acad. Sci. (USA), 106 (26), 10552-10557, 2009.
3. R. Alizadeh, J. J. Beaudoin and L. Raki, Viscoelastic nature of calcium silicate hydrate, Cem. Concr. Comp., 32, 369-376, 2010.
4. D.-T. Nguyen, R. Alizadeh, J. J. Beaudoin, and L. Raki, Microindentation Creep of Monophasic Calcium-Silicate-Hydrates, submitted to Cem. Concr. Comp., June 2012.
5. H.F.W. Taylor, Proposed structure for Calcium Silicate Hydrate Gel, J. Amer. Ceram. Soc. 69, (6), 464-467, 1986.
6. I. Soroka and P.J. Sereda, The structure of cement- stone and use of compacts as structural models, Proc. 5th Int. Symp. on the Chem. of Cem., Vol. 3., Tokyo, 67-73, 1968.
7. Feldman R.F., Factors affecting the Young's modulus-porosity relation of hydrated Portland cement compacts, Cem. Concr. Res., 2(4), 375-386, 1972.
8. P.J. Sereda and R.F.Feldman, Compacts of powdered material as porous bodies for use in sorption studies, J. Appl. Chem., 13, 150-158, 1963.
9. J.J. Beaudoin, Comparison of mechanical properties of compacted calcium hydroxide and Portland cement paste systems, Cem. Concr. Res., 13, 319-324, 1983.
10. P.J. Sereda, R.F. Feldman and E.G. Swenson, Effect of sorbed water on some mechanical properties of hydrated Portland cement pastes and compacts, Highway Research Board, Special Report 90, 58-73, 1966.

11. W.C. Oliver and G.M. Pharr, An improved technique for determining hardness and elastic modulus using load and displacement sensing indentation experiments, J. Mater. Res.7, 1564-1583, 1992.

12. R. Alizadeh, J.J. Beaudoin and L. Raki, Mechanical properties of calcium silicate hydrates, Mat. and Struct., 44, 13-28, 2011.

13. R.J.-M. Pellenq, N. Lequeux and H. Van Damme, Engineering the bonding scheme in C-S-H: the iono-covalent framework, Cem. Concr. Res. 38, 159-174, 2008.

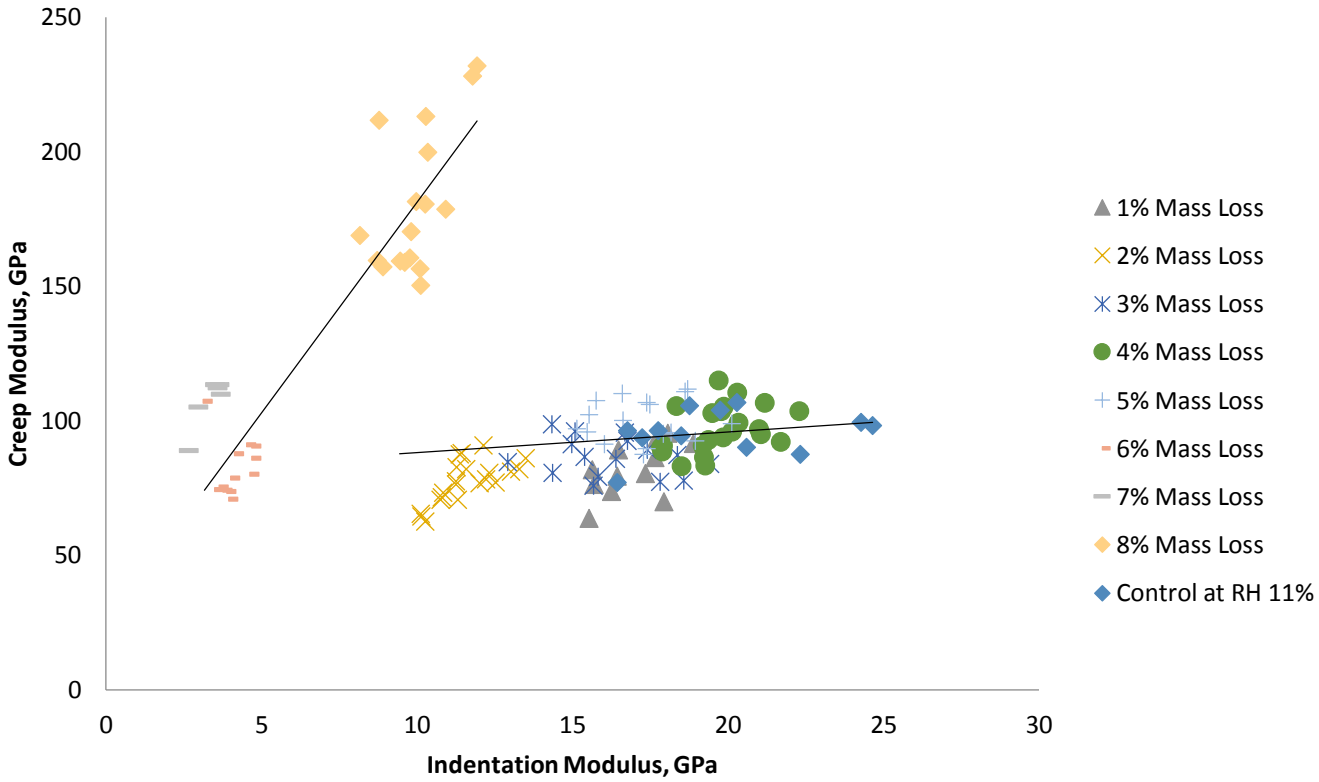

Figure 1: Creep Modulus versus Indentation Modulus for C-S-H (C/S = 0.8) dried incrementally from 11% RH.

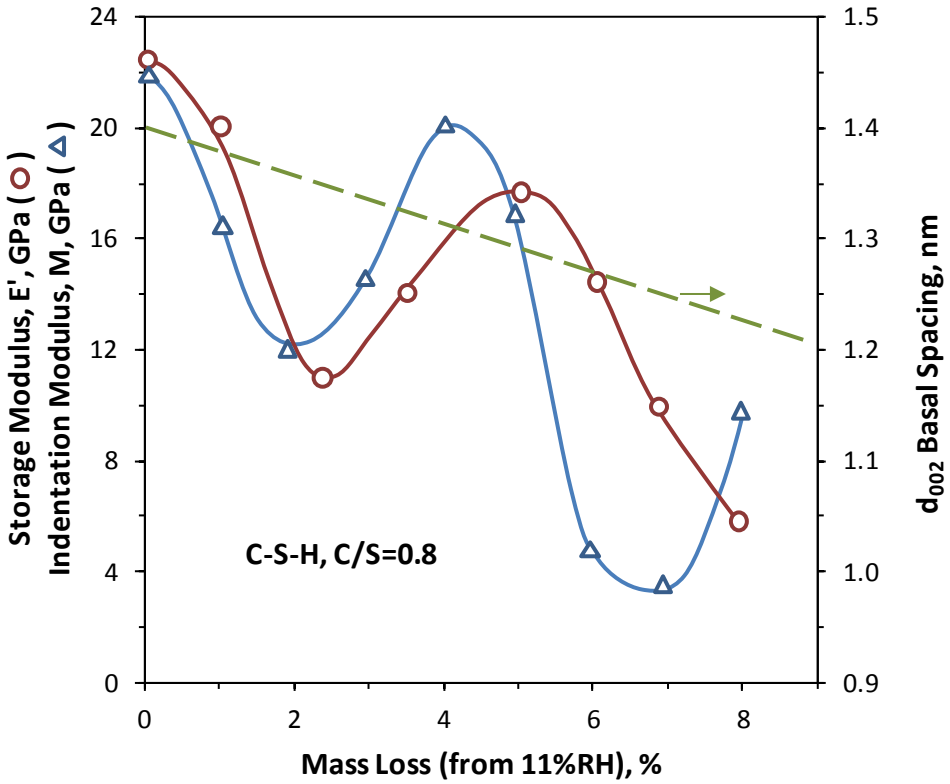

Figure 2: Indentation Modulus and Storage Modulus versus Mass-Loss for C-S-H (C/S = 0.80). The change in 002 basal-spacing is also indicated.

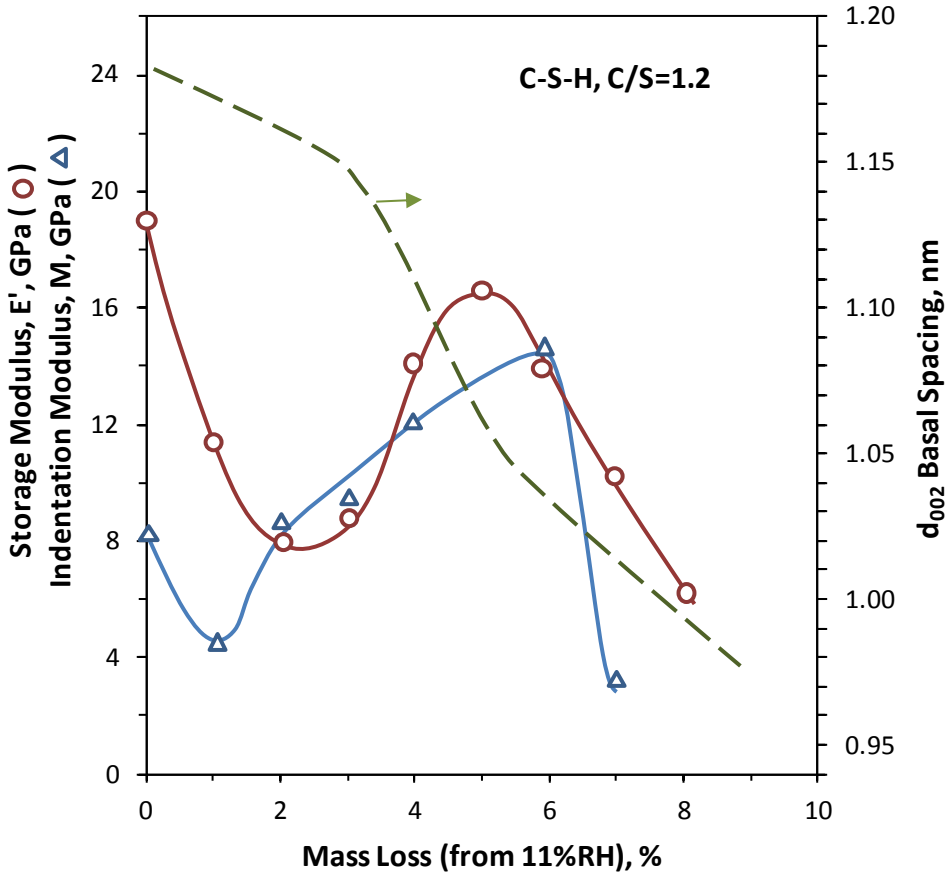

Figure 3: Indentation Modulus and Storage Modulus versus Mass-Loss for C-S-H (C/S = 1.20). The change in 002 basal-spacing is also indicated.

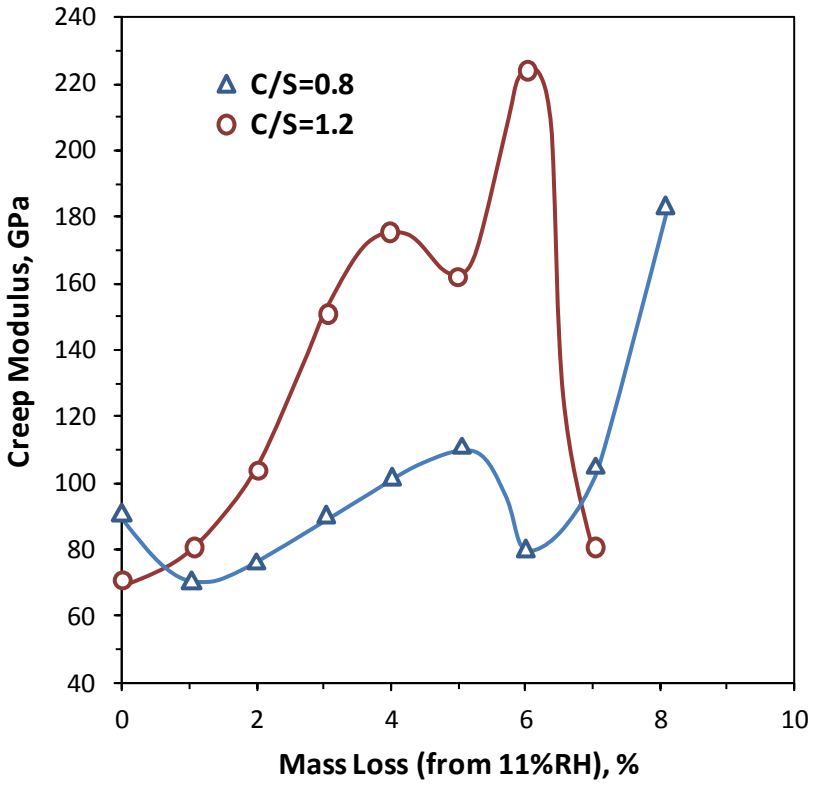

Figure 4: Creep Modulus versus Mass-Loss for C-S-H (C/S = 0.80 and 1.20)

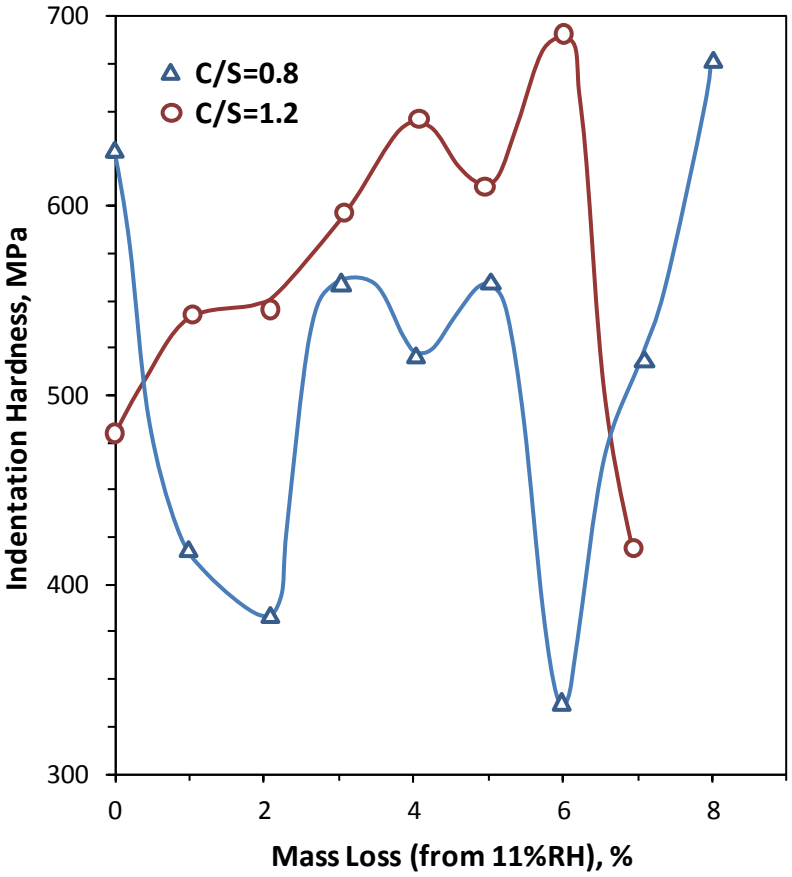

Figure 5: Indentation Hardness versus Mass-Loss for C-S-H (C/S = 0.80 and 1.20)

4.5 Paper 4: Creep of Calcium-Silicate-Hydrates: A Particle Sliding Mechanism

Results of a microindentation creep study of synthetic C-S-H (C/S = 0.8 and 1.20) and hydrated Portland cement paste are presented in the fourth paper. The mass-loss dependencies, starting from the 11% RH condition, of internal friction (tan ∂) and the creep modulus were determined using dynamic mechanical analysis and microindentation methods. The nanostructural role of interlayer water in C-S-H has a significant influence on the creep process.

Creep of Calcium-Silicate-Hydrates: A Particle Sliding Mechanism

(Submitted for publication)

D.-T. Nguyen[a], , J. J. Beaudoin[c], R. Alizadeh[b] and L. Raki[c]

[a] Department of Civil Engineering, University of Ottawa, Ottawa, ON, Canada
[b] Giatec Scientific Inc., Ottawa, ON, Canada
[c] National Research Council Canada, Construction Portfolio, Ottawa, ON, Canada

Abstract

Results of a microindentation creep study of synthetic C-S-H (C/S = 0.8 and 1.20) and hydrated Portland cement paste are reported. A systematic investigation was conducted to determine the mass-loss dependencies (starting from the 11% RH condition) of internal friction (tan ð) obtained using dynamic mechanical analysis and the creep modulus. Evidence was obtained to support the view that a contributing creep mechanism may involve the sliding of C-S-H layers relative to one another. This mechanism is a factor in the creep process for all three systems studied. It is apparent that interlayer water has a structural role in the creep process of cement-based materials.

1. Introduction

Neville, in his book on creep [1], provides an historical note indicating that the first data on the behavior of concrete under a sustained load was published in 1907 [2]. A plethora of publications have since documented theoretical and experimental observations of the time-dependent deformation of cement-based materials. Various mechanisms responsible for creep have been proposed [3]. Feldman and Sereda have argued that the layered nature of C-S-H and interlayer water relocation plays an important role [4]. Many authors have postulated that several processes can occur simultaneously [5-10]. These include

viscous flow, delayed elasticity, seepage, aging, intercrystalline slip and bond rupture. Other authors have described processes involving shearing action occurring as a result of multiplate crystal surfaces sliding over one another [1, 4]. Microstructural and more recently nanostructural investigations have advocated that the origins of creep are rooted in a particle sliding mechanism [4, 11, 12]. Feldman proposed that creep is a manifestation of gradual crystallization or aging in a poorly crystallized material accelerated by drying or stress [4]. Water transport from entrances to interlayer spaces occurs and probably controls creep rate at early stages. Solid-volume increases were actually observed during drying and re-exposure of cement paste to various humidities. He concluded, however, that the process in the early stage may activate the rate determining processes at later stages including crystal slippage, microcracking, bond breaking and reforming. Alizadeh et al. in stress relaxation experiments with synthetic C-S-H (conducted at 11% to 0% relative humidity) showed that the viscoelastic performance depends considerably on the presence of interlayer water [13]. It was argued that the results supported the validity of the theory of sliding of C-S-H sheets as a time-dependent deformation mechanism responsible for creep and stress relaxation of cement-based materials. Vandamme and Ulm hypothesized that creep of C-S-H is due to nano-particle sliding resulting in a local increase of the packing density providing a plausible explanation for the dependence of creep rate and magnitude on this parameter [12]. The role of interlayer water or structural water on creep of C-S-H was not discussed.

The role of interlayer water on the creep behavior of synthetic C-S-H (C/S = 0.80 and 1.20) and cement paste hydrated for 2 months is investigated and the results reported in this paper. Microindentation measurements and dynamic mechanical analysis (DMA) are utilized to assess the correspondence between creep and internal friction (tan ð) as a function of mass-loss. Inferences (based on internal friction determinations) regarding the creep recovery process in saturated cement paste (w/c = 0.35) have been previously reported [14, 15]. It was concluded that a short-term transition exhibited in the creep

recovery curves was caused by a stress-induced redistribution of capillary water. Creep modulus versus mass-loss data starting from the 11% RH condition (where no capillary or pore water is present) for the three systems studied in conjunction with the tan ð versus mass-loss data are considered in terms of supporting a potential creep mechanism based on sliding of C-S-H layers. This data is supplemented by basal-spacing (d_{002}) versus mass-loss data for the C-S-H in addition to helium inflow versus mass-loss data for hydrated cement paste under sustained load. It is emphasized that multiple creep mechanisms in hydrated cements may be operative simultaneously. The focus here is, however, to provide evidence for the possibility of a particle-sliding mechanism and its dependence on interlayer water.

2. Experimental

2.1 Materials

C-S-H: synthetic C-S-H was produced from the pozzolanic reaction between CaO and amorphous silica in excess water. Calcium oxide was obtained by calcining reagent grade calcium carbonate at 900°C. Reactive silica (CAB-O-SIL, grade M-5 from Cabot Corporation, USA) was heated at 110°C to remove any surface adsorbed water. Distilled water was de-aired and used for the reactions. All materials were kept sealed in N_2 purged bottles until they were used. Variation in C/S ratio was achieved by adjusting the stoichiometric amounts of the reactants. Preparations had C/S ratios of 0.8 and 1.2. The reaction period was 6 months. The material was then filtered and dried under vacuum for 4 days at room temperature. The dried C-S-H was stored in nitrogen purged glass vials before the experiments. Characterization of these materials by X-ray diffraction (XRD) and thermal methods gave results directly comparable to C-S-H (I) as reported by Taylor [16].

Hydrated Cement Paste: The paste was prepared using a water/solid ratio of 0.42. Specimens with circular cross-section (25 mm in diameter) were cast in glass cylinders. The specimens were demolded after 24h and sheathed in a rubber membrane containing a few drops of lime saturated water. They were then stored in stoppered glass tubes for 2 months. Slices 1 mm thick were then cut and conditioned at 11% RH for several weeks prior to microindentation measurements.

2.2 Humidity Conditioning

Specimens for all systems were conditioned for several days at 11% RH in vacuum desiccators containing saturated lithium chloride solution. The powders were conditioned at 11% RH before compaction and for a few days after compaction. Theoretically there is a monolayer of water on the surfaces of the particles in addition to interlayer water at this humidity.

2.3 Preparation of Compacted Specimens

Solid circular disc samples for all the powdered materials (i.e. both C-S-H preparations) were prepared by pressure compaction in steel moulds with a cross-section of 25 mm. The thickness of most of the disc samples was nominally 1 mm. Numerous studies on the use and validity of compacts as models for hydrated cement systems have been published [17-21]. It has been shown that compacted specimens of powdered hydrated Portland cement have similar mechanical property-porosity relationships to that of the original hardened paste of the same material [21].

2.4 Porosity Determinations

The porosity values of the compacted samples and the paste samples were determined using helium pycnometry or by calculation using published density values. The calculation is made knowing the apparent volume and the solid volume of the sample.

2.5 Microindentation measurements

All the microindentation tests were performed using a CSM Instruments Instrumented Indentation Tester. The apparatus is housed in an environmental chamber. All tests were conducted at 11% RH on specimens equilibrated at 11% RH.Tests were conducted using a Berkovich indenter. The nanoindentor tip is a three-sided pyramid which is geometrically self-similar. It has a flat profile with a total included angle of 142.3 degrees and a half angle of 65.35 degrees measured from the axis to one of the pyramid flats. The Berkovich tip has the same projected area-to-depth ratio as a Vickers indentor. The CSM microindentation instrument has a load range of 0.03-30 N with a resolution of 0.3 mN. The specimens were tested over a wide range of porosity values varying from about 10% to as high as 60%. There were approximately 25 indents on each sample at each porosity level for a total of approximately 125 indents for each material system. The composition of the solid phase for monophasic systems remains constant. Pure materials do not require as many indents as composite materials as phase separation procedures such as the use of deconvolution are not necessary.

The indentation depth (h) was recorded as a function of time at the maximum load of 1000 mN for a 600 s dwell period. The loading rate was 2000 mN/min. The logarithmic creep was determined through curve fitting of the indentation-depth versus time curves during the 600 s dwell time by the following equation:

$$\Delta h(t) = x_1 ln(x_2 t + 1) + x_3 + x_4 \qquad (1)$$

The creep modulus, C, is then calculated from: $C = P_{max}/(2a_U x_1)$ where $a_U = [A_c/\pi]^{1/2}$. A_c is the projected area of contact between the indenter probe and the indenter surface. It is determined using the Oliver and Pharr method as a function of the maximum indentation depth [22]. The indentation modulus (M) and indentation hardness (H) were obtained from the software that uses the Oliver and Pharr method. $M = \pi^{1/2}S/[2(A_c)^{1/2}]$ where $S = dP/dh|_{h = hmax}$ is the initial slope of the unloading branch of the P-h curve. P is the maximum indentation load. Indentation hardness (H) was estimated from the relation $H = P/A_c$.

2.6 Dynamic Mechanical Analysis (DMA) – Internal Friction (Tan ∂) Measurements

The dynamic mechanical analysis (DMA) method involves the application of an oscillating force to the sample and measurement of displacement [23]. There is usually a time lag between the applied force and the resulting displacement. The time lag can be quantified in terms of a phase angle between the load and the displacement due to their ideally sinusoidal nature. The tangent of this angle (tan ∂) represents the damping property of the material often referred to as internal friction. The DMA tests in this study were conducted on test samples at room temperature. The experiments involved the incremental removal of water from each sample prior to a test run. Tan ∂ versus mass-loss curves were constructed for each test specimen. The construction of each curve involved up to 15 DMA tests and took up to two weeks to complete. Additional details are given in a previous publication [24]. The DMA analysis was conducted using a Rheometrics RSA II instrument on all samples in this investigation.

3. Results and Discussion

3.1 C-S-H (C/S = 1.20)-DMA and Creep Modulus Measurements

The tan ð versus mass-loss and creep modulus versus mass-loss curves for C-S-H (C/S = 1.20) dried in increments from 11% RH are plotted in Figure 1. The curves are of similar shape up to about 6%-7% mass-loss i.e. tan ð and creep modulus values generally increase to a maximum and then decrease to values of similar magnitude to those obtained at 11% RH. The maximum in this mass-loss range occurs at about 2%-3% for the tan ð curve and shifts to between 5% and 6% for the creep modulus curve. The significance of this shift will be discussed later. Measurements of tan ð were continued up to a mass-loss of 9.6% with a second maximum obtained at 7.5%. It was not possible to obtain creep modulus data beyond 7% mass-loss due to the nature of the test and the degree of brittleness of the sample. The increase in tan ð on drying up to the maximum at 2-3% mass-loss is accompanied by the loss of adsorbed and interlayer water. The initial loss of some of the interlayer water likely occurs at the ends of the layers. The ends of the layers come into closer proximity but translation is inhibited by the remaining interlayer water that structurally reinforces the system by bridging the central part of the layers. Further removal of interlayer water up to 6% mass-loss results in a decrease in tan ð values as the C-S-H sheets are brought closer together. This corresponds with a maximum observed in the creep modulus data (i.e. minimum creep rate). These observations are compatible with cross-linking of the C-S-H sheets and possible interaction of the calcium ions with the silicate lamellae possibly through Si-O-Si or $\equiv SiO^{-}Ca^{2+}$ linkages. Lower internal friction and enhanced rigidity in the system are compatible with lower values of creep rate.

Mass-losses at about the 6% level appear to have structural significance. Maxima with respect to mass-loss (on drying from 11% RH) as an argument are observed in all cases for the following: helium inflow experiments on unloaded samples (C-S-H/C/S = 1.20, cement paste); helium inflow experiments on cement paste while under sustained load; creep modulus measurements (C-S-H, cement paste). In addition the degree of polymerization of the C-S-H begins to increase at this moisture level and a significant decrease in the 002 basal-spacing occurs for the C/S = 1.20 preparation. Helium inflow (40h)

and 002 basal-spacing versus mass-loss curves are plotted in Figure 2 [25]. The changes observed in these plots will be put in context (with respect to creep behavior) later in the discussion. Further removal of water beyond the 6% level results in a significant decrease in creep modulus or increase in creep rate compatible with the lower values of internal friction. A 'collapse' of the layered structure has been initiated involving further densification and of equal importance the removal of more water from the central core of the layers. This also coincides with the significant decreases in helium inflow and the 002 basal-spacing observed in Figure 2. The increase in tan ð at mass-losses greater than 7% may be due to the sliding of the silicate layers as they come closer together upon further removal of interlayer water. The decline in internal friction may also be attributed to loss of the final amounts of interlayer water and possibly some constitutional water.

A simplified illustration of nanostructural changes to C-S-H due to the application of sustained load at various stages of mass-loss from the 11% RH condition is given in Figure 3 (a)-3(e). The silicate layers are essentially full of interlayer water at 11% RH. A significant contribution toward the relatively high creep rate (low creep modulus) is attributed to the surface adsorbed water (Figure 3(a)). The exit of water primarily from the layer ends is illustrated in Figure 3(b). Some water is likely to exit from defect points where there are missing bridging tetrahedra. A continual increase in shear stress to a maximum is illustrated. Structural restraint is still provided by the interlayer water. The effect of chemical interactions between the silicate sheets as described previously is illustrated in Figure 3(c). Collapse of structure and the removal of interlayer from central core positions is depicted in Figure 3(d). The effect of the 'final' collapse of the layers that are in closest proximity to each other is shown in Figure 3(e). The length of the arrows depicting shear stress represents the relative magnitude of the internal friction generated.

3.2 C-S-H (C/S = 0.80)-DMA and Creep Modulus Measurements

The tan ð versus mass-loss and creep modulus versus mass-loss curves for C-S-H (C/S = 0.80) dried in increments from 11% RH are plotted in Figure 4. There is a qualitative similarity of the tan ð and creep modulus results with those for C/S = 1.20. Tan ð and creep modulus values (in general) increase to a maximum at mass-loss values of 2.5% and 5% respectively. Tan ð (internal friction) then decreases to a minimum at 5% mass-loss coinciding with the maximum reached by the creep modulus data. These observations are also compatible with cross-linking of the C-S-H sheets and possible interaction of the calcium ions with the silicate lamellae possibly through Si-O-Si or $\equiv SiO^{-}Ca^{2+}$ linkages. Lower internal friction and enhanced rigidity in the system are compatible with lower values of creep rate (i.e. higher creep modulus). The significance of the tan ð and creep modulus parameters and their dependence on mass-loss up to this point as it relates to the creep process is similar to that described in the previous section for C/S = 1.20. Further removal of water up to 6% corresponds with an increase in tan ð and a decrease in creep modulus as the silicate sheets come into closer proximity and additional interlayer water is removed from the central core of the layers improving the ability of the layers to translate. Creep modulus and tan ð values subsequently increase at mass-losses up to 7 and 8% respectively. The potential for creep reduces as additional removal of interlayer water appears to enhance the interaction between the silicate chains restricting translation or sliding.

Helium inflow and 002 basal-spacing are plotted versus mass-loss for C/S = 0.80 in Figure 5. There are significant differences in the mass-loss dependencies of these parameters in comparison to those of the C/S = 1.20 preparation. The initial basal-spacing for the low C/S ratio sample is significantly larger and removal of interlayer water results in a more gradual decrease. The helium inflow for the low C/S ratio preparation has an oscillatory character i.e. there are several maxima and minima in the helium inflow versus mass-loss curve, maxima occurring at 1.5, 3.8, 6.4% mass-loss. Low C/S ratio preparations typically

have longer silicate chain lengths than those with high C/S ratio. It is apparent that this could affect the exit process for the removal of interlayer water which is likely to be highly variable and 'site' specific along the length of the silicate chain. It is possible that sites of 'local' collapse of structure exist. These individual sites would affect other sites including factors that influence mass-transfer and creep. It is noted in Figure 5 that there is the presence of a maximum at 6.4% mass-loss which coincides with maxima observed in the vicinity of this mass-loss for the other silicate systems studied. The higher C/S ratio preparations with shorter chain lengths do not exhibit multiple maxima as mass transfer and structural collapse is more uniform.

The magnitude of creep modulus for C/S = 1.20 and 0.80 at their maximum (6% and 5% mass-loss) respectively is significantly higher for the higher C/S ratio preparation i.e. 240 GPa as compared to 110 GPa. Inversely the creep rate is lower for the high C/S ratio preparation. The magnitude of the internal friction up to this mass-loss is similar. It would therefore seem that structural factors such as chain length that influence the relative movement of the silicate sheets also influence mass transfer and hence creep rate. Collapse of structure is more pronounced at mass-loss values above 6% for the C/S = 1.20 preparation as the creep modulus decreases significantly. The creep modulus of the low C/S ratio preparation increases dramatically at mass-loss values in excess of 6%. This indicates that the structural collapse in this region of mass-loss for the low C/S ratio preparation is more complete resulting in a significantly lower creep rate. In summary the creep rate up to the 'intrinsic' structural collapse involving the removal of water in core interlayer positions is lower for the high C/S ratio preparation. Conversely, it is higher at higher levels of mass-loss. This higher creep rate may be influenced by the larger number of nanostructural defects (missing bridging silica tetrahedral) in the silicate sheets of the higher C/S ratio preparation.

3.3 Hydrated Portland Cement Paste

The tan ð versus mass-loss and creep modulus versus mass-loss curves for hydrated cement paste (water/cement ratio = 0.42) dried in increments from 11% RH are plotted in Figure 6. It is noted that the tan ð and creep modulus curves mimic each other with maxima at about 2% and 6% mass-loss. There are two maxima for the tan ð parameter over the entire range of mass-loss data as was observed for the C-S-H measurements. The magnitude of the tan ð (internal friction) values is substantially lower than those for the C-S-H preparations. The C-S-H present in hydrated Portland cement is ill-crystalline and no basal-spacing can be detected. The C-S-H phase exhibits short range order [26]. Nevertheless, it exhibits many of the characteristics of a layered material [27]. The shifting of the initial creep modulus maximum to lower values of mass-loss (relative to the maxima observed for the C-S-H preparations) may be related to the short chain-length and high degree of disorder of the silicate phase in hydrated cement. Arguably there are a larger number of calcium-silicate-hydrate units per unit volume of specimen. In addition the amount of interlayer water per structural unit would likely be much smaller than in the more crystalline synthetic C-S-H. This would influence the rate of mass-transfer and possibly account for the shift of the creep modulus curve to lower values of mass-loss. The second maximum in the tan ð curve also occurs at about 6.5% mass-loss close to the second maximum in the tan ð curve. This mass-loss corresponds with a maximum that has been observed in the helium inflow (40h)-mass-loss curve [28]. It also corresponds well with the maximum observed in a plot of the decrease in helium inflow (40h) versus mass-loss for cement paste under a sustained load (Figure 7). It is suggested that the rate of creep for cement paste is sensitive to the removal of nanostructural water. It also indicates that the contribution of structural water to the creep process in hydrated cement paste is sensitive to the internal friction generated by its removal. It is arguable that the internal friction is manifested in the form of energy dissipation as a result of a 'sliding' process involving the translation of silicate sheets relative to one another.

4. Conclusions

1. The nanostructural role of interlayer water in C-S-H has a significant influence on the creep process.
2. Creep of C-S-H is dependent on C/S ratio and the equilibrium state of mass-loss from 11% RH.
3. The internal friction parameter (tan ð) obtained from dynamic mechanical analysis is dependent on mass-loss from the 11% RH position.
4. A comparison of tan ð and creep modulus versus mass-loss data for C-S-H and cement paste provides support for the view that a contributing creep mechanism is rooted in a 'sliding' or translation process of C-S-H layers relative to each other.
5. The creep modulus versus mass-loss (with reference to 11% RH) dependence of cement paste is shifted to lower values of mass-loss. This may be due to the short range order and length of the C-S-H structural units in hydrated cement and their influence on the mass transfer process as interlayer water is removed from the structure.
6. The creep process for synthetic layered calcium-silicate-hydrates and the structural role of interlayer water appears to be similar to that of hydrated cement paste. Interparticle sliding or translation appears to be an operative creep mechanism for both synthetic C-S-H and hydrated cement paste.
7. Microindentation methods appear to be effective for determining the creep response of pure calcium silicate hydrates of interest to cement science researchers.

5. References

1. A.M. Neville, Creep of concrete: plain, reinforced and prestressed, North Holland Pub. Co., pp. 622, 1970.
2. W.K. Hatt, Notes on the effect of time element in loading reinforced concrete beams, ASTM Proc., 7, 421-433, 1907.
3. F.H. Wittmann, Creep and shrinkage mechanisms, in Creep and Shrinkage of Concrete Structures, Eds. Z. P. Bazant and F.H. Wittmann, 129-163, Wiley & Sons, New York, 1982.
4. R.F. Feldman, Mechanism of creep of hydrated Portland cement paste, Cem. Concr. Res. 2 (5), 521-540, 1972.
5. B.L. Meyers and F.O. Slate, Creep and creep recovery of plain concrete as influenced by moisture conditions and associated variables, Magazine of Concrete Research, 22(70), 37-41, 1970.
6. W. Ruetz, A hypothesis for the creep of hardened cement paste and the influence of simultaneous shrinkage, Proc. Int. Conf on the Structure of Concrete, London, Cement and Concrete Association, 365-387, 1968.
7. D.J. Hannant, The mechanism of creep in concrete, Materials and Structures, 1, 403-410, 1968.
8. I. Ali and C.E. Kesler, Mechanisms of creep, Symposium on Creep of Concrete, ACI Special Publication No. 9, 35-63, 1964.
9. Z.N. Cilosani, On the probable mechanism of the creep of concrete, Beton I Zhelezobeton, Moscow, No. 2, 75-78, 1964.
10. R.G. L'Hermite, Volume changes of concrete, Proc. Fourth Int. Symp. Chem. Cem., Vol. II, 659-694, Washington D.C., 1960.
11. R.F. Feldman and J.J. Beaudoin, Effect of applied stress on the helium inflow characteristics of hydrated Portland cement, Cem. Concr. Res., 13(4), 470-476, 1983.
12. M. Vandamme and F.-J. Ulm, Nanogranular origin of creep, Proc. Nat. Acad. Sci. (USA), 106 (26), 10552-10557, 2009.

13. R. Alizadeh, J.J. Beaudoin and L. Raki, Viscoelastic nature of calcium silicate hydrate, Cem. Concr. Comp., 32, 369-376, 2010.

14. E.J. Sellevold, Low frequency internal friction and short-time creep of hardened cement paste: An experimental correlation, Hydraulic Cement Pastes: Their Structure and Properties, Proc. of a Conference, University of Sheffield, Cem. Concr. Assoc., 330-337, 1976.

15. E J. Sellevold and C.W. Richards, Short-time creep transition for hardened cement Paste, J. Amer. Ceram. Soc., 55(6), 284-289, 1972.

16. H.F.W. Taylor, Proposed structure for Calcium Silicate Hydrate Gel, J. Amer. Ceram. Soc. 69, (6), 464-467, 1986.

17. I. Soroka and P.J. Sereda, The structure of cement- stone and use of compacts as structural models, Proc. 5th Int. Symp. on the Chem. of Cem., Vol. 3., Tokyo, 67-73,1968.

18. R.F. Feldman, Factors affecting the Young's modulus-porosity relation of hydrated Portland cement compacts, Cem. Concr. Res., 2(4), 375-386, 1972.

19. P.J. Sereda and R.F. Feldman, Compacts of powdered material as porous bodies for use in sorption studies, J. Appl. Chem., 13, 150-158, 1963.

20. J.J. Beaudoin, Comparison of mechanical properties of compacted calcium hydroxide and Portland cement paste systems, Cem. Concr. Res., 13, 319-324, 1983.

21. P.J. Sereda, R.F. Feldman and E.G. Swenson, Effect of sorbed water on some mechanical properties of hydrated Portland cement pastes and compacts, Highway Research Board, Special Report 90, 58-73, 1966.

22. W.C. Oliver and G.M. Pharr, An improved technique for determining hardness and elastic modulus using load and displacement sensing indentation experiments, J. Mater.Res.7, 1564-1583, 1992.

23. K.P. Menard, Dynamic Mechanical Analysis-A Practical Introduction, CRC Press LLC, Boca Raton, pp. 208, 1999.

24. R. Alizadeh, J.J Beaudoin and L. Raki, Mechanical properties of calcium silicate hydrates, Matls. and Struct., 44, 13-28, 2011.

25. R. Alizadeh, J.J. Beaudoin and L. Raki, C-S-H – A nanostructural model for the removal of water from hydrated cement paste, J. Amer. Ceram. Soc., 90 (2), 670-672, 2007.

26. D. Viehland, J.-F. Li, L.-J. Yuan and Z. Xu, Mesostructure of calcium silicate hydrate (C-S-H) gels in Portland cement paste: Short-range oerdering, nanocrystallinity and local compositional order, J. Amer. Ceram. Soc., 79 (7), 1731-1744, 1996.

27. R.F. Feldman, Assessment of experimental evidence for models of hydrated Portland cement, Highway Research Record, No 370, 8-24, 1972.

28. R.F. Feldman, The flow of helium into the interlayer spaces of hydrated Portland cement paste, Cem, Concr. Res., 1 (3), 285-300, 1971.

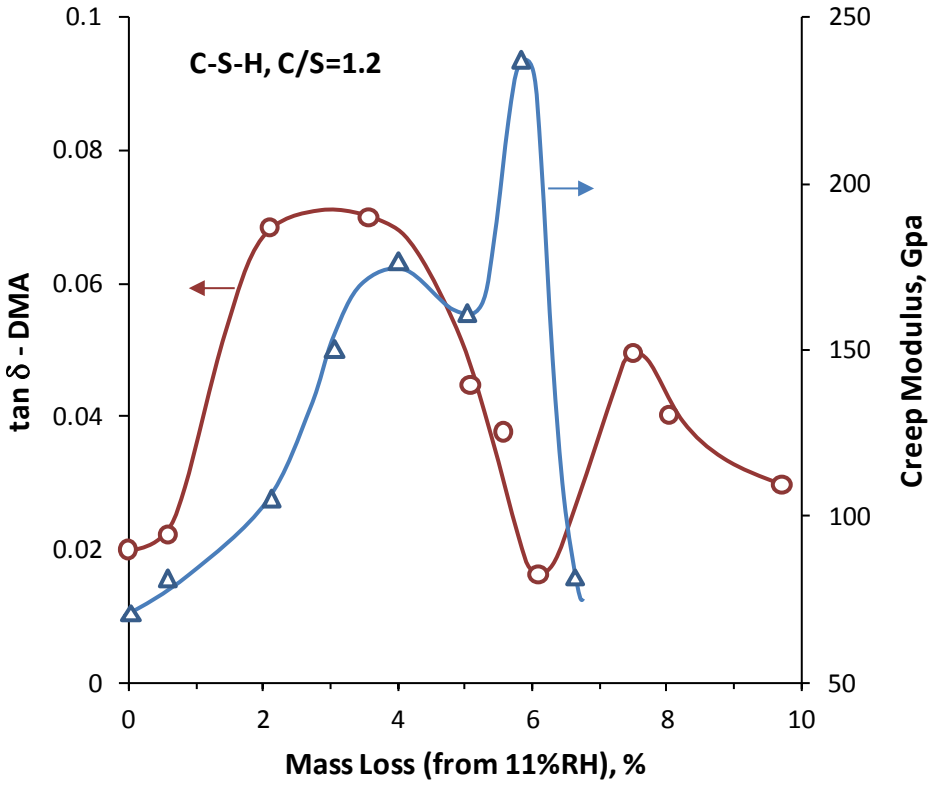

Figure 1: Creep modulus and tan ð versus mass-loss curves (on drying from 11% RH) for C-S-H (C/S = 1.20) preparations.

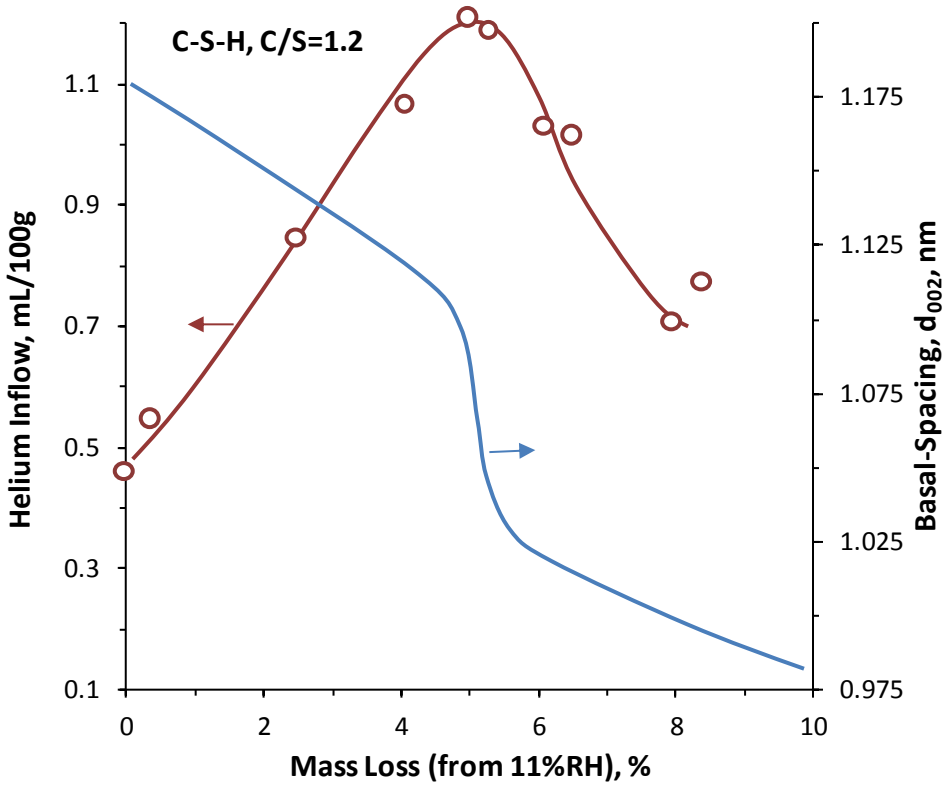

Figure 2: Helium-inflow (40h) and basal-spacing versus mass-loss curves (on drying from 11% RH) for C-S-H (C/S = 1.20) preparations.

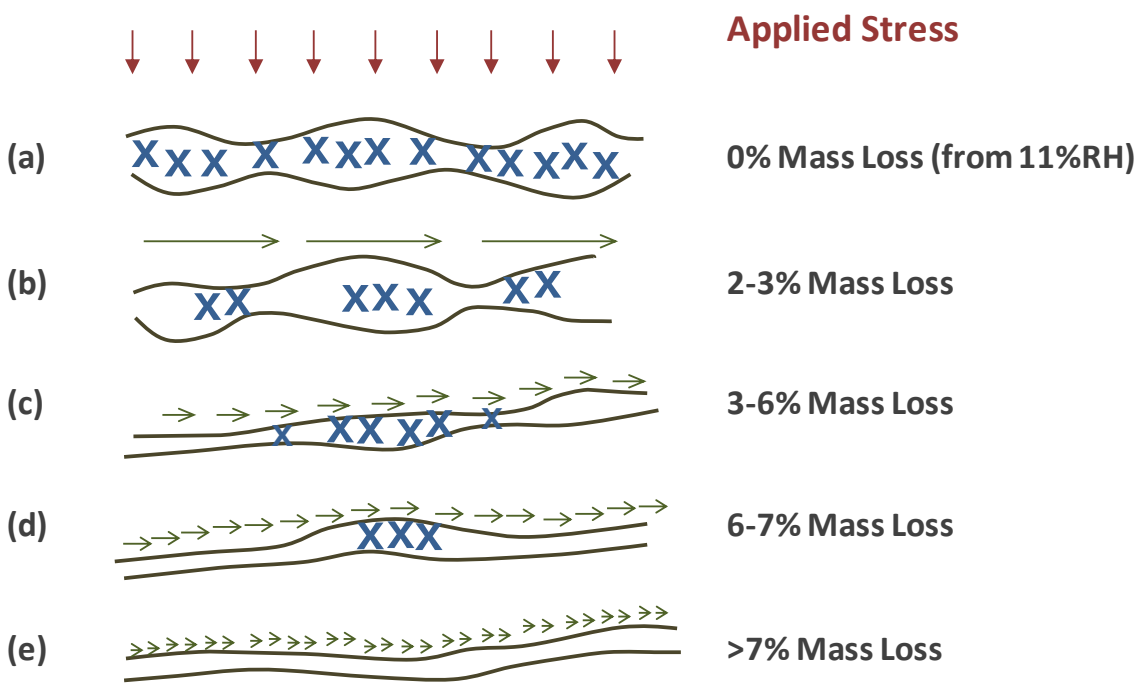

Figure 3: A simplified illustration of nanostructural changes to C-S-H due to application of sustained load at various stages of mass-loss from the 11% RH condition. Symbols: o adsorbed water; x interlayer water; → shear stress due to translation of layers.

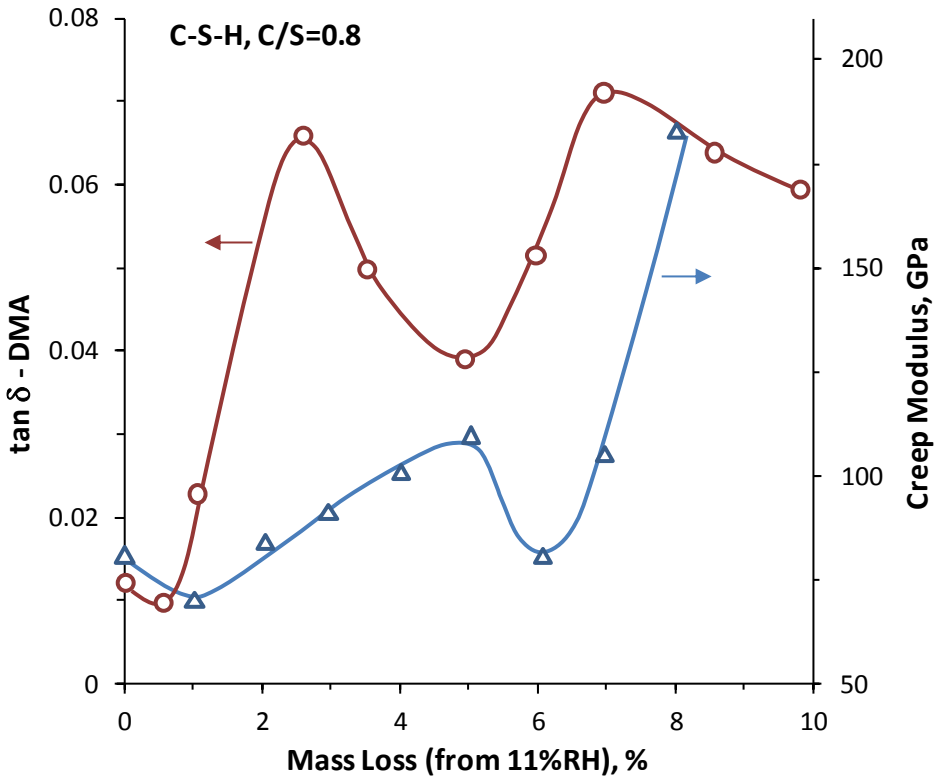

Figure 4: Creep modulus and tan ð versus mass-loss curves (on drying from 11% RH) for C-S-H (C/S = 0.80) preparations.

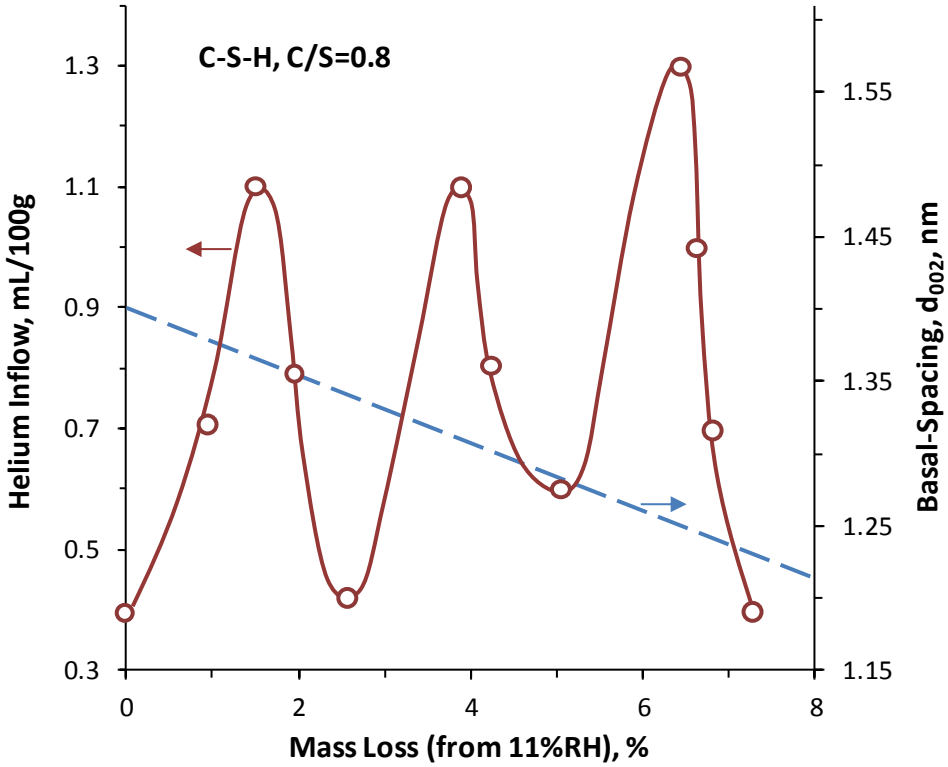

Figure 5: Helium-inflow (40h) and basal-spacing versus mass-loss curves (on drying from 11% RH) for C-S-H (C/S = 0.80) preparations.

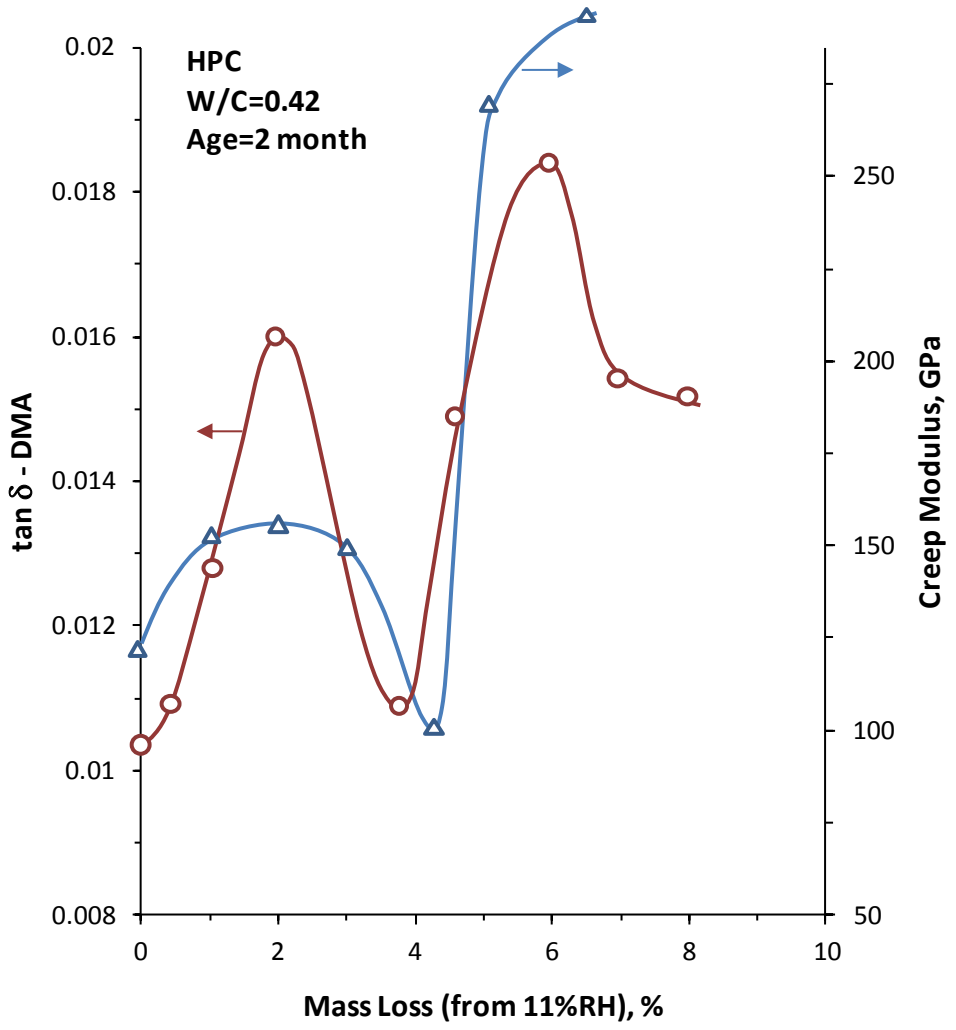

Figure 6: Creep modulus and tan ∂ versus mass-loss curves (on drying from 11% RH) for hydrated Portland cement paste (w/c = 0.42; 2months hydration).

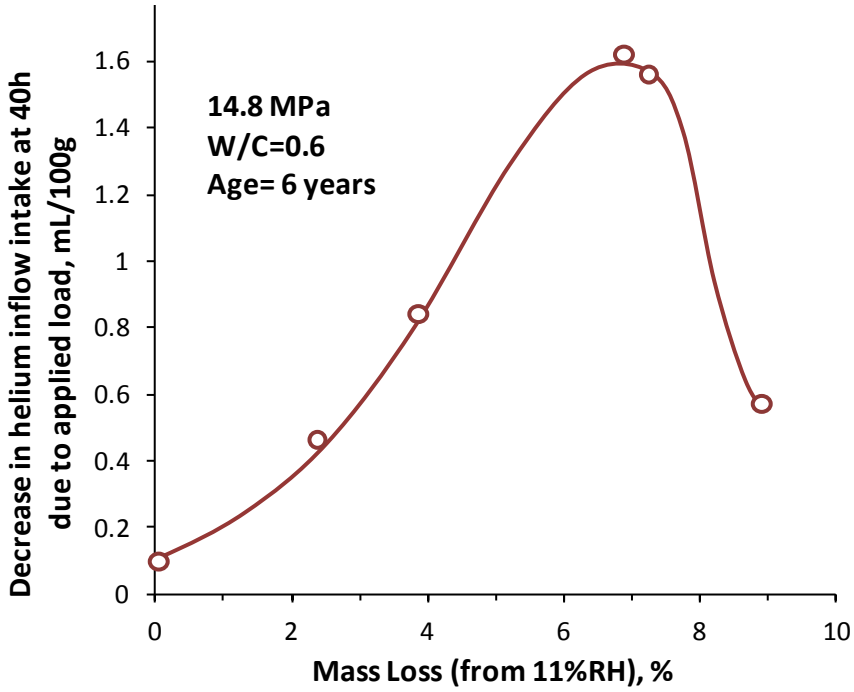

Figure 7: Decrease in helium intake at 40h due to applied stress (14.8 MPa) versus mass-loss for Portland cement paste (w/c = 0.60) hydrated 6 years.

5

Summary and Future Work

Detailed conclusions are an integral part of each paper. Presented in the previous chapters, the most significant achievements are the identification of major differences in the engineering performance of two C-S-H (I) phases, C/S = 0.8 and 1.2, establishing a link between the chemistry and engineering performance of C-S-H systems, and demonstrating the possibility and advantages of controlling the nature of the hydration products in cement paste. In the following section, the main findings of various parts of this research are summarized. Recommendations for future research work are made.

5.1 Summary

This thesis was designed to improve the current understanding of the nanostructure and engineering properties of C-S-H systems and modified C-S-H systems. Many of the controversial issues in cement science were identified and were addressed in a comprehensive research study, which examined the key features of the C-S-H systems at the nano-structure level. In Chapter 4, each paper presented new evidence for a number of mechanical aspects of C-S-H materials. Numerous advanced analytical tools were used in order to verify the observations made in each section. The major achievements of the current work are mentioned briefly as follows:

Paper 1: Microindentation Creep of Monophasic Calcium-Silicate-Hydrates

It was determined that microindentation is a useful method for determining the creep behavior of monophasic calcium-silicate-hydrates. It was found that creep of pure C-S-H phases is greater than the creep of hydrated cement paste or hydrated C_3S due to the restraining effect of calcium hydroxide and clinker phases in the paste. The C/S ratio of the C-S-H preparations studied appeared to influence the three primary microindentation parameters. In general lower C/S ratio preparations have lower values of creep modulus, indentation modulus and indentation hardness. The preparation with C/S = 0.8 had the lowest creep modulus or highest creep possibly due to the high degree of polymerization and low number of defects. Nanostructural models of C-S-H comprised of 1.4nm tobermorite and jennite structural units are compatible with the indentation creep observations made in this study. Creep data for C-S-H obtained from micro and nanoindentation measurements available with literature is co-linear. The porosity dependence of the creep measurements is similar for both scales. Further, the linear porosity dependence of indentation creep over a wide porosity range and the convergence of pycnometric density

determinations with crystallographic determinations supports the view that only one type of C-S-H is present. This is in agreement with the findings of Trtik et al. who have questioned the interpretation of frequency diagrams for indentation modulus and indentation hardness and hence the existence of two types of C-S-H.

Paper 2: Microindentation Creep of Secondary Hydrated Cement Phases and C-S-H

Microindentation parameters i.e. creep modulus, indentation modulus and indentation hardness are porosity dependent. Porosity is an important parameter in determining creep rate as equivalent values of indentation hardness and modulus are obtained at different values of porosity for different hydrated cement phases. It was found that C-S-H generally had a greater creep rate than that of the other hydrated cement phases over a wide range of porosity. The results obtained showed that ettringite, calcium hydroxide and hydrated C_3S had a relatively low creep rate on a porosity basis, whereas gypsum and calcium carbonate had a relatively high creep rate approaching that of C-S-H. Creep of cement phases depends on many factors including crystal structure, defects, translation of cleavage planes, intrinsic mechanical properties in addition to porosity effects. Consideration should be given to determining the influence of 'secondary' phases in hydrated cement when assessing the creep behavior of cement-based materials.

Paper 3: Microindentation Creep, Elasticity and Hardness of C-S-H: The Structural Role of Water

Microindentation creep measurements on C-S-H (C/S = 0.80 and 1.20) demonstrated that creep modulus, indentation modulus and indentation hardness are all dependent on mass-loss from the 11% RH condition. The oscillatory nature of the indentation modulus versus mass-loss curve (C/S = 0.80 and 1.20) mimics both qualitatively and quantitatively the storage modulus (E') versus mass-loss curve obtained

independently using dynamic mechanical analysis methods. The character of these curves was also mimicked by the indentation hardness and creep modulus versus mass-loss curves. Differences in the magnitude of the microindentation parameters at mass-losses greater than 2% for the two C-S-H systems studied as a result of drying may be due to the structural collapse that occurs on drying that would appear to bring the C-S-H sheets (C/S = 1.20) much closer together possibly with an attendant strengthening effect. The oscillatory nature of the microindentation parameters as a function of mass-loss can be explained in terms of removal of adsorbed and interlayer water, increase in the degree of polymerization, possible cross-linking of the silicate chains and the role of calcium ions in the interlayer region. It was also found that a possible creep mechanism may involve the relative displacement of C-S-H sheets relative to one another.

Paper 4: Creep of Calcium-Silicate-Hydrates: A Particle Sliding Mechanism

Evidence was presented that the nanostructural role of interlayer water in C-S-H has a significant influence on the creep process. Creep of C-S-H is dependent on C/S ratio and the equilibrium state of mass-loss from 11% RH. It was found that a comparison of tan ð and creep modulus versus mass-loss data for C-S-H and cement paste provided support for the view that a contributing creep mechanism is rooted in a 'sliding' process of C-S-H layers relative to each other. The creep modulus versus mass-loss (with reference to 11% RH) dependence of cement paste is shifted to lower values of mass-loss. It was also found that the creep process for synthetic layered calcium-silicate-hydrates and the structural role of interlayer water appeared to be similar to that of hydrated cement paste. Interparticle sliding or translation appeared to be an operative creep mechanism for both synthetic C-S-H and hydrated cement paste. Furthermore, it was found that microindentation methods appeared to be effective for determining the creep response of pure calcium silicate hydrates of interest to cement science researchers.

5.2 Recommendations for Future Work

Although a great deal of research on the nature and properties of C-S-H has been conducted, numerous aspects of the characteristics and engineering behaviour of this material still remain unclear. Working with phase pure synthetic C-S-H systems is beneficial as their chemical composition can be readily controlled. The advancements in experimental procedures provide an opportunity to re-examine and clarify some of the controversial issues in cement and concrete science. A few relevant topics that merit detailed investigation in the future are suggested as follows:

1. C-S-H undergoes ageing (increase in degree of crystallization) that is dependent on the hydration time. It is suggested that a comprehensive set of C-S-H (I) samples utilizing various hydration periods be synthesized as the aging of the C-S-H is likely to be an important factor in the development of its mechanical properties. C-S-H can be studied at various stages in the ageing process using a variety of methods including microindentation or dynamic mechanical analysis.
2. The removal of water from the 11% RH condition and its effect on microstructural and mechanical properties of C-S-H systems was investigated in the current work. The water adsorption-desorption isotherm is highly irreversible exhibiting both primary and secondary hysteresis. It is therefore suggested that a study should be conducted on the rehydration of the dried C-S-H materials and the change in various properties, such as creep, as water enters the interlayer region at positions along the adsorption branch of the isotherm.

Appendix A: Vita

Dan-Tam Nguyen received her B.A.Sc. in Civil Engineering with a specialization in Environmental and Water Resources Engineering from the University of Ottawa in 2011. She was admitted to the M.A.Sc. Program in Civil Engineering at the University of Ottawa in 2012. Cement and concrete science has been at the core of her research during the past two years. She has made the following contributions during the course of her master's research:

Peer-Reviewed Journal Publications:

Nguyen, D.-T., Alizadeh, R., Beaudoin, J.J., & Raki, L., "Microindentation creep of monophasic calcium silicate-hydrates," *Cement and Concrete Composites*, 48, 118-126, 2014.

Nguyen, D.-T., Alizadeh, R., Beaudoin, J.J., & Raki, L., "Microindentation creep of secondary hydrated cement phases and C-S-H," *Materials and Structures*, 46(9), 1519-1525, 2013.

Pourbeik, P., Alizadeh, R., Beaudoin, J.J., Nguyen, D.-T., & Raki, L., "Microindentation creep of 45 year old hydrated Portland cement paste," *Advances in Cement Research*, 25(5), 301-306, 2013.

Nguyen, D.-T., Alizadeh, R., Beaudoin, J.J., & Raki, L., "Microindentation creep, elasticity, and hardness of C-S-H: the structural role of water," submitted for publication, 2014.

Nguyen, D.-T., Alizadeh, R., Beaudoin, J.J., & Raki, L., "Creep of calcium-silicate-hydrates; a particle sliding mechanism," submitted for publication, 2014.